KINETICS AND PHOTOCHEMISTRY OF TRANSIENT FREE-RADICALS

A THESIS

SUBMITTED IN PARTIAL FULFILMENT OF THE REQUIREMENTS

FOR THE DEGREE OF

Doctor of Philosophy in Chemistry

IN THE

University of Canterbury

BY

Roger Francis Meads

University of Canterbury

1992

To my parents

Beverley Ada Meads

and

George Percival Meads

how fortunate I am

The machine does not isolate man from the great problems of nature
but plunges him more deeply into them.

Saint-Exupéry

Let us learn to dream, gentlemen, then perhaps we shall discover the truth;
But let us beware of publishing our dreams abroad before they have been scrutinized
by our vigilant intellect ...
Let us always allow the fruit to hang until it is ripe.
Unripe fruit brings even the grower but little profit;
It damages the health of those who consume it;
It endangers particularly the youth who cannot yet distinguish between ripe and
unripe fruit.

Kekulé, 1890

Abstract

We report here several experimental and theoretical studies of free-radicals in the gas phase. Bimolecular rate constants for the reactions

$$\begin{aligned}
BH + NO &\longrightarrow \text{products} & k &= 1.26 \pm 0.07 \times 10^{-10}\ \text{cm}^3\ \text{s}^{-1} \\
BH + C_2H_4 &\longrightarrow \text{products} & k &= 1.41 \pm 0.09 \times 10^{-10}\ \text{cm}^3\ \text{s}^{-1} \\
CN + NH_3 &\longrightarrow HCN + NH_2 & k &= 3.0 \pm 0.4 \times 10^{-11}\ \text{cm}^3\ \text{s}^{-1} \\
CN + ND_3 &\longrightarrow DCN + ND_2 & k &= 1.5 \pm 0.3 \times 10^{-11}\ \text{cm}^3\ \text{s}^{-1}
\end{aligned}$$

have been measured and upper limits to the rate constants for the reactions

$$\begin{aligned}
BH + CO &\longrightarrow \text{products} & k &< 1.1 \times 10^{-11}\ \text{cm}^3\ \text{s}^{-1} \\
BH + CH_4 &\longrightarrow \text{products} & k &< 1.6 \times 10^{-12}\ \text{cm}^3\ \text{s}^{-1} \\
BH + C_2H_6 &\longrightarrow \text{products} & k &< 9.1 \times 10^{-13}\ \text{cm}^3\ \text{s}^{-1} \\
BH + O_2 &\longrightarrow \text{products} & k &< 1.3 \times 10^{-13}\ \text{cm}^3\ \text{s}^{-1}
\end{aligned}$$

have been set. BH ($^1\Sigma$) radicals were generated by excimer-laser photolysis of diborane at 193 nm and detected by time-resolved laser-induced fluorescence. The effects of varying the temperature and the nature of the buffer gas on the reactions of BH with NO and C_2H_4 have been investigated. CN ($^2\Sigma^+$) radicals were generated by excimer-laser photolysis of C_2N_2 at 193 nm and their time evolution was monitored by absorption spectroscopy.

In addition to the rate constant measurements, the products of the reactions of CN with NH_3 and ND_3 have been determined using mass spectrometry and infrared absorption spectroscopy. The methods of *ab initio* molecular orbital theory have been used to determine structures and relative energies of species which could

conceivably be involved in these reactions. The results of all studies have been interpreted in relation to the mechanisms of the reactions concerned.

Prompt emission observed during the 193 nm excimer-laser photolyses of diborane and stannane has been characterised and the identity of the probable emitting species for each band observed has been assigned on the basis of band structure, known thermochemistry and the dependence of band intensity on photolysis laser power. The results obtained have been interpreted in terms of the nature of the photodissociation processes.

Acknowledgements

The successful completion of this work has been aided by the valued contributions of a number of people. First and foremost I would like to thank my family, for their continual support, patience and love.

I am very grateful to my supervisors for their guidance during the course of this work. I would like to thank Professor Leon F. Phillips for his supervision during the past four years and similarly, Dr. Peter W. Harland and Dr. Robert G. A. R. Maclagan for their support and encouragement. Thanks also to Professor Michael P. Hartshorn, Dr. Donald A. House and Dr. Murray J. McEwan.

The contribution made by the technical staff of this department is greatly appreciated. In particular I wish to thank Messrs Peter C. Chadwick, John E. Davis, Alexander M. Fergusson, Russell W. Gillard, David J. MacDonald, Robert M. McGregor, David W. Morrison, Bruce A. Reid, Geoffery Speer, Derek T. Williams, Barrie Wood and John J. York for their advice and assistance.

The friendship, advice and amusement provided by fellow researchers; Dr. John Harrison, Dr. Jayantha Wimalasena, Brett Cameron, David Marsden, Michael Tavendale and Murray Salt is also greatly appreciated.

R F Meads

Roger F. Meads.

March 1, 1992

Table of Contents

List of Tables

List of Figures

Chapter 1

Introduction

The fields of experimental kinetics, spectroscopy and dynamics of small molecules have seen a number of advances in recent years as part of the continuing quest to understand the fundamental interactions of atoms and molecules with each other and with electromagnetic radiation. Gas-phase systems are of particular interest in this regard since the finer details of these elementary processes are not masked by the effects of interference from the matrix which is a complex problem in condensed phases. The use of molecular beam apparatus can extend this ideal further allowing the study of species under essentially collisionless conditions. In a recent series of very elegant experiments, this phenomenon has allowed the characterization of species *in transition* between reactants and products both for unimolecular photodissociation [1,2] and bimolecular chemical reactions [3,4,5].

Despite these advances, the field of gas-phase kinetics remains as one of the most important and fruitful means of obtaining fundamental information on the rates at which these interactions occur. The realm of the gas-phase kineticist extends to cover both intermolecular and intramolecular processes and includes processes by which atoms and molecules interact with electromagnetic radiation. The results of such studies provide information on the potential-energy surfaces characterizing these interactions and are vital for use in modelling studies of the complex chemistry occurring in many practical chemical systems.

Progress in experimental chemical kinetics has been closely linked to technical innovation. In this regard, the advent of commercially available lasers, of which there are now many types employing gas, liquid and solid-state lasing media [6,7], has provided a major impetus in the development of this, and many other areas of chemistry [8,9]. Lasers possess a number of properties which make them an essential part of most modern kinetics experiments. Foremost among these are the very high photon densities (brightness) and monochromaticity (narrow bandwidth) of lasers and the wide regions of the electromagnetic spectrum that they now cover. In combination with frequency mixing techniques and methods of discrete shifting [10,11], "continuously" tunable, monochromatic, coherent light sources are available at nearly any desired wavelength in the range 150–1100 nm with many other regions extending well into the infra-red and vacuum-ultraviolet [9] also covered.

The application of lasers to the study of chemical kinetics has become the focus for many research groups. High power lasers operating at discrete wavelengths in the ultraviolet and vacuum-ultraviolet regions are ideal sources for the generation of transient species such as atoms, molecules, radicals and ions by laser-photolysis of a stable precursor molecule. Single and multi-photon photolysis can provide the experimentalist with access to a large number of rovibronic states of the photofragments [12]. However, photofragments produced in this manner can often have large excesses of internal energy, which introduces additional problems involving cascading and thermalization. Measurement of the energy distributions of the photolysis products can provide information on the photolysis process [13]. In addition to the characteristics already mentioned, the short pulse-widths and high spatial coherence of these pulsed-laser beams have the major advantage, over other means of production such as pulse-radiolysis or discharge-flow techniques, of being able to produce high concentrations of photofragments in a well defined volume, instantaneously and with comparative cleanliness [14]. Judicious choice of the precursor and reactant molecules with respect to the photolysing wavelength can substantially reduce the co-production of unwanted species which can interfere with the process being studied by competing reaction, quenching or absorption of the analysing laser-light.

This method also allows for a simpler interpretation of the experimental data as opposed to, for example, shock-tube [15] and combustion systems [16,17], where extensive numerical modelling is required to determine the kinetic information for the reactions of interest.

Lasers have also proven to be very powerful tools for the detection of transient species whether produced by laser photolysis or by other means. The most widely used laser based detection technique is laser-induced fluorescence [14] in which fluorescence is excited from one or more rovibronic transition of the species of interest by a pulsed, or more recently continuous-wave, dye-laser. Dye-lasers generally lase in the visible and near ultra-violet regions and are tunable over the fluorescence band of the organic dye being used. The detection of fluorescence excited in this manner has proven to be very sensitive to low molecular concentrations although it has the disadvantage of often being limited by fluorescence quenching, sometimes at relatively low pressures. There is the additional problem that not all species will fluoresce as energy degradation of the laser-excited state by non-radiative means may be more efficient.

Since the initial experiments by Laguna and Baughcum [18], detection of transient species by infra-red diode-laser absorption has become more popular. This method has the advantage that almost all species, with the exception of homonuclear diatomic molecules, will absorb infra-red radiation and the very narrow bandwidth of diode-lasers provides for high chemical selectivity between species produced by the photolysis laser pulse. Being an absorption technique, it can be used to study reactions over a wide range of temperatures and pressures but has the disadvantage of being generally less sensitive than detection by laser-induced fluorescence, since a change in signal needs to be detected as opposed to emission above an essentially zero background. Multiple pass optical arrangements are often used to increase the sensitivity of this method of detection.

In conjunction with experimental studies, recent developments in theoretical methods have an important contribution to make to our understanding of the potential-energy surfaces characterizing chemical processes. The development of *ab*

initio molecular orbital theory [19,20,21] and the implementation and commercial distribution of software based on these methods, predominantly by Gaussian Inc, has meant that the ability to calculate these potential-energy surfaces is now available to the non-specialist. A recent review provides a useful guide to the concepts and features of many of the currently used methods of *ab initio* quantum chemistry [22].

Current computational capabilities generally preclude calculation of entire potential-energy surfaces for all but the simplest of systems, since they may span many degrees of freedom. However, by probing the stationary points of the surface which correspond to intermediate and transition state species, much information can be obtained. Knowledge of the relative energies of reactants, products, intermediates and transition states gives good insight into the possible mechanism(s) of a chemical reaction and the relative importance of each, while calculations of the relative energies and/or Morse-type potential curves for the possible electronic states of a molecule have great value in spectroscopic applications.

Other theoretical methods, either statistically based, such as Rice-Ramsperger-Kassel-Marcus theory [23] and Activated-Complex theory [24] or dynamically based, such as Quasi-classical trajectory theory [25,26] can use the results of these *ab initio* studies to calculate the rates of various processes such as chemical reactions or unimolecular decompositions under experimentally inaccessible conditions. Although there is no substitute for experimental data, theoretical studies are certain to feature prominently as our understanding of chemical reactivity increases.

1.1 Scope of the Present Work

The work described in this thesis consists of five studies, four experimental and one theoretical, involving the reactions of cyanogen (CN) and boron hydride (BH) radicals and the spectroscopy of the products of the photodissociations of diborane (B_2H_6) and stannane (SnH_4). Studies of reactions of free-radicals such as these are

particularly relevant to the chemistry of atmospheric and/or combustion processes as well as being amenable to theoretical treatments due to the relative simplicity of the species involved. The combination of experiment and theory is able to provide a far greater insight into elementary processes such as these than either one alone.

General descriptions of experimental equipment and procedures used are given in chapter 2, with details of specific methodology relevant to individual experiments give in the appropriate chapter. In each of the experimental studies, the radical(s) of interest were produced by laser photolysis of a stable precursor molecule in a flow-system. In the kinetics experiments, the time-evolution of these species was monitored by either laser-induced fluorescence (chapter 3) or absorption spectroscopy (chapter 6). The emissions observed during the multi-photon photolysis of diborane and stannane were characterised and the probable emitting species of each band observed was assigned on the basis of band structure, known thermochemistry and laser power dependences (chapter 4).

In addition to these experimental studies, an *ab initio* molecular orbital theory study of the reaction of CN with NH_3 is presented (chapter 5). In conjunction with the kinetic (chapter 6) and product analysis (chapter 7) studies done on this reaction the most likely mechanism of reaction is deduced.

Finally, in chapter 8 some general conclusions about the work presented in the preceeding chapters are drawn and areas for possible extension of this work are discussed.

Chapter 2

Experimental

2.1 Introduction

In this chapter the major pieces of equipment used in the experiments discussed herein will be described. Technical specifications and considerations regarding the use of this equipment will be outlined together with data reduction procedures and methods of preparation and purification of reagents used. Specific methodology detailing the use of the equipment is deferred until the experimental section of the appropriate chapter. In all experiments, free-radicals were produced by laser-photolysis of a stable precursor molecule in a flow-system. These radicals were then characterised by either their spectroscopic or kinetic behaviour.

2.2 Apparatus

2.2.1 Excimer Laser

The photolysis light source used was a Lumonics model TE861-T, thyratron-switched, multigas, Excimer Laser. Gas mixtures of argon fluoride (ArF) and krypton

fluoride (KrF) were used to produce output at 193.3 and 248.5 nm respectively. Pulse energies, measured by a Scientech model 364 power/energy meter, were typically 50–70 millijoules. The laser output beam had a rectangular cross-section of approximately 2×1 cm^2 which, for experiments involving the production of either B_2H_6 or SnH_4 photofragments, was focussed to a point of approximately 2×1 mm^2. In all experiments the effective pulse energy incident upon the radical precursor was less than the maximum energy measured as a result of spatial filtering, due either to apertures or cell design, and scattering of the light by cell windows and optical elements. Knowledge of the absolute laser power was only important in the emission spectroscopy experiments of chapter 4. The high pulse energies and short pulse widths ($\approx$ 10 ns) of excimer lasers make them well suited to the present experiments.

2.2.2 Diode Laser

The probe light source used in the studies of CN-radical reactions was a Laser Analytics Infra-red Diode Laser. The laser diodes were cooled to cryogenic temperatures by a CTI-Cryogenics model 22C Cryodyne, Closed Cycle Helium Refrigerator. The cooled lead-salt diodes lase in many tunable, monochromatic modes. Frequency tuning of the infra-red radiation is achieved by varying either the refrigerator temperature (coarse tuning) or the injection current (fine tuning). Individual modes were selected using a monochromator (Laser Analytics model SP5151) adjacent to the cold-head, which has a grating blazed at *ca.* 10 microns. The wavelength scale of the monochromator was calibrated using the output of a helium-neon laser. Individual modes could generally be tuned over a range of *ca.* 1 cm^{-1} with a maximum continuous-wave power output of *ca.* 1 mW. The total range covered by a single diode (semi-continuously with many mode-breaks) is approximately 100 cm^{-1}. The narrow bandwidth of the diode-laser provides for high chemical selectivity between moieties produced by the photolysis laser pulse and is applicable to the observation of both the decay of reactant species (chapter 6) and the buildup of products (chapter 7).

The diode-laser system also incorporates an internally-coupled, confocal Etalon (Laser Analytics model SP5945) which provides infra-red Fabry-Perot calibration fringes while the laser frequency is scanned, to assist in the determination of the absolute lasing frequency in the manner described by Reich *et al.* [27]. The etalon has the added feature of being able to be used to *lock* the laser emission frequency to the etalon path-difference [27,28]. This allows the stabilization of the laser emission frequency, or for varying the laser frequency by scanning the path difference around it's mean value *via* an internal scanner plate. Alignment of the infra-red beam through the etalon and reaction cells was done using the collimated output of a visible helium-neon laser on a co-linear path to the diode-laser beam.

2.2.3 Dye Laser

The probe light source used in the studies of BH-radical reactions was an AVCO model C5000/4000 Nitrogen Pumped Dye Laser. The thyratron-switched nitrogen laser produces 10 ns, 1 mJ pulses at 337.1 nm which are coupled onto a flowing-dye cassette. To produce output at 433.4 nm needed for these experiments, the dye Stilbene 420 (Exciton Chemical Company) was used. Tuning of the output wavelength over the dye's fluorescence band is accomplished *via* a gear box attached to the diffraction-grating drive. The dye-laser output pulses had typical energies of a few microjoules and a bandwidth of less than 0.1 nm (fwhm) when the laser was properly tuned. Spectral profiles were measured using a McPherson model 218, 0.3 m monochromator.

2.2.4 Detection Systems

In the experiments described here, three different types of detector were used: namely infra-red detectors, photomultipliers and a quadrupole mass spectrometer.

Infra-red detectors

The intensity of the infra-red diode-laser beam was monitored using Judson J15D14-M204-S01M-60 liquid-nitrogen cooled, mercury-cadmium-telluride detectors. Peak response is at *ca.* 11 microns falling to 60% at 4 microns. Detector output was amplified by a matched Judson PA-100 pre-amplifier (55 dB gain). Cable lengths between the detector and pre-amplifier were shielded and kept as short as possible to minimize the possibility of pick-up.

Photomultipliers

Prompt emission and laser-induced fluorescence was detected using either an EMI 9813QA, bi-alkali cathode, high-gain photomultiplier (peak response at *ca.* 360 nm) or an EMI 9558QB, tri-alkali cathode, red sensitive photomultiplier (peak response at *ca.* 400 nm). Both the photomultipliers and their pre-amplifiers were housed in a cylinder of μ-metal as a shield against electromagnetic noise.

Mass Spectrometer

A Spectramass Dataquad Quadrupole Mass Spectrometer was used for mass analysis of gaseous samples. Gaseous ions were detected using a secondary-electron multiplier. The quadrupole was pumped to pressures of *ca.* 10^{-8} torr by a Varian VHS-4 diffusion pump backed by a Welch Duo-Seal model 1376 mechanical pump. Analysis was done at pressures ranging from 10^{-7} to 10^{-5} torr as measured by an ion-gauge adjacent to the quadrupole. The diffusion pump and quadrupole are separated by a large liquid-nitrogen cold trap to prevent contamination of samples with diffusion pump oil fragments.

2.2.5 Monochromators

Three monochromators were used during the course of the experiments described here: namely a McPherson model 218, 0.3 m monochromator, a Jarrell-Ash 0.75 m Czerny-Turner monochromator and a Laser Analytics model SP5151 monochromator, used for mode selection of the diode-laser output, which has been described previously. Both the McPherson and the Jarrell-Ash monochromators were used to resolve the emission spectra described in chapter 4 and the McPherson monochromator was also used for a variety of other functions which included determining spectral profiles of the dye-laser and tuning of the dye-laser to the desired wavelength. Three different interchangeable gratings were used in the McPherson monochromator, all of which have 1200 grooves/mm, blazed at 500, 300 and 150 nm while the grating used in the Jarrell-Ash monochromator was blazed at 300 nm. The wavelength scales of the both these monochromators were calibrated using the emission of a mercury Pen-Ray lamp.

2.2.6 Reaction Cells

General considerations relevant to the design of the photolysis cells used in the laser-induced fluorescence (chapter 3) and the laser absorption (chapter 6) experiments will be discussed here. Additional details pertinent to the individual cells will be given in the experimental section of the appropriate chapter. The object of this section is to illustrate the differing criteria borne in mind during the design and construction of the two cells.

The cell used for the laser-induced fluorescence experiments was designed with respect to two major criteria; namely the need for temperature control and the need to minimize the effects of stray light. Temperature control was achieved by constructing the sidearms of the cell from a double layer of glass tubing and circulating a variety a liquids between the layers. The temperature of the liquids used was thermostatically controlled in a reservoir and circulated by an in-line pump. Insulation

of the cell with several layers of Cayo-wool allowed experiments in the temperature range 250–350K to be carried out.

A number of approaches were used to suppress stray light. Room light was eliminated by painting the cell with several layers of black paint. The effects of broad-band fluorescence excited from the Suprasil windows (most likely caused by defects, impurities and non-linear processes within the quartz) were minimized by the use of long sidearms on the cell, as the observed fluorescence intensity decreased with distance from the photomultiplier. Scattering of the photolysis and probe laser-light by the optics and the windows was also a problem. Angling the windows from perpendicular to the optical axis and using appropriate combinations of Corning glass filters to give a narrow bandpass in the region of interest helped minimize this and the effects of the window fluorescence. Despite these measures, it was necessary to wait 50 μs after the photolysis laser pulse before collecting data. This period also served to ensure that all species were thermalized and equilibrated with the cell wall temperature.

The cell used for the diode-laser absorption experiments was designed with one major consideration in mind: the need to maximize the length of the path along which the photolysis and probe laser beams overlapped. While overlap between the photolysis and probe laser beams was also necessary for the laser-induced fluorescence experiments, the decrease in sensitivity of laser absorption compared to laser-induced fluorescence made it especially necessary to maximize the overlap path length in these experiments.

Cell windows of calcium fluoride were used to enable the probe (infra-red) laser beam to be introduced co-linearly into the volume swept out by the photolysis (ultra-violet) laser beam. This proved to be far superior to introducing the two laser beams through different windows (each transparent to only one or other of the laser beams), which resulted in the probe laser beam being unable to pass through the entire length of the volume swept out by the photolysis laser beam in the cell. The number of passes attainable through this volume was a compromise between the need to have the excimer laser close to the cell and the (external) mirrors in

front of it as far back as possible to facilitate more reflections, and the diameter of the CaF_2 windows available limiting spatial resolution. The length of the cell was limited by the size of the annealing oven in the departmental glassblowing workshop to *ca.* 1.2 metres.

Both cells were evacuated by a Welch duo-seal model 1397 rotary pump backing a Heraeus R150 Roots blower. The pumps were separated from the cell and reagent manifold by a large liquid-nitrogen cold-trap which served the dual purpose of removing corrosive gases before passage through the pump and preventing contamination of the cell with pump oil. The actual pumping speed was controlled by a throttling valve situated immediately before the cold-trap.

Both cells were constructed of Schott-Duran glass in the glassblowing workshop of this department. Cell pressure was monitored *via* a B19 ground-glass joint by a MKS type 222CA 0-10 torr Baratron and, in the case of the CN experiments, also by a Texas Instruments model 144 quartz-spiral gauge. The reference vacuum for this instrument was provided by a two-stage glass diffusion-pump. All joints were lubricated with Apiezon N or H grade vacuum grease.

2.2.7 Reagent Manifold

Preparation and control of gas mixtures for laser photolysis was done in a glass vacuum-manifold. Incorporated in this were glass-bulbs and a variety of cold-traps for the purification and storage of reagent gases together with metered lines for the buffer, reactant and radical precursor constituents of each gas mixture. There was some flexibility in the system *via* interconnections between the lines so that, for example buffer could also be channeled through the radical precursor line and into a saturator which was used to admit vapor from solid ICN into the cell on the stream of buffer gas.

Gas flows were measured by Tylan model FM360 mass flow-meters, calibrated by standard bubble-tube techniques, and regulated by either Whitey (for flows less than

50 sccm) or Edwards needle-valves in conjunction with glass stop-cocks (J. Young Scientific Glassware Limited). The requirements of the experiment being undertaken dictated which of the available flow-meters, from a range having capacities 10, 50, 200 and 500 sccm, were used on which line. All the flow-meters used had calibration factors (actual flow/indicated flow) which were linear over their entire range. The flow-meters were connected to a Tylan model RO20A readout box which gave the flow in standard cubic centimetres per second (sccm) directly.

The pressure in any of the lines could be measured by a MKS 0-1000 torr, type 315BH-1000 capacitance manometer, controlled by a type MKS type 170M controller. The reference vacuum for this instrument was provided by an Edwards 1″ diffusion pump. The manifold was constructed of Schott-Duran glass so that modifications, of which there were many, could be done cheaply and with relative ease. The ultimate geometry of the manifold was dependent on the experiment being undertaken.

Diborane and stannane were prepared in a separate vacuum line housed remotely from the main laboratory. Both manifolds were leak tested regularly using a tesla-coil and by monitoring the pressure in the manifold as a function of time when the pumps were blocked off. All vacuum pumps, including the diffusion pump, were separated from the manifold by large liquid-nitrogen cold-traps.

2.2.8 Microcomputers and Software

Experiments in which data was acquired using the Boxcar Integrator were controlled using a Digital Equipment Corporation (DEC) LSI 11/23 minicomputer *via* a DEC AXV-11C A/D-D/A interface, incorporating sixteen 12-bit analogue-to-digital input channels and two 12-bit digital-to-analogue output channels. This system has twin floppy-disk drives for data storage. The DEC system controlled experimental parameters such as the boxcar gate delay (as a fraction of the preset timebase), the sampling rate and the number of points taken before collecting and storing the data for later analysis. All programs for the collection of data using the boxcar,

both kinetic and spectroscopic, and subsequent analysis of this data were written by Professor L. F. Phillips.

Experiments in which data was acquired using the LeCroy transient recorder were controlled using the LeCroy Waveform Catalyst software run on an IBM-clone 80386DX (with 80387 math co-processor) personal computer. In the configuration used for our experiments the LeCroy system essentially functioned as a 32 MHz dual-channel, digital oscilloscope. Data transfer between the computer and transient recorder was *via* a GPIB interface (LeCroy 8901A, PC IEEE-488 AT-GPIB (16-bit) interface card). Data was stored on the computer's hard-disk and analysed using software written by the author.

2.2.9 Instrumentation

Oscilloscope

Many diagnostic procedures throughout the course of these experiments were performed using a Tektronix model 7904, 500 MHz oscilloscope. This instrument is capable of being used with a variety of amplifying and timebase modules which provide a wide range of display options. Those modules most commonly used were a 7A26 dual-trace amplifier, a 7A22 differential amplifier, a 7B85 delaying timebase and a 7B80 timebase. The oscilloscope was routinely used for checking timing aspects of each piece of equipment as well as their timing relationships to other equipment relative to a trigger pulse. It was also used for signal monitoring especially when maximizing the signal-to-noise ratio with respect to experimental parameters.

Boxcar Integrator

The main data acquisition device used for the BH-radical kinetic experiments and the emission studies was a Princeton Applied Research (PAR) model 160 Boxcar Integrator. This instrument was used for gating and averaging the signal relative to

a trigger pulse, either directly or as a slave to a minicomputer. Further aspects of the boxcar's pulse generation capabilities will be outlined in chapter 3. All boxcar parameters were optimised to ensure that the maximum signal-to-noise ratio was obtained and care was taken to ensure that the time-constants, inherent in the boxcar's operation, did not distort the signal in any way.

Transient Recorder

The main data acquisition device used for the CN-radical kinetic experiments was a LeCroy transient recorder. This instrument consists of two LeCroy TR8837F transient digitizers whose input and timing pulses are provided by a LeCroy 6103 dual-channel amplifier/attenuator all situated in a LeCroy 8013A Camac crate. All modules were programmable *via* the LeCroy Waveform Catalyst software and have the capability to run in *autosequence* mode, which was used in our experiments to increase the signal-to-noise ratio while the diode-laser frequency was being scanned to locate the transient absorption. The transient digitizers were configured to allow a portion of the *pretrigger* region (the time immediately before the CN radicals are produced) of the trace to be collected for the determination of I_0 (intensity at $t = 0$) values needed for data reduction procedures.

2.3 Reagent Chemicals and Handling Techniques

The reagent chemicals used during the course of these experiments may be divided into three categories according to the purpose they served. These are buffer/carrier gases, reactant gases and radical precursors.

Helium (New Zealand Industrial Gases Scientific or Instrument grades, nominal purity > 99.99%), argon (NZIG Welding grade, np > 99.99%), nitrogen (NZIG oxygen-free grade, np > 99.995%) and sulphur hexafluoride (Air Products Instrument grade, np > 99.99%) were used as buffer and/or carrier gases. Helium, argon

and nitrogen were purified by passage over reduced BASF BTS catalyst heated to 150°C followed by passage through a silica-gel cold-trap (liquid-nitrogen cooled for helium and dry-ice/ethanol cooled for argon and nitrogen). Sulphur hexafluoride was used without further purification.

Ethane dinitrile (C_2N_2, Matheson Gas Products, np > 99.99%), iodine cyanide (ICN), stannane and diborane were used as radical precursors. C_2N_2 was purified by trap-to-trap distillation and freeze-pump-thaw cycles. ICN was prepared using the method outlined in Organic Syntheses, Volume 4 [29] and purified using the recrystallization methods suggested. Diborane was prepared using the methods of Jeffers [30] and of Freeguard and Long [31]. Purification of samples prepared by either method was done *via* trap-to-trap distillation and by freeze-pump-thaw cycles. Despite these measures diborane prepared by the method of Jeffers proved unsuitable for the borane emission spectroscopy experiments (see chapter 4) due to contamination with SnH_4. Stannane was prepared using the method of Schaeffer and Emilius [32] and used without further purification.

Nitric oxide (Matheson Gas Products CP grade, np > 99.2%), nitrogen dioxide, ammonia (Christchurch Gas, Coal and Coke Co, np > 99.9%), oxygen (Matheson Gas Products UHP grade, np > 99.99%), methane (NZIG UHP grade, np > 99.97%), ethane (Matheson Gas Products CP grade, np > 99%), ethene (NZIG CP grade, np > 99.5%), carbon monoxide (Matheson Gas Products CP grade, np > 99.5%) and d_3-ammonia (ND_3) were used as reactant gases. Nitric oxide was purified by passage through a silica-gel dry-ice/ethanol cooled cold-trap (−78°C). Ammonia was purified by trap-to-trap distillation and by freeze-pump-thaw cycles over anhydrous potassium hydroxide. Nitrogen dioxide was synthesised by mixing excess oxygen with nitric oxide in a 10-ℓ bulb. The reaction mixture was purified by freeze-pump-thaw cycles with a pure sample being indicated by the lack of any blue-green colouration in the frozen (white) solid. d_3-Ammonia was synthesised by reaction of D_2O with MgN_3 in a vacuum system. The product gas mixture was purified by distillation into a 5-ℓ bulb followed by freeze-pump-thaw cycles. The purity of our sample was checked using mass spectrometry which showed no evidence

for the presence of contaminants. The remaining gases were used without further purification.

2.4 Data Reduction Procedures

Brief details regarding the determination of bimolecular rate coefficients from experimental data are given here. Further details, pertinent to individual experiments, are given in the experimental section of the appropriate chapter.

The concentrations (number densities) of the constituents of each gas mixture were calculated from their partial pressures and the temperature at which the experiment was conducted. Partial pressures were determined from the indicated flow-rates, corrected with pre-determined flow-meter calibration factors (actual flow/indicated flow) and heat capacity correction factors supplied by the flow-meter manufacturer, and total pressure. In the case of ND_3 the heat capacity correction factor was calculated using the manufacturer's formulae and data taken from the JANAF thermochemical tables [33].

The data collected in the BH-radical kinetics experiments, in the form of laser-induced fluorescence intensities *vs.* time, were corrected for background signal (measured with the dye-laser blocked) and then converted to ln(I) *vs.* time format. The pseudo first-order decay constant k', is determined from the slope of a plot of these values. These constants were determined for all the reactant (NO, C_2H_4, etc) concentrations for which experimental data had been collected. The bimolecular rate constant is obtained from the slope of a plot of k' *vs.* [reactant]. The degree of accuracy of the rate constants obtained was reflected by the 95% confidence intervals calculated from a Student-t test of the linear least-squares fit.

The data collected in the CN-radical kinetics experiments was in the form of infra-red intensities *vs.* time. The value of I_0 was determined from the pre-trigger portion of the data and the post-trigger data was then converted to $\ln\left(\frac{I_0}{I}\right)$ *vs.* time format. The pseudo first-order decay constant k', is determined from the slope of

a plot of these values. Once these values had been determined the rest of the data reduction procedure was identical to that carried out in the BH-radical experiments.

Chapter 3

Kinetics of Reactions of BH with NO, C_2H_4, O_2, CH_4, C_2H_6 and CO

3.1 Introduction

The combustion chemistry of boron has long been of interest due to the potential of elemental boron and boron-containing systems as high energy fuels. On a volumetric basis, the theoretical energy release from elemental boron exceeds that available from conventional liquid-hydrocarbon fuels or aluminium-based fuels by factors of three and two [34] respectively. This has stimulated a great deal of interest in the enhancement of liquid-hydrocarbon fuel combustion *via* the use of boron-hydrocarbon slurry suspensions. Practical difficulties encountered due to the inhibiting effect of the buildup of boron oxide coatings on unburned boron particles, preventing complete oxidation of boron to B_2O_3, has meant that the full potential of such systems is yet to be realised.

Similarly, there has also been considerable interest in the combustion of boranes, due to their high energy release, wide limits of flammability and small quenching

diameters [35] and a number of studies of borane oxidation have been undertaken. From a study of the reactions of oxygen and nitrogen atoms with diborane and borane carbonyl, Anderson and Bauer [36] concluded that to account for the energetics of the observed products, the reaction pathway must involve hydrogen abstraction from the initial adduct to form BH and BH_2. Further work by Jeffers and Bauer [37] confirmed that only the reactions

$$\begin{aligned} BH + O &\longrightarrow BO^* + H \\ BH_2 + O &\longrightarrow BO^* + H_2 \end{aligned}$$

were exoergic enough to produce BO in the electronically excited states observed as well as verifying the presence of BH from the detection of BH $\tilde{A} \rightarrow \tilde{X}$ emission. Subsequent to these studies Borchardt *et al.* [38] have proposed a detailed mechanism for the oxidation of diborane in which reactions involving boron hydrides play an important part in the overall reaction scheme.

Despite their potential importance, very little is known about the rates of fundamental processes involving boron hydride radicals. At the time this work was done, no previous measurements of the kinetics of BH reactions had been made. Pasternak *et al.* [39] had reported room-temperature rate constants for the reactions of BH_3 with CO, NO and C_2H_4 and upper limits to the rate constants for reactions with O_2 and H_2O. Since this work, Rice *et al.* [40] have reported measurements of the room-temperature rate coefficients of BH reactions and more recently Garland *et al.* [41] have reported a similar study including measurements made at elevated temperatures. A theoretical and experimental study of the association reaction of BH with D_2 has also been reported [42]. All other studies of the reactions of boranes have been conducted in the same laboratory.

3.2 Experimental

Boron hydride (BH) radicals were produced by the 193.3 nm photolysis of diborane (B_2H_6) using the focussed output of an ArF excimer laser. The laser was operated at

a frequency of *ca.* 17 Hz and produced pulses with energies of 50–70 mJ, as measured by a Scientech model 364 power/energy meter. The laser repetition frequency was chosen so that the pumping speed on the reaction cell was sufficient for the contents of the cell to be swept out between pulses. The low pulse energies combined with the small absorption cross-section of diborane at 193 nm (*ca.* 4.4×10^{-20} cm^2 [43]) ensured that pseudo first-order conditions were maintained in all experiments with [Reactant] $\gg$ [BH].

The reaction cell used in these experiments (see section 2.2.6) essentially consisted of a six-way glass cross comprising two long (30 cm) side-arms, a pump-out port, two B34 tapered ground-glass sockets, used to provide optical access to the viewing region for the photomultiplier and the monochromator, and a B19 tapered ground-glass socket used to allow pressure and temperature monitoring. This arrangement of the photomultiplier and monochromator eliminated the need for the use of collection optics. Suprasil-quartz windows were attached to the end of the side-arms with epoxy resin. The reactant gas mixture was introduced from both ends of the cell to minimize dead space. Some buildup of photolysis products on the windows did occur, predominantly on the window through which the photolysis laser beam entered, however the high photon flux of the photolysis laser beam acted as a efficient cleaner of the area of the window through which it passed. A diagram of this cell can be found on page 110 of reference [44].

BH-radicals were monitored by laser-induced fluorescence, excited in the Q_{00} branch of the $\tilde{A} \rightarrow \tilde{X}$ transition at 433.4nm [45], with an AVCO C5000/4000 nitrogen-pumped dye-laser using Stilbene-420 dye. The laser-induced fluorescence was detected at right angles to the plane of the photolysis and probe-laser beams, through Corning 7–69 and 3–73 glass filters with a combined bandpass of 410–490 nm (peak transmission 37% at 430 nm), by an EMI 9813QA photomultiplier. The photomultiplier output was amplified and taken to a computer controlled PAR model 160 Boxcar Integrator.

The experimental setup is shown in figure 1. A 10 volt TTL pulse produced by

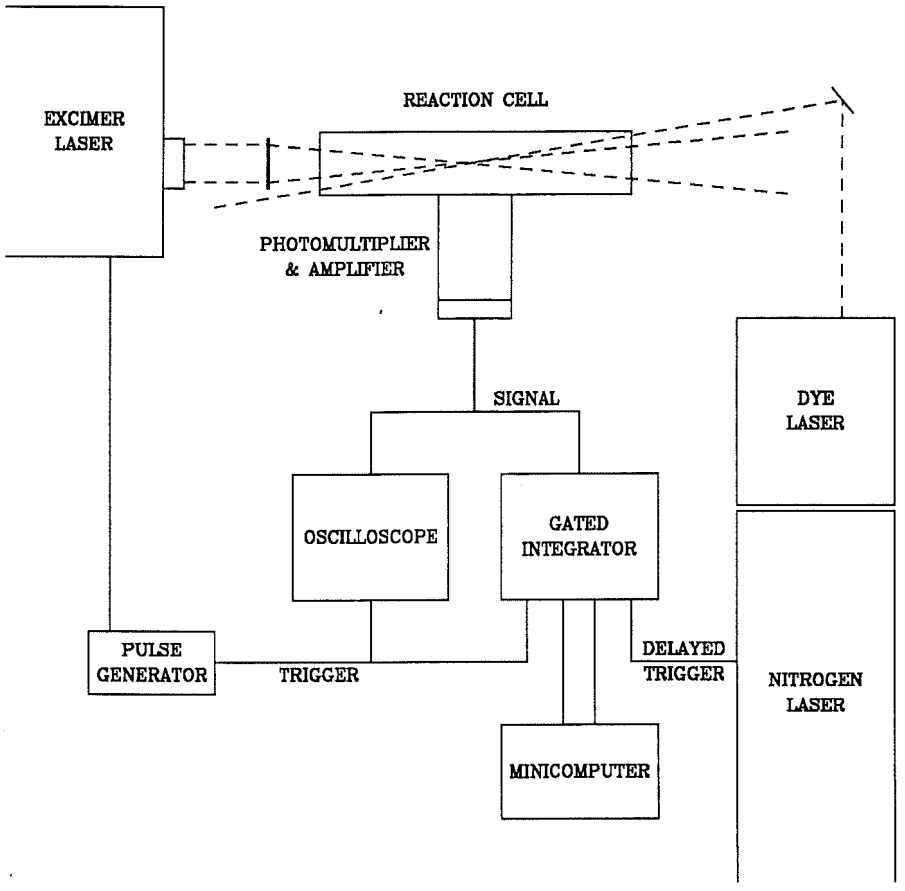

Figure 1: Experimental configuration for the collection of kinetic data using excimer-laser photolysis/dye-laser-induced fluorescence

a variable frequency, square-wave generator simultaneously triggers the photolysis laser and the boxcar integrator, initiating the timebase ramp. The decay of laser-induced fluorescence from BH-radicals is measured by varying the delay between the photolysis and probe lasers in the following way. The boxcar integrator has the facility to produce a 5V output pulse essentially synchronous with the opening of the input gate and this is used to trigger the probe laser. With the gate delay, as a fraction of the timebase, varied under the external control of a microcomputer, the laser-induced fluorescence decay profile can be measured. Additional flexibility in the timing system was provided by the addition of a variable delay between the

opening of the gate and the probe laser being triggered. Both the timing system and the input gate were optimised to maximize the signal-to-noise ratio.

Cell pressure was measured using a MKS model 222CA 0-10 torr Baratron. The range of pressures we could use were limited by fluorescence quenching at greater than approximately 2.5 torr and signals being too small to be accurately measured at pressure less than *ca.* 0.3 torr. For this reason we chose to investigate the effect of pressure on the reaction by varying the nature of the buffer gas rather than the total pressure. The temperature of the gas stream was measured by a calibrated copper-constantan thermocouple situated just below the viewing region. Flow rates of reactant molecules were measured with calibrated Tylan mass flow-meters and controlled with needle valves. Reactant partial pressures were calculated from the measured flow rates and total pressure. The purity, handling and preparation of gases used in this experiment have been discussed previously in section 2.3.

3.3 Results and Discussion

Typical pseudo first-order decay plots for BH in the presence of varying concentrations of NO are shown in figure 2. Signals from the first 60 microseconds of each decay are not included in the plots due to a significant background arising mainly from window fluorescence in this time period. The linearity of plots obtained confirms that BH was being removed by first-order processes. The bimolecular rate coefficient is obtained from the slope of a plot of the first-order rate constants as a function of the NO concentration (figure 3). The results we obtain show that the rates at which BH reacts with NO and C_2H_4 are both fast and exhibit a negative dependence on temperature, as illustrated in figure 4. The error bars in figure 4 represent the 95% confidence intervals obtained from a Students-t test of the linear least-squares fit. Removal of the rate constants at the lowest temperature measured, which have large 95% confidence intervals, does not significantly affect the slopes of these plots.

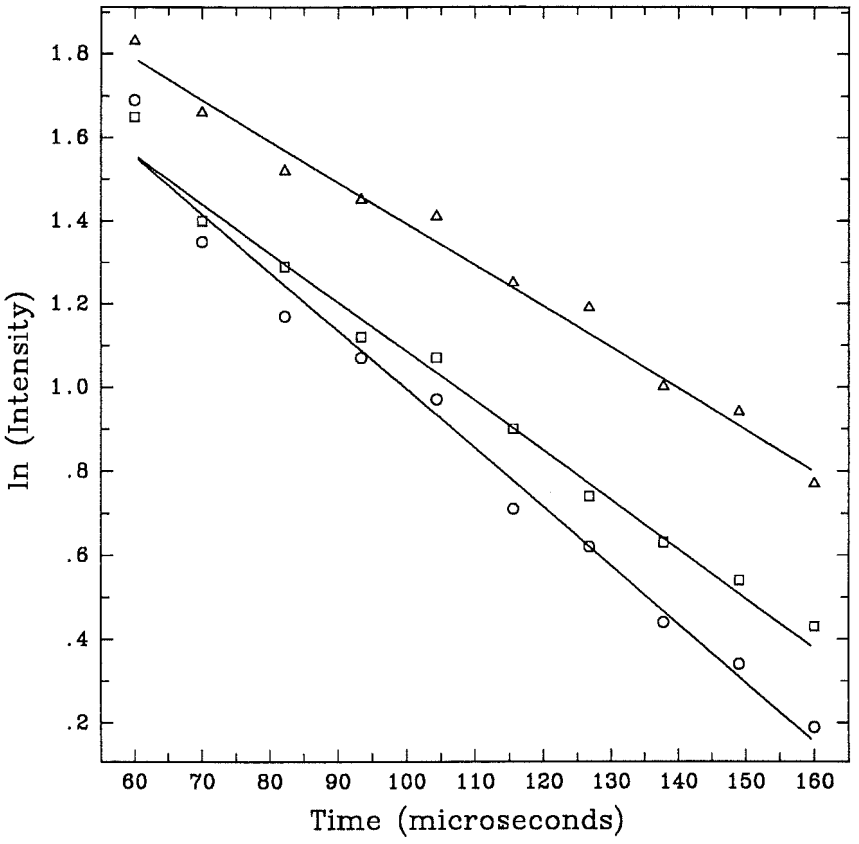

Figure 2: Laser-induced fluorescence decay profiles of BH in the presence of NO: circles [NO] = 1.25×10^{14} cm^{-3}; squares [NO] = 0.89×10^{14} cm^{-3}; triangles [NO] = 0.56×10^{14} cm^{-3}

3.3.1 BH + NO

We measure the rate constant[1] for the room-temperature reaction of BH with NO to be $(1.26 \pm 0.07) \times 10^{-10}$ cm^3 s^{-1}, in 0.5–2.0 torr of He. This is in good agreement with the later determinations of Rice *et al.* [40] ($(1.35 \pm 0.06) \times 10^{-10}$ cm^3 s^{-1})

[1]Previously reported rate constants from this study [46,44] differ slightly from those presented here due to a small error made in previous data reduction procedures

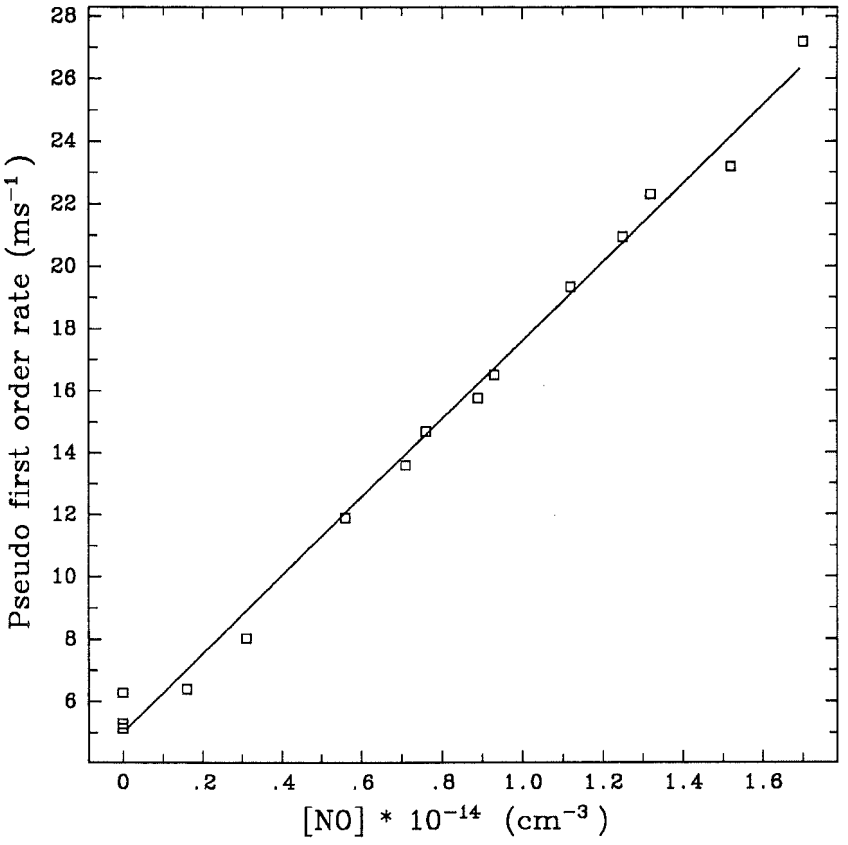

Figure 3: Stern-Volmer plot for the decay of BH in the presence of NO

and Garland *et al.* [41] ($(9.4 \pm 0.9) \times 10^{-11}$ cm^3 s^{-1}). Garland *et al's.* measurements, made in the temperature range 298–600K, confirm the negative temperature dependence we observe. Their results were fitted to the Arrhenius expression[2] $k(\mathrm{T}) = 4.5 \pm 0.8 \exp\left(\frac{2.0 \pm 0.6}{\mathrm{RT}}\right) \times 10^{-11}$ cm^3 s^{-1}. Rice *et al's.* measurements show the rate constant is independent of pressure in the range 5–100 torr of He. This result appears to contradict the dependence of the rate constant on the nature of the buffer gas we find in our study, where an increase in the collision efficiency of the buffer gas appears to decrease the rate of reaction (table 1).

[2]Throughout this thesis R = 8.314 J K^{-1} mol^{-1}.

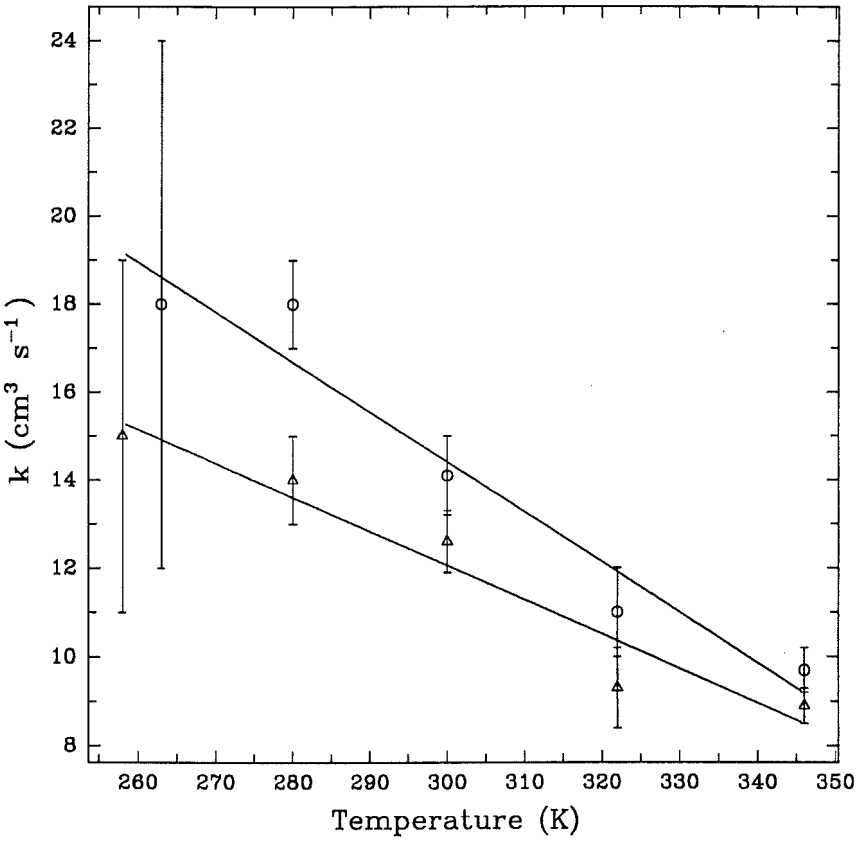

Figure 4: Temperature dependences of the reactions of BH with NO (triangles) and C_2H_4 (circles)

We attribute this dependence to depletion of NO in the viewing region by a radical chain reaction involving diborane photolysis products as well as other species such as NH, N and O atoms. The observed rate is then dependent on the rate of diffusion of NO into the viewing region and as a result would exhibit the observed dependence on the buffer gas. Due to the limitations of our system and the small single-photon absorption cross section of diborane at 193 nm, we were unable to have more than a ten-fold excess of NO over the precursor B_2H_6 in order to obtain measurable signals over the timebase used whereas Rice *et al's.* measurements were performed with at least a 100-fold excess of NO over borane carbonyl precursor. Any

Buffer	k_{BH+NO}	$k_{BH+C_2H_4}$
He	$1.26 \pm 0.07 \times 10^{-10}$	$1.41 \pm 0.09 \times 10^{-10}$
Ar	$9.5 \pm 0.6 \times 10^{-11}$	$1.39 \pm 0.09 \times 10^{-10}$
N_2	$9 \pm 1 \times 10^{-11}$	$1.71 \pm 0.09 \times 10^{-10}$
SF_6	$6 \pm 2 \times 10^{-11}$	$1.33 \pm 0.05 \times 10^{-10}$

Table 1: Dependence of the rate constants of the reactions of BH with NO and C_2H_4 on the nature of the buffer gas.

effects due to NO depletion in the manner we suspect would be more noticeable in our system. The observed lifetime of BH in our system in the absence of NO, is considerably less than that reported by Rice *et al.* which provides support for the existence of the radical chain reaction we propose.

Harrison and Maclagan [47] have reported an *ab initio* molecular orbital theory study of this reaction in which they have calculated the MP4SDQ/6–31G*//HF/6–31G* energies of species conceivably involved. Their results indicate that there are four spin-allowed, exothermic product channel possible in this reaction.

$$\begin{aligned}
BH + NO &\longrightarrow [HBNO]^{\dagger} \longrightarrow HNB + O && \Delta E = -7.2 \text{ kJ mol}^{-1} \\
&\qquad\qquad\quad \longrightarrow HBNO && \Delta E = -299.0 \text{ kJ mol}^{-1} \\
&\longrightarrow [HBON]^{\dagger} \longrightarrow BO + NH && \Delta E = -193.5 \text{ kJ mol}^{-1} \\
&\qquad\qquad\quad \longrightarrow HBO + N(^2D) && \Delta E = -136.9 \text{ kJ mol}^{-1}
\end{aligned}$$

Reaction to form HNB + O involves a hydrogen shift in the intermediate HBNO complex. Harrison and Maclagan suggest that, by analogy to the HBN⇌HNB rearrangement which has a substantial barrier, that the barrier to the H migration would close this barely exothermic product channel. Stabilization of the HBNO adduct is also unlikely to be occurring since Rice *et al.* did not observe any dependence of the rate on total pressure which would be expected if this were the case. Harrison and Maclagan report the barrier to a hydrogen shift in the HBON adduct to be 75.2 kJ mol^{-1} above the *cis* isomer at 0K. This barrier is thus 57.2 kJ mol^{-1} below

the energy of the reactants so that formation of BO and NH *via* this channel or fragmentation to form HBO and N(^{2}D) are the most likely product channels in this reaction.

Although the actual products of reaction have not, as yet, been determined, Kawashima *et al.* [48,49] have observed the HBO species spectroscopically, in the ν_1, ν_2, $2\nu_2$ and ν_3 vibrational states during their studies of ac-discharges in B_2H_6/O_2 and B_2H_6/NO mixtures using infra-red diode-laser absorption.

Phillips [46] has calculated the dynamical *capture* rate of BH and NO to form the HBON adduct over the centrifugal barrier of a dipole-dipole potential. The results of these calculations show the capture rate to be essentially temperature independent over the range 200–400K and slightly greater than or equal to the observed rate of reaction. Inclusion of a factor for the rates of rearrangement and dissociation of the intermediate gives calculated reaction rates slightly less than or equal to the observed rates and exhibiting a small negative temperature dependence. The observed data generally lies between the two extremes and so therefore it would seem that this model adequately accounts for both the observed rate of reaction and temperature dependence. Phillips notes the following points regarding the application of this model to the BH/NO system. Although the factor for barrier crossings is statistical, the dynamical lifetime of the HBON complex (time taken for successive barrier crossings) must be used since a shorter lifetime, as calculated statistically, is not physically possible. Even though the dynamical lifetime is used, it is only of the order of 1 picosecond and there would seem barely enough time to allow statistical redistribution of energy from the newly formed B–O bond. Secondly the overall rate constants, with such a small system, are very strongly dependent on the nature of the activated complex assumed for the process of dissociation back to reactants. He concludes that a larger system would more thoroughly explore the capabilities of this model.

3.3.2 BH + C_2H_4

We measure the rate constant for the room-temperature reaction of BH with C_2H_4 to be $(1.41 \pm 0.09) \times 10^{-10}$ cm^3 s^{-1} at pressures near 1 torr. This is in good agreement with value reported by Rice *et al.* ($(1.17 \pm 0.04) \times 10^{-10}$ cm^3 s^{-1}), at 11 and 50 torr total pressure, and reasonable agreement with the value of Garland *et al.* ($(9.5 \pm 0.8) \times 10^{-11}$ cm^3 s^{-1}). Garland *et al.*, whose measurements span the temperature range 298–600K, confirm that the rate exhibits a negative temperature dependence and were able to fit their data to the expression $k(\mathrm{T}) = 4.0 \pm 0.7 \exp\left(\frac{2.1 \pm 0.6}{\mathrm{RT}}\right) \times 10^{-11}$ cm^3 s^{-1}. All workers observe the reaction to be independent of pressure.

Subsequently Rice *et al.* have suggested that the reaction proceeds *via* addition of BH to the carbon-carbon double bond analogous to the isoelectronic reaction of C(^{1}D) atoms with C_2H_4, in which labelling studies indicate that addition to the double bond is the major reaction channel [50]. In the related reaction of BH with 2,3-dimethyl-2-butene, Rice *et al.* measure the rate constant to be $(1.9 \pm 0.1) \times 10^{-10}$ cm^3 s^{-1}. This enhancement in the rate constant was attributed by these workers to be due to the increase in electron donating ability of the methyl substituents over hydrogen and also implies that the major mechanism of the reactions of BH with double-bond containing species is addition, since in this case, other processes such as insertion or abstraction are essentially blocked.

3.3.3 BH + CH_4, C_2H_6, O_2 and CO

We have set upper limits (k + 95% confidence intervals) to the rate constants for the room temperature reactions of BH with CH_4, C_2H_6, O_2 and CO. Strong chemiluminescence transmitted through the Corning filters, decaying on the timescales we collected data, prevented us from measuring the rate at which BH reacts with NO_2 and from using N_2O as a buffer gas. Chemiluminescence was also a problem with the BH + O_2 reaction but the intensity was not such that it prevented us from

measuring the BH laser-induced fluorescence decays. The emissions are probably due to the formation of $BO^{\star}$ and $BO_2^{\star}$ by reaction of $B(^2P)$ atoms formed in our system (see chapter 4) with the oxygen-containing species [51,52,53].

BH + O_2

Our upper limit for the room-temperature reaction of BH with O_2 ($k < 1.3 \times 10^{-13}$ $cm^3\ s^{-1}$) is consistent with the rate constant of Rice *et al.* ($8 \pm 1 \times 10^{-13}$ $cm^3\ s^{-1}$) and the temperature dependant data of Garland *et al.* ($k(T) = 4.9 \pm 0.6 \exp\left(\frac{-10.0 \pm 0.4}{RT}\right) \times 10^{-11}$ $cm^3\ s^{-1}$). These workers find the reaction to be independent of pressure in the range 10–50 torr. Exothermic pathways possible in this reaction are

$$\begin{aligned} BH + O_2 &\longrightarrow HBO + O \quad \Delta H = -488\ kJ\ mol^{-1} \\ &\longrightarrow BOH + O \quad \Delta H = -274\ kJ\ mol^{-1} \\ &\longrightarrow BO + OH \quad \Delta H = -402\ kJ\ mol^{-1} \\ &\longrightarrow BO_2 + H \quad \Delta H = -502\ kJ\ mol^{-1} \\ &\longrightarrow HOBO \quad \Delta H = -996\ kJ\ mol^{-1} \end{aligned}$$

In their modelling study of diborane/O_2 flames, Shaub and Lin [54] assumed the dominant reaction pathway produces BO and OH and estimated the rate constant to be 6×10^{-14} $cm^3\ s^{-1}$. Since it was the intention of these workers to model the combustion features qualitatively, the higher value measured would not significantly affect any conclusions they formed.

BH + CO

Rice *et al.* find the reaction of BH with CO to be pressure dependent using He ($k = (3.9 \pm 0.3) \times 10^{-13}$ (10 torr), $(5.8 \pm 0.2) \times 10^{-12}$ (404 torr) $cm^3\ s^{-1}$), CF_4 and SF_6 as buffer gases. Our upper limit ($k < 1.1 \times 10^{-11}$ $cm^3\ s^{-1}$), measured in 1 torr of He, is effectively an extrapolation of their data. They assume the reaction proceeds through a HBCO complex which is stabilized by collisions with the bath gas. However, to attain agreement between the TST-RRKM type model they use

and their data for BH and BH_3 reactions with CO, which show relatively similar pressure dependences, they had to assume a B–C bond strength approximately twice that in BH_3CO for this complex. This would suggest that their model provides an inadequate description of this reaction.

BH + CH_4 and C_2H_6

Our upper limits for the reactions of BH with CH_4 and C_2H_6 are $k < 1.6 \times 10^{-12}$ and $k < 9.1 \times 10^{-13}$ cm^3 s^{-1} respectively. Both upper limits are likely to be inflated by the presence of C_2H_4 as an impurity, especially the upper limit set for C_2H_6. Obtaining sufficiently pure samples of C_2H_6 was a problem also mentioned by other workers.

3.4 Conclusions

We have measured rate constants for the reactions of BH with NO and C_2H_4 and set upper limits to the rate constants for the reactions of BH with O_2, C_2H_6, CH_4 and CO. BH was produced by laser photolysis of B_2H_6 and detected by time resolved laser-induced fluorescence. The results obtained were

BH + NO	$k = 1.26 \pm 0.07 \times 10^{-10}$ cm^3 s^{-1}
BH + C_2H_4	$k = 1.41 \pm 0.09 \times 10^{-10}$ cm^3 s^{-1}
BH + CH_4	$k < 1.6 \times 10^{-12}$ cm^3 s^{-1}
BH + C_2H_6	$k < 9.1 \times 10^{-13}$ cm^3 s^{-1}
BH + O_2	$k < 1.3 \times 10^{-13}$ cm^3 s^{-1}
BH + CO	$k < 1.1 \times 10^{-11}$ cm^3 s^{-1}

at room temperature. The reactions of BH with NO and C_2H_4 have been found to exhibit negative temperature dependences over the range 260–350K. The reaction of BH with NO also exhibits a dependence on the nature of the buffer gas used.

All measurements are in good agreement with the later measurements of Rice *et al.* [40] and Garland *et al.* [41]. In each case the results obtained have been interpreted in terms of the likely mechanism and products of reaction.

This work has been previously reported [46].

Chapter 4

Photoexcitation of Diborane and Stannane at 193 nm

4.1 Introduction

Laser Photolysis is a commonly used technique for generating gas phase free-radicals in order to study their kinetics and spectroscopy. Since the high power ultra-violet lasers used for photolysis generally deliver more energy to the radical-precursor than is needed for dissociation, analysis of prompt emission from excited photofragments can yield information about the energetics and dynamics of the fragmentation process. Work of this kind has been done to obtain information about the various photodissociation mechanisms of H_2O and ICN at 248 nm [55], acrylonitrile and acrolein at 193 nm [56,57] and ammonia and hydrazine at 193 nm [58,59,60,61]. Differences in selection rules governing transitions between states of differing geometry in absorption and emission, means that laser photolysis has considerable potential for generating new spectra.

The aim of this work was to characterize the emissions observed during the 193 nm photolyses of diborane and stannane in terms of the identity of the emitting species and the gross nature of the photodissociation processes by which they

are produced. The interest in the photodecomposition of stannane arose due to the presence of this molecule as an impurity in the initial samples of diborane we prepared by reaction of $NaBH_4$ with anhydrous $SnCl_2$ [30].

The ultra-violet photochemistry of diborane has not been extensively investigated. The ultra-violet absorption spectrum of diborane has been reported by Blum and Herzberg [62] and by Price [63] and shows two maxima, at approximately 155 and 180 nm. In the first reported investigation of the photochemical decomposition of diborane, Hirata and Gunning [64] used Hg ($^3P_1$) atoms to photosensitize the process at 253.7 nm and concluded that products they observed were consistent with

$$B_2H_6 + h\nu \longrightarrow B_2H_5 + H$$

being the primary photochemical step. Further studies of the diborane photolysis by Bufalini and Todd [65] and by Kreye and Marcus [66], both using the 184.9 nm emission of a mercury-lamp, also found that their data, primarily comprising time-dependent pressure changes and product analyses, was consistent with the initial formation of B_2H_5 and H. Postulation of the formation of BH_3 in these experiments was necessary to explain the production of B_5H_{11} although the quantum yield for the production of BH_3 was thought to be a order of magnitude less than that for the production of B_2H_5 + H. Consistently, but again without any direct evidence, Clark and Anderson [67] proposed a method for the photochemical purification of silane contaminated with species including diborane, using an ArF excimer-laser at 193 nm, and discussed the findings in terms of the photolysis initially producing B_2H_5 + H.

Direct evidence as to the identity of the primary photolysis products was first provided by the work of Irion and Kompa. From the results of a study of the photo-induced reaction of B_2H_6 with D_2, they concluded that the observed kinetics and isotopically exchanged products were consistent with BH_3 being a chain-carrier [43]. They postulated that the polymer and higher borane products observed in previous studies did implicate the presence of B_2H_5, but that B_2H_5 was formed by reaction of the secondary photolysis products of BH_3, notably BH_2 and BH, with

BH_3 and not from the photolysis of B_2H_6. The continuous-wave photolysis sources used in the previous experiments would have photolysed any BH_3 formed before it could be detected whereas the pulsed photolysis source used in Irion and Kompa's experiments did not.

Further experiments by these workers provided additional evidence for the production of BH_3 in the photolysis step. By adding PF_3 to the photolysis mixture, they were able to *trap* the BH_3 as it was produced in the form of a $BH_3 \bullet PF_3$ complex. Quantitative infra-red spectroscopy of this complex enabled them to determine the quantum yield for the production of BH_3, from the 193 nm photolysis of diborane, to be 2.00 ± 0.25 [68]. This work also confirmed their former postulate of BH_3 as a chain carrier in the 193 nm photo-induced B_2H_6/D_2 exchange.

The amount of spectroscopic information known about either BH_3 or BH_2 is limited. The infra-red diode-laser absorption study of Kawaguchi *et al.* [69] is the only observation of the gas-phase spectrum of BH_3. These workers used kinetic-spectroscopy and discharge-modulation to detect lines belonging to a Q-branch series of the ν_2 band. Similarly, the only spectrum of BH_2 reported is the $\tilde{A} \rightarrow \tilde{X}$ transition between 600 and 840 nm observed by Herzberg and Johns [70] in their flash-photolysis studies. By comparison, extensive spectra of the BH radical have been observed and many electronic states of BH have been characterised [45,71].

To date, it would seem that there is virtually nothing is known about the photochemistry of stannane at 193 nm. The vacuum ultra-violet absorption spectrum of stannane has been reported by Fernandez *et al.* [72] but these workers observed no notable absorption above 160 nm making our work the first reported above this wavelength.

4.2 Experimental

Samples of diborane and stannane (see section 2.3) were prepared according to the methods of Freeguard and Long [31] and Schaeffer and Emilius [32] respectively and

were photolysed using the output of an ArF excimer-laser at 193.3 nm. Typical pulse energies, measured by a Scientech model 364 power/energy meter, corresponded to fluences of 35 mJ cm^{-2} unfocussed and 3 J cm^{-2} at most, when focussed.

Emission spectra were observed in the first and second orders of a McPherson model 218 0.3 m monochromator and a Jarrell-Ash 0.75 m Czerny-Turner monochromator and detected by either a EMI 9558QB or an EMI 9813QA photomultiplier. Combinations of Corning glass filters were used to select the wavelength region of interest as well as to prevent interference from higher-order spectra. The two monochromators were optically-coupled to different photolysis cells; the McPherson to the photolysis cell described in chapter 3, adjacent to the photolysis region and the Jarrell-Ash to a smaller, 15 cm long glass cell with the optics reconfigured so that the focussed 193 nm radiation traversed the cell in a direction parallel to the monochromator entrance slit. With either arrangement, the emission was so weak that the best resolution attainable corresponded to a triangular slit function of *ca.* 0.08 nm.

The photomultiplier output was amplified and taken to a PAR model 160 Box-car Integrator before being digitized and stored on a DEC LSI 11/23 minicomputer. Emission lifetime measurements were made by digitizing the photomultiplier output using a LeCroy 32MHz transient recorder controlled by an IBM-clone personal computer. Discharge spectra were obtained by flowing diborane or diborane-rare-gas mixtures through either a microwave or weak tesla discharge. In these experiments the photomultiplier output was detected by a high-speed Keithley model 417 pi-coammeter and displayed on a chart-recorder.

Diborane and stannane were flowed slowly through the cells at pressures less than *ca.* 25 millitorr. All emissions observed were *prompt*, and only detected on a sub-microsecond timescale. All spectra shown here are uncorrected for the wavelength response of the photomultiplier/monochromator combination.

4.3 Results and Discussion

Process	Number of Photons	Products	Excess energy (kJ mol^{-1})	Emission maximum (nm)
1	1	$2BH_3$	454 ± 33	263 ± 18
2	1	$BH_3 + BH_2 + H$	25 ± 8	–
3	2	$BH_3 + BH_2 + H$	644 ± 33	186 ± 9
4	2	$BH_3 + BH + 2H$	296 ± 33	404 ± 44
5	2	$BH_3 + B + 3H$	-35 ± 42	–
6	2	$2BH_2 + 2H$	218 ± 33	550 ± 83
7	3	$BH_3 + B + 3H$	584 ± 42	205 ± 14
8	3	$BH_2 + BH + 3H$	488 ± 33	245 ± 17
9	3	$BH_2 + B + 4H$	157 ± 42	760 ± 200
10	3	$2BH + 4H$	140 ± 33	850 ± 200
11	4	$BH + B + 5H$	428 ± 42	280 ± 27

Table 2: Thermochemistry of the possible products from the photodissociation of diborane at 193 nm

Table 2 summarizes the thermochemistry associated with the photodissociation of diborane by 1 to 4 photons at 193 nm. Heats of formation were taken from the JANAF thermochemical tables [73] for B_2H_6, BH, B and H, from Pople *et al.* [74] for BH_2 and from Page *et al.* [75] for BH_3. Process involving the elimination of H_2 might also have been included but they are not required to account for the present observations.

The emission we observe from the photolysis of diborane comprises three distinct regions: atomic boron(I) lines at 249.7 nm and 208.9 nm with intensity proportional to the laser power *ca.* cubed; a structured region between 320 and 390 nm attributed to two bands of BH_2^*, with intensity proportional to the square of the laser power (figure 5); the BH $\tilde{A}^1\Pi \rightarrow \tilde{X}^1\Sigma$ transition [45] between 420 and 450 nm also with intensity proportional to the square of the laser power (figure 6). The power dependences given were generally found to be within 10% of their stated integral values

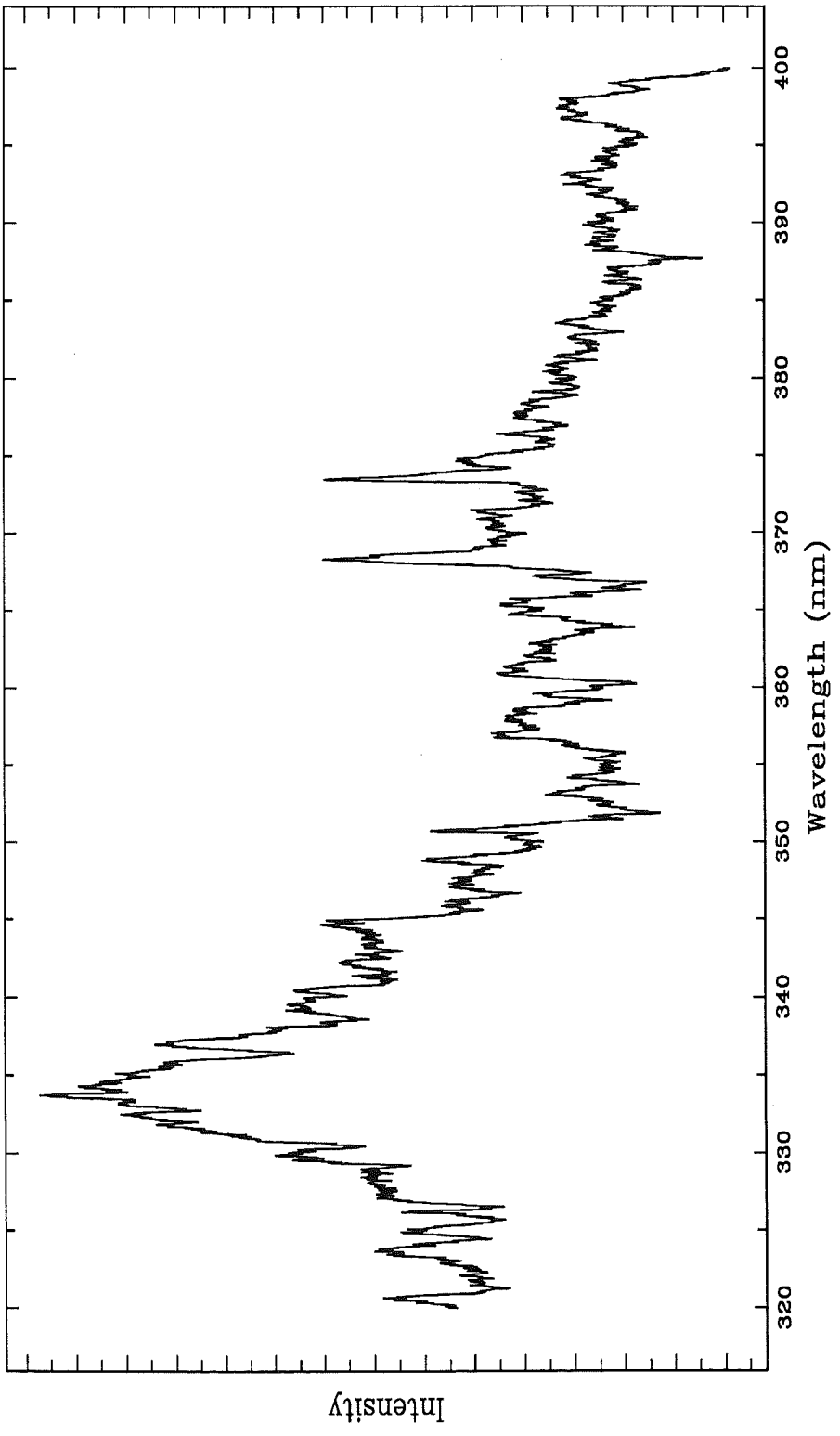

Figure 5: Emission from excited BH_2 observed during the 193 nm photolysis of diborane

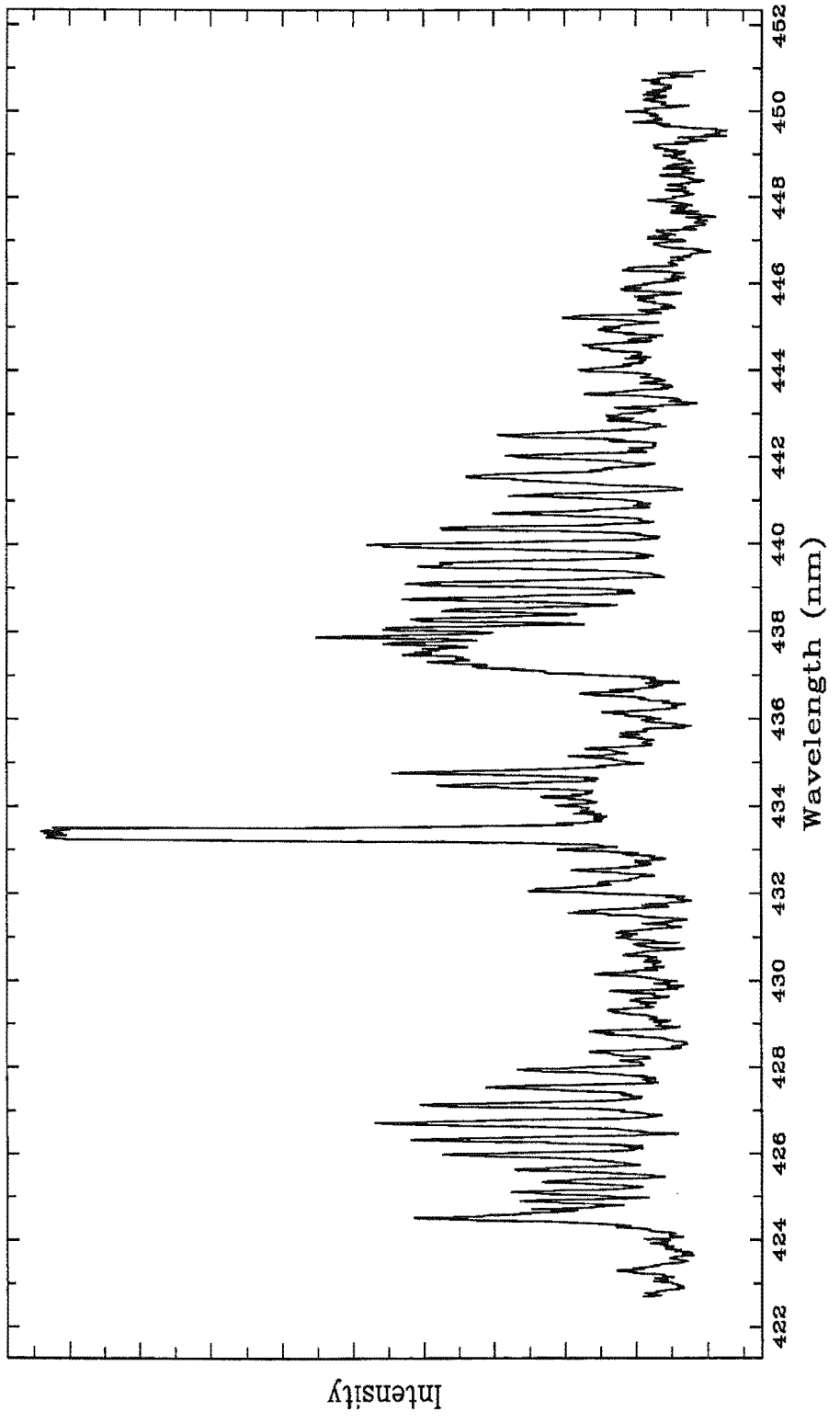

Figure 6: Emission from excited BH observed during the 193 nm photolysis of diborane

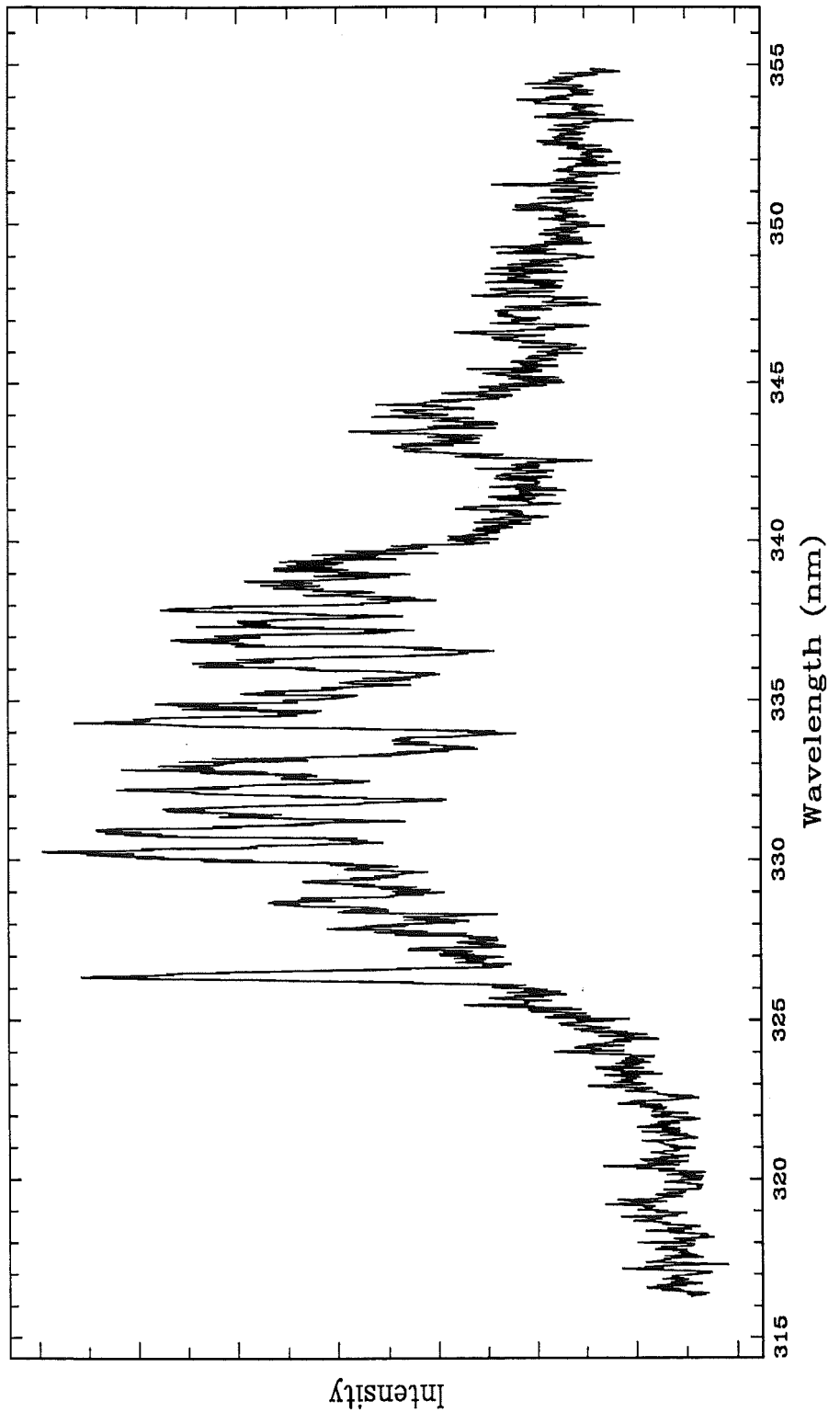

Figure 7: Expanded view of the emission from excited BH_2 in the region 320 to 345 nm. The line at 326.3 nm is from Sn(I).

and there was no appreciable variation of band shape with laser intensity.

The band lying between 320 and 345 nm, shown in figure 7, exhibits evident K-structure with peak separations averaging 52 cm^{-1} on the blue side of the apparent band origin at 334 cm^{-1} and 42 cm^{-1} on the red side. These separations, which correspond to approximately 2(A′−B′) of a prolate near-symmetric top, seem reasonable for BH_2 (A″ = 41.6 cm^{-1}, B″ ≈ C″ ≈ 6.6 cm^{-1}) but not for BH_3 (A″ = B″ = 8 cm^{-1}, C″ = 4 cm^{-1}). This band has a dependence on laser power that is consistent with the production of excited BH_2 by process 3 of table 2. Phillips [76] has simulated this band as a perpendicular transition of a near symmetric top. He found it necessary to use an extremely non-Boltzmann distribution over the initial rotational levels, restricting J′ to the range 12–32 with a rotational temperature of 1250K in this J′ range. The results qualitatively predict the band shape and subband spacings. The narrow spectral range of this band suggests that the geometries of the upper and lower states are quite similar.

The band lying between 360 and 390 nm also has an intensity proportional to the square of the laser power and on this basis it is also assigned to BH_2^*. This band has some sharp features at approximately 368 and 373 nm and like the band between 320 and 345 nm, the narrow spectral range of this band implies that the electronic transition does not involve a large change in geometry.

The observed BH $\tilde{A}\rightarrow\tilde{X}$ emission band lying between 420 and 450 nm has a power dependence consistent with production of BH ($\tilde{A}$) *via* process 4 of table 2. This band exhibits a markedly non-Boltzmann distribution indicating that dissociation to form BH* was rapid. Comparison with theoretical spectra indicates that the emitting population is both rotationally and vibrationally excited with rotational and vibrational temperatures of *ca.* 2750K. As noted by Johns *et al.* [45], the $\tilde{A}\rightarrow\tilde{X}$ emission breaks off at J′ = 26 of the (0,0) band and the (3,3) band is absent from the observed spectrum.

At high laser fluences, two atomic boron(I) transitions, $^2S \rightarrow {}^2P$ (249.7 nm) and $^2D \rightarrow {}^2P$ (208.9 nm), were observed. The production of ^2D or ^2S boron atoms

from diborane can result from the absorption of a single 193 nm photon by BH ($\tilde{A}$) or excited BH ($\tilde{X}$) or from multiphoton absorption by larger BH_n fragments. The observed power dependence is consistent with production of boron atoms *via* process 7 of table 2.

The BH_2 $\tilde{A}\rightarrow\tilde{X}$ bands [70] were not observed following laser excitation but were a prominent feature of microwave discharge spectra obtained. The low detection sensitivity above 700 nm in the laser excitation experiments means that there were possibly bands in this region we did not detect. We measure a value for the BH $\tilde{A}\rightarrow\tilde{X}$, Q_{00} emission lifetime of 540 ns which is considerably longer than the literature value of 125 ± 5 ns [77,78] and implies that the $v' = 0$ level was being repopulated by cascade processes. No emission was observed from the photolysis of diborane at 248 nm, which was attributed to the negligible single-photon absorption coefficient of diborane at this wavelength.

J″		J′		Wavelength (nm)	Intensity
0	($^3P_0$)	1	($^1P_1^o$)	254.73	≈ 1
0	($^3P_0$)	1	($^3P_1^o$)	286.42	35
1	($^3P_1$)	1	($^1P_1^o$)	266.20	0
1	($^3P_1$)	2	($^3P_2^o$)	270.73	8
1	($^3P_1$)	1	($^3P_1^o$)	301.00	33
1	($^3P_1$)	0	($^3P_0^o$)	303.50	100
2	($^3P_2$)	1	($^1P_1^o$)	279.10	0
2	($^3P_2$)	2	($^3P_2^o$)	284.08	23
2	($^3P_2$)	1	($^3P_1^o$)	317.60	86
2	($^1D_2$)	1	($^1P_1^o$)	326.33	20
2	($^1D_2$)	2	($^3P_2^o$)	333.16	≈ 10
2	($^1D_2$)	1	($^3P_1^o$)	380.21	60

Table 3: Atomic tin lines observed during the 193 nm photolysis of stannane

The atomic tin lines observed during the 193 nm photolysis of stannane are listed in table 3. The intensity of these lines is linearly proportional to the photolysis laser

power which implies they result from the absorption of a single 193 nm photon. Since the energy of the highest populated Sn(I) state is 39257.1 cm^{-1}, this leaves only 150 kJ mol^{-1} available for the dissociation of SnH_4 to products which must include gas-phase atomic tin.

By taking the enthalpy of formation of $SnH_{4(g)}$ at 0K to be 174.8 kJ mol^{-1} [79], we are forced to rule out the process

$$SnH_{4(g)} + h\nu \longrightarrow Sn_{(g)} + 4H_{(g)}$$

as a primary excitation step since ΔH_0^0 for this process is 991 kJ mol^{-1} for the production of ground state $Sn_{(g)}$. This would require more energy than is available from a single 193 nm photon. However for the process

$$SnH_{4(g)} + h\nu \longrightarrow Sn_{(g)} + 2H_{2(g)} \qquad (1)$$

we find $\Delta H_0^0 = 127.2$ kJ mol^{-1} which permits the unusual photoexcitation step

$$SnH_{4(g)} + h\nu_{193} \longrightarrow Sn_{(g)}(^1P_1^o) + 2H_{2(g)}$$

The same energy limitations require that photodissociation to give $Sn(^3P)$ follows a similar process. Similar primary processes involving the elimination of a single hydrogen molecule have been previously proposed for the photolysis of CH_4 at 123.6 nm and [80], and silane at 147 nm [81]. The low intensities of the tin lines we observe suggest that photodissociation *via* process 1 may only be a minor primary channel relative to

$$SnH_{4(g)} + h\nu_{193} \longrightarrow SnH_{2(g)} + H_{2(g)}$$

Further work is warranted to show the presence of H_2 and to determine whether SnH_2 also forms from the photodissociation process.

4.4 Conclusions

Emission observed during the 193.3 nm photolyses of stannane and diborane have been characterised and the identity of the probable emitter has been assigned, in each

case, on the basis of photolysis-laser power dependences, known thermochemistry and band structure.

The emissions observed during the photolysis of diborane, together with the probable emitter, were

320–390 nm	BH_2^* (two bands)
420–450 nm	BH $\tilde{A}^1\Pi \rightarrow \tilde{X}^1\Sigma$
208.9,249.7 nm	Boron(I) atoms

The emissions attributed to BH_2^* are new transitions.

The emissions observed during the photolysis of stannane were all assigned to known electronic transitions of atomic Sn(I).

In both cases the results obtained have been interpreted in terms of the nature of the respective photodissociation processes.

This work has been previously reported [76,82].

Chapter 5

Theoretical study of the reaction of CN with NH_3

5.1 Introduction

During the past decade, the rate at which CN-radicals react with other radicals, atoms and molecules has become of interest to an increasing number of experimental research groups (see chapter 6), for a variety of reasons. Despite these efforts, only a few theoretical studies of these systems have been reported. In conjunction with experiments, theoretical studies of the type we present here, are useful for elucidation of the mechanism(s) by which the reaction proceeds and of the likely product channels open to reactants. The results of such studies, providing information on the form and relative energetics of the potential energy surface over which the reaction occurs, can then be used in dynamical or statistical type calculations to enable prediction of the rate coefficients under experimentally inaccessible reaction conditions.

Previous *ab initio* studies have been reported for the reactions of CN with H_2 [83] and CN with HCl [84]. Rate coefficients for the reaction of CN with H_2 have been calculated using these *ab initio* results in a transition-state theory approach [85] and by using reduced-dimensionality reaction probabilities [86]. There have

been no reported theoretical studies of the reaction of CN with NH_3.

The aims of this study were to determine the mechanism by which CN reacts with NH_3 and the likely products of reaction in conjunction with the experimental studies reported in chapters 6 and 7. The mechanism of reaction in particular, is not well understood. This reaction has been shown experimentally to exhibit the characteristics normally associated with radical-radical reactions [87]. This is unexpected since the reaction of CN with NH_3 is between a radical and a neutral molecule.

Discussion of the implications of the *ab initio* results we present in relation to the experimentally determined kinetic properties and products of reaction is deferred to chapters 6 and 7 respectively. Only the characteristics and properties expected to be displayed by each possible reaction channel will be discussed here.

5.2 Principles of *ab initio* molecular orbital theory[1]

5.2.1 The potential energy surface

The course of a chemical reaction is governed by the form of the potential energy surface $U(q_i)$, over which it occurs. The potential energy surface represents the dependence of the total potential energy (U) of the system on the co-ordinates (q_i) of the constituent nuclei. For a system of N nuclei, the potential energy surface is a function of 3N–6 (3N–5 for linear systems) independent variables and is therefore a *surface* in a *space* of 3N–6 dimensions.

To determine the form of the potential energy surface it is necessary to solve the non-relativistic time-independent Schrödinger wave equation

$$\mathcal{H}\Psi = \mathcal{E}\Psi$$

[1]The content of this section is based primarily on the excellent texts by Szabo and Ostlund [19], Levine [20] and Hehre *et al.* [21].

where $\mathcal{H}$ is the Hamiltonian for a system of N nuclei and n electrons, at a number of points for each of the 3N–6 variables. For all but the smallest systems, this is currently impractical. Usually only the important features of the potential energy surface are determined such as stationary points (points where the gradient, the first derivative of U with respect q_i, is zero). Stationary points may be characterised by the eigenvalues of the force constant (second derivative of U with respect q_i) matrix or *Hessian*, as either intermediates or transition states. Intermediates are local minima which have all real eigenvalues while transition states are saddle points (first order saddle points, convex in one dimension) and have one negative eigenvalue. Knowledge of the relative energies of reactants, products, intermediates and transition states gives good insight into the possible reaction mechanism(s) and the relative importance of each.

Within the framework of the Born-Oppenheimer approximation, in which by virtue of their much smaller mass, the electrons can be considered as moving in a field of fixed nuclei, terms in the Hamiltonian corresponding to kinetic energy of the nuclei and the repulsion between the nuclei, can be ignored and considered constant respectively. Hence the Hamiltonian (in atomic units) reduces to

$$\mathcal{H} = -\sum_{i=1}^{n}\frac{1}{2}\nabla_i^2 - \sum_{i=1}^{n}\sum_{A=1}^{N}\frac{Z_A}{r_{iA}} + \sum_{i=1}^{n}\sum_{j>i}^{n}\frac{1}{r_{ij}} \qquad (2)$$

where Z_A is the atomic number of nucleus A and the Laplacian ∇_i^2 involves differentiation with respect to the co-ordinates of the ith electron. The first term in equation 2 is the operator for the kinetic energy of the electrons; the second term represents coulomb attraction between the nuclei and electrons and the third term represents repulsion between the electrons. The Hamiltonian of this form is termed the *electronic Hamiltonian* and solution of the Schrödinger wave equation

$$\mathcal{H}_{elec}\Psi = \mathcal{E}_{elec}\Psi \qquad (3)$$

yields the *electronic energy* of the system. The total energy of the system for fixed nuclei is obtained by addition of the constant term representing nuclear repulsion.

$$\mathcal{E}_{total} = \mathcal{E}_{elec} + \sum_{A=1}^{N}\sum_{B>A}^{N}\frac{Z_A Z_B}{R_{AB}}$$

where R_{AB} is the distance between nuclei A and B. Solution of equation 3 is achieved by allocating each electron to its own spin orbital and combining these into an N-electron wavefunction. Spin orbitals have dependence on both spatial and spin co-ordinates. A Slater determinant is used to give a wavefunction which is an antisymmetrised product of the spin orbitals in order to obey the antisymmetry or Pauli Exclusion principle. For a closed-shell N-electron system

$$\Psi(\mathbf{x}_1, \mathbf{x}_2, \cdots, \mathbf{x}_N) = (N!)^{-\frac{1}{2}} \begin{vmatrix} \chi_i(\mathbf{x}_1) & \chi_j(\mathbf{x}_1) & \cdots & \chi_k(\mathbf{x}_1) \\ \chi_i(\mathbf{x}_2) & \chi_j(\mathbf{x}_2) & \cdots & \chi_k(\mathbf{x}_2) \\ \vdots & \vdots & & \vdots \\ \chi_i(\mathbf{x}_N) & \chi_j(\mathbf{x}_N) & \cdots & \chi_k(\mathbf{x}_N) \end{vmatrix}$$

where $\mathbf{x}_i$ represent the space and spin co-ordinates of electron i. Slater determinants correlate the motions of electrons with the same spin while the motion of electrons with opposite spin are uncorrelated. If a single Slater determinant is used as the approximation to the true wavefunction then this is called the Hartree-Fock approximation.

5.2.2 The Hartree-Fock approximation

The simplest wave function that can be used to describe the ground state of a closed-shell N-electron system is a single Slater determinant. The best wavefunction is determined variationally to give the lowest energy, which is an upper bound to the true energy of the system. Minimization of the energy with respect to the choice of the spin orbitals leads to the Hartree-Fock equations

$$f|\chi_a\rangle = \epsilon_a|\chi_a\rangle$$

where ϵ_a is the energy of spin orbital χ_a and f is the Fock operator which represents the sum of a core Hamiltonian operator and the Hartree-Fock potential. The Hartree-Fock potential is the average potential experienced by an electron due to the presence of the other electrons and hence depends on the spin orbitals of the other electrons. The Hartree-Fock equations are thus non-linear and must be solved

iteratively. This is done using the Self-Consistent-Field procedure in which the spin orbitals are varied until those used to construct the Fock operator are also its eigenfunctions. The Hartree-Fock equations are reduced to a set of matrix equations by expansion of the spin orbitals in a set of basis functions to allow their solution for molecular species

$$\chi_i(\mathbf{r}) = \sum_{\mu=1}^{k} C_{\mu i}\phi_\mu(\mathbf{r})$$

for k basis functions.

The ground state wavefunction Ψ_0 corresponds to filling the N lowest energy spin orbitals with the N-electrons. The ground state energy is thus given by

$$\mathcal{E}_0 = \langle\Psi_0|\mathcal{H}|\Psi_0\rangle$$

Hartree Fock calculations are usually classified as either restricted or unrestricted depending on whether or not orbitals of different spin are constrained to having the same spatial form. Unrestricted determinants generally produce lower energies than restricted determinants but they are contaminated by spin states of higher multiplicity (that is, they are not eigenfunctions of the total spin operator).

The lowest energy attainable using the Hartree-Fock approximation is achieved by using a complete (infinite) basis set and is termed the Hartree-Fock limit. For the sake of computational manageability a finite basis set must be used so that energies higher than the Hartree-Fock limit generally result.

5.2.3 Post Hartree-Fock theory

The major assumptions inherent in the Hartree-Fock approximation limit it's accuracy, so that even the energy attained at the Hartree-Fock limit represents an upper bound to the *true* energy of the system. It can be shown that the exact wavefunction for the ground and excited states of an N-electron system can be written as a linear combination of all possible N-electron Slater determinants formed from a complete

set of spin orbitals. The variational determination of the wavefunction in this manner is called *configuration interaction* (CI) as each determinant represents a unique electron configuration. Determinants are referred to as N-tuply excited, relative to the ground state configuration, corresponding to the promotion of N-electrons from the occupied spin orbitals to the unoccupied spin orbitals. The lowest energy eigenvalue of the Hamiltonian is the exact ground state energy of the system within the Born-Oppenheimer approximation. The difference between the exact energy $\mathcal{E}$ and the Hartree-Fock limit energy is called the *correlation energy*

$$\mathcal{E}_{corr} = \mathcal{E} - \mathcal{E}_{HF}$$

since motion of electrons of opposite spin are uncorrelated in the Hartree-Fock approach.

An alternative multideterminantal approach to the calculation of correlation energy is to use perturbation theory. In this approach the correlation energy is calculated by including correlation effects as a perturbation $\mathcal{V}$ on the reference determinant $\mathcal{H}_0$.

$$\mathcal{H}|\Psi\rangle = (\mathcal{H}_0 + \lambda\mathcal{V})\,|\Psi\rangle = \mathcal{E}|\Psi\rangle$$

The exact ground-state energy $\mathcal{E}$ and wavefunction Ψ can then be expanded as infinite series of the form

$$\begin{aligned} \Psi &= \Psi^{(0)} + \lambda\Psi^{(1)} + \lambda^2\Psi^{(2)} + \cdots \\ \mathcal{E} &= \mathcal{E}^{(0)} + \lambda\mathcal{E}^{(1)} + \lambda^2\mathcal{E}^{(2)} + \cdots \end{aligned}$$

The energy and wavefunction are formulated by setting $\lambda = 1$ and truncating the series to various orders. The Hartree-Fock Hamiltonian is chosen as $\mathcal{H}_0$ as we are interested in obtaining a perturbation expansion of the correlation energy. This choice of Hamiltonian is known as Møller-Plesset perturbation theory and in this case the perturbation is the difference between the true interelectronic repulsion and the Hartree-Fock average interelectronic potential. Møller-Plesset perturbation theory is referred to by the highest order energy term allowed[2] so that truncation

[2]The Hartree-Fock energy represents the sum of the zeroeth and first order terms.

after third order is termed MP3. For computational manageability, terms higher than fourth order are seldom included.

Second and higher order terms in the expansion contain matrix elements of the perturbation operator involving excited determinants. In the Hamiltonian matrix, elements involving the ground state with singly-excited determinants vanish due to Brillouin's theorem while matrix elements involving the ground state with triply and higher order excited determinants vanish because the Hamiltonian contains only one and two electron terms. The result is that only doubly-excited determinants contribute to MP2 and MP3 energies while MP4 energies also have contributions from singly, triply and quadruply-excited determinants since they have non-zero matrix elements with doubly-excited determinants. MP4 calculations have the additional terminology indicating the excitations that are included so that an MP4SD calculation includes only contributions from singly and doubly-excited determinants. Triply-excited determinants are the hardest to handle computationally and consequently are sometimes excluded.

5.2.4 Basis Sets

The most commonly used basis functions for the expansion of spin orbitals are Slater functions and Gaussian functions

$$\begin{aligned} \phi_{Slater}(\zeta, r) &= N(\zeta) S \exp^{-\zeta r} \\ \phi_{Gaussian}(\alpha, r) &= N(\alpha) G \exp^{-\alpha r^2} \end{aligned}$$

where N is a normalization factor, α and ζ are Gaussian and Slater exponents respectively, and r is the distance from the centre of the function. G and S specify the type (s, p, d, ...) of Gaussian or Slater function as a dependence on the cartesian co-ordinates x, y and z. Slater functions better represent atomic orbitals than do Gaussian functions, mainly due to the failure of Gaussian functions to give the desired *cusp* at the origin and so require fewer terms for a representation of comparable quality. Gaussian functions however provide for more efficient evaluation of

integrals and can be evaluated explicitly without recourse to numerical integration, which increases accuracy. By use of a basis set in which each basis function is a fixed linear-combination (contraction) of Gaussian functions (primitives), approximation of functions with the desired qualities can be attained while retaining rapid integral evaluation.

The simplest basis set is one which comprises the number of functions required to accommodate all of the electrons of the atom while maintaining overall spherical symmetry and is called a *minimal* basis set. Minimal basis sets are useful for calculations on large molecules where large amounts of computation must be done but can only be used for the prediction of chemical properties in a qualitative manner. The most commonly used minimal basis set is the STO-3G basis set in which three primitive Gaussians are contracted for each basis function to approximate a Slater type orbital.

The minimal basis set may be improved by using two basis functions for each minimal basis function. The resulting *double-zeta* basis set is capable of allowing for anisotropic effects within the molecule. A further improvement is achieved by using a *split-valence* basis set in which the valence region of the molecule is represented by two basis functions. The chemical properties of a molecule are generally dominated by valence shell electrons. Use of a split valence basis set in which the valence region is separated into inner and outer regions, described by separate basis functions, allows for greater flexibility in the optimization of the molecular orbitals and so a better description of these properties.

Allowance for the effects of anisotropic charge distribution experienced by an atom in a molecule can be accounted for by the addition of polarization functions to the basis set, generally as a set of d-type functions for non-hydrogen atoms and p-type functions for hydrogen. It has been empirically determined that addition of d-functions to heavy atoms is more important than adding p-functions to hydrogen. The basis set used in this study, the 6-31G* is an example of a split-valence basis set with a set of d-type polarization functions on the non-hydrogen atoms. A good description of the inner shell electrons by the basis set is also important, since

although inner shell electrons generally contribute little to the chemical properties of the molecule, they do contribute to the electronic energy. The criterion of energy minimization may otherwise cause valence functions to be *borrowed* by the inner shell to lower the electronic energy, to the detriment of the representation of the valence shell and thus the description of the bonding and molecular properties of the molecule.

5.3 Details of Calculations

The geometries of species conceivably involved in the reaction of CN with NH_3 were optimised at the HF and, in certain cases, the MP2 levels of theory. Harmonic vibrational frequencies, MP4SDQ and QCISD(T) energies were calculated using these geometries. All calculations were done with a 6-31G* basis set using either Gaussian82 [88] or Gaussian90 [89].

5.4 Results and Discussion

The geometries of species conceivably involved in the reaction of CN with NH_3, optimized at the HF/6–31G* level of theory, are summarized in table 4, over the following four pages, in standard Z-matrix format. The rows of values in {braces} are MP2 geometries. In tables defining multiple structures, Z_x refers to the ordering of atoms for that structure while distances and angles should be read from the first line before the second line for each species.

To ensure that these tables are interpreted correctly, let us consider the structure of the transition-state species TS_4 as an example. The Z-matrix defining the structure of this species has an ordering of atoms listed under Z_1; Z_2–Z_5 should be ignored in this case. The bond distances and angles are then read from the table first line before second line for each *group* of parameters. In this case the HF values

are: $r_1 = 1.18$, $r_2 = 1.44$, $r_3 = 1.34$, $r_4 = 1.00$, $r_5 = 1.00$; $\angle_1 = 121.7$, $\angle_2 = 67.5$, $\angle_3 = 115.9$, $\angle_4 = 116.9$; and $\phi_1 = 180.0$, $\phi_2 = 187.9$, $\phi_3 = -23.3$, $\phi_4 = 196.9$ For this species an MP2 geometry has been calculated. The MP2 values are: $r_1 = 1.18$, $r_2 = 1.44$, $r_3 = 1.34$, $r_4 = 1.02$, $r_5 = 1.01$; $\angle_1 = 121.4$, $\angle_2 = 78.0$, $\angle_3 = 116.5$, $\angle_4 = 117.1$; and $\phi_1 = 180.0$, $\phi_2 = 172.1$, $\phi_3 = -23.2$, $\phi_4 = 196.2$.

Transition state species are labelled TS_x, while intermediates, reactants and products are labelled according to their connectivity of atoms. TS_9 and TS_{10} are most likely torsional transition states of the intermediate species.

Species	Geometry r_x(Å) $\angle_x, \phi_x$ (deg)					
CN	r_{CN}	1.16 {1.13}				
NH	r_{NH}	1.02				
N_2	r_{NN}	1.08				
CH_2 ($^3B_1$)	r_{CH}	1.07	$\angle_{HCH}$	130.8		
CH_2 ($^1A_1$)	r_{CH}	1.10	$\angle_{HCH}$	103.3		
NH_2	r_{NH}	1.01	$\angle_{HNH}$	104.4		
N_2H	r_{NN}	1.18	r_{NH}	1.03	$\angle_{NNH}$	113.0
HCN	r_{CH}	1.06	r_{CN}	1.13	$\angle_{HCN}$	180.0
HNC	r_{HN}	0.99	r_{NC}	1.15	$\angle_{HNC}$	180.0
CH_3	r_{CH}	1.07	$\angle_{HCH}$	120.0	ϕ_{HCHH}	180.0
NH_3	r_{NH}	1.00	$\angle_{HNH}$	107.2	ϕ_{HNHH}	114.8
		{1.02		106.4		113.1}
H_2CN	r_{HC}	1.08	r_{CN}	1.26	$\angle_{HCN}$	120.8
	ϕ_{HCNH}	180.0				
cis HCNH	r_{HC}	1.08	r_{CN}	1.23	r_{NH}	1.01
	$\angle_{HCN}$	133.8	$\angle_{CNH}$	115.2	ϕ_{HCNH}	0.0
trans HCNH	r_{HC}	1.08	r_{CN}	1.23	r_{NH}	1.01
	$\angle_{HCN}$	126.9	$\angle_{CNH}$	114.5	ϕ_{HCNH}	180.0

Z_1	Z_2	Z_3	Z_4	Z_5		r_x		$\angle_x$		ϕ_x
C	N	N	H	H						
N	N	C	N	C	1	r_1				
X	X	X	X	X	1	1.0	2	90.0		
X	X	X	X	X	2	1.0	1	90.0	3	0.0
H	H	H	C	N	2	r_2	4	$\angle_1$	1	ϕ_1
N	C	N	N	N	1	r_3	3	$\angle_2$	2	ϕ_2
H	H	H	H	H	6	r_4	1	$\angle_3$	3	ϕ_3
H	H	H	H	H	6	r_5	1	$\angle_4$	3	ϕ_4

Species	Z_x	r_1,r_2,r_3,r_4,r_5 (Å)			$\angle_1$,$\angle_2$,$\angle_3$,$\angle_4$ (deg)		ϕ_1,ϕ_2,ϕ_3,ϕ_4 (deg)	
HHNHNC	4	1.00	1.15	2.00	90.2	90.6	180.0	180.0
		1.01	1.01		127.0	127.0	91.2	−91.2
HHNHCN	5	1.07	1.13	2.21	90.0	90.6	180.0	180.0
		1.01	1.01		127.4	127.4	91.0	−91.0
cis	1	1.23	1.01	1.36	26.6	47.2	187.7	177.5
H_2NCNH		1.00	1.00		116.6	117.4	192.4	−27.0
trans	1	1.24	1.00	1.35	25.2	139.7	184.3	187.5
H_2NCNH		1.00	1.00		116.6	117.2	185.6	−31.9
TS_2	4	1.56	1.17	1.07	151.8	140.5	180.0	180.0
		1.00	1.00		115.9	115.9	110.4	−110.4
TS_3	5	1.54	1.15	1.09	83.5	132.6	180.0	180.0
		1.01	1.01		107.6	107.6	121.8	−121.8
TS_4	1	1.18	1.44	1.34	121.7	67.5	180.0	187.9
		1.00	1.00		115.9	116.9	−23.3	196.9
		{1.18	1.44	1.34	121.4	78.0	180.0	172.1
		1.02	1.01		116.5	117.1	−23.2	196.2}
TS_5	1	1.19	1.00	1.91	107.4	109.6	132.9	234.5
		1.01	1.01		99.4	99.5	228.4	−25.0
		{1.19	1.00	1.99	100.8	111.6	157.1	232.3
		1.03	1.03		95.8	96.0	230.7	−26.0}
TS_6	1	1.24	1.02	1.31	25.5	92.2	182.9	180.1
		1.00	1.00		121.7	122.2	178.5	−1.5
TS_9	2	1.28	1.01	1.24	162.5	81.9	180.0	180.0
		1.08	1.08		121.5	121.5	90.7	−90.7
TS_{10}	3	1.24	1.08	1.44	36.5	150.5	180.0	180.0
		1.00	1.00		107.5	107.5	122.8	−122.8

Z_1	Z_2		r_x		$\angle_x$		ϕ_x
C	N						
N	C	1	r_1				
H	H	1	r_2	2	$\angle_1$		
N	N	1	r_3	2	$\angle_2$	3	ϕ_1
H	H	4	r_4	1	$\angle_3$	3	ϕ_2
H	H	4	r_5	1	$\angle_4$	3	ϕ_3

Species	Z_x	r_1,r_2,r_3,r_4,r_5 (Å)			$\angle_1$,$\angle_2$,$\angle_3$,$\angle_4$ (deg)		ϕ_1,ϕ_2,ϕ_3 (deg)		
H_2NHCN	1	1.26	1.08	1.38	119.0	125.5	176.9	−33.7	193.6
		1.00	1.00		115.0	114.6			
TS_7	1	1.17	1.83	1.35	102.9	98.9	177.4	−24.8	200.8
		1.00	1.00		114.0	115.7			
		{1.17	1.63	1.36	102.8	97.7	176.9	−25.8	201.4
		1.01	1.01		112.8	115.5}			
TS_8	1	1.18	1.06	1.96	111.8	147.3	180.0	126.8	−126.8
		1.01	1.01		98.9	98.9			
H_2NHNC	2	1.29	1.00	1.42	122.7	125.7	180.0	121.9	121.9
		1.00	1.00		107.9	107.9			

HN_2CH_2							HNCHNH						
C							C						
N	1	1.42					N	1	1.32				
N	2	1.39	1	60.4			H	2	1.01	1	110.7		
H	3	1.00	1	110.5	2	250.9	H	1	1.08	2	122.0	3	0.0
H	1	1.08	3	118.7	2	−104.2	N	1	1.33	2	121.6	4	180.0
H	1	1.08	3	115.4	2	112.1	H	5	1.01	1	108.1	4	180.0

Z_1	Z_2	Z_3		r_x		$\angle_x$		ϕ_x
C	N	C						
N	N	N	1	r_1				
N	C	N	1	r_2	2	$\angle_1$		
H	H	X	3	r_3	1	$\angle_2$	2	ϕ_1
H	H	H	3	r_4	1	$\angle_3$	2	ϕ_2
H	H	H	3	r_5	1	$\angle_4$	2	ϕ_3

Species	Z_x	r_1,r_2,r_3,r_4,r_5 (Å)			$\angle_1$,$\angle_2$,$\angle_3$,$\angle_4$ (deg)		ϕ_1,ϕ_2,ϕ_3 (deg)		
H_3NCN	1	1.16	2.35	1.00	180.0	109.8	0.0	120.0	−120.0
		1.00	1.00		109.8	109.8			
		{1.14	2.16	1.01	180.0	105.8	0.0	120.0	−120.0
		1.01	1.01		105.8	105.8}			
TS_1	1	1.16	1.45	1.30	142.6	129.5	−0.1	122.1	−122.0
		1.01	1.01		108.1	108.1			
CH_3N_2	2	1.18	1.49	1.08	118.3	108.9	0.0	120.8	−120.8
		1.08	1.08		108.9	108.9			
H_2NCN	3	1.14	1.34	1.00	178.2	90.0	0.0	113.6	−113.6
		1.00	1.00		114.5	114.5			

HCN_2H_2						
N						
N	1	1.51				
N	1	1.32	2	62.5		
H	3	1.09	1	126.9	2	107.2
H	2	1.00	1	113.7	3	−114.3
H	2	1.00	1	117.0	3	107.2

Table 4: Optimized Hartree-Fock and MP2 geometries

Species		−HF//HF	−MP4SDQ//HF	−MP4SDQ//MP2	ZPVE
	H	0.49823	0.49823	0.49823	
$(^3\Sigma)$	NH	54.95943	55.07668		21.1
$(^1\Sigma_g)$	N_2	108.94395	109.25323		16.5
$(^2B_1)$	NH_2	55.55770	55.70801		54.0
$(^2A')$	N_2H	109.42540	109.72814		37.0
$(^2B_2)$	H_2CN	93.43231	93.69658		70.1
$(^2A')$	*cis* HCNH	93.39296	93.66992		70.8
$(^2A')$	*trans* HCNH	93.39875	93.67926		72.6
$(^3B_1)$	CH_2	38.92150	39.01990		48.4
$(^1A_1)$	CH_2	38.87237	38.99199		47.2
	NH_3	56.18436	56.36828	56.36894 {56.37210}	97.2
	CH_3	39.55899	39.68759		81.3
$(^2\Sigma)$	CN	92.20483	92.45165	92.45154 {92.48100}	11.9
$(^1\Sigma)$	HNC	92.85533	93.13711		44.8
$(^1\Sigma)$	HCN	92.87520	93.15973		47.2
	NH_3 + CN	148.38919	148.81993	148.82048 {148.85309}	109.1
	H_2NCN	147.90866	148.36089		97.2
	CH_3N_2	148.46201	148.90581		121.8
	HNCHNH	148.46452	148.89329		124.1
	HN_2CH_2	148.40203	148.83625		128.2
	HCN_2H_2	148.33630	148.79398		127.1
	H_2NHNC	148.36843	148.80955		128.1
	H_3NCN	148.39970	148.84083	148.84367 {148.86940}	115.8
	HHNHNC	148.42681	148.86105		108.1
	cis H_2NCNH	148.43537	148.88253		123.8
	HHNHCN	148.44280	148.88263		108.3
	H_2NHCN	148.46726	148.90307		125.9
	trans H_2NCNH	148.44412	148.89416		125.8

Species		−HF//HF	−MP4SDQ//HF	−MP4SDQ//MP2	ZPVE
	TS_1	148.33274	148.80557		104.8
	TS_2	148.36319	148.81372		107.1
	TS_3	148.37265	148.82743		101.6
	TS_4	148.38240	148.83249	148.83462 {148.85665}	99.1
	TS_5	148.38825	148.83593	148.83660	112.0
	TS_6	148.40229	148.85436		117.8
	TS_7	148.39037	148.83878	148.83928	100.3
$(^2A')$	TS_8	148.41344	148.85192		110.0
	TS_9	148.38204	148.83354		115.6
	TS_{10}	148.37786	148.82571		121.2

Table 5: Calculated HF//HF, MP4SDQ//HF, MP4SDQ//MP2 and QCISD(T)//MP2 {in braces} energies (hartree[3]) and zero-point vibrational energy (kJ mol^{-1})

As can be seen from table 4, a number of the calculated geometries contain *stretched* bonds. It has been noted that fourth-order unrestricted Møller-Plesset energies, which include contributions from triple substitutions show poor results for geometries of this kind due to slow convergence of the unrestricted Møller-Plesset series [90]. Overestimation of the effects of triple substitutions in the MP4 energy has also been noted to occur for unsaturated radicals, such as cyano, and in some molecules which contain multiple bonds [91,92]. As a result of this we have only calculated MP4 energies at the MP4SDQ level rather than at the MP4SDTQ level.

For species which warranted higher level calculations, QCISD(T)//MP2 energies were calculated. The QCISD(T) method [93] is known to give energies close to the full-CI results, particularly for geometries close to equilibrium, however since the relative computational time for a QCISD(T) energy calculation is several days compared to several hours for an MP4SDQ energy calculation, QCISD(T) energies were only calculated for species corresponding to important features of the potential

[3] 1 Hartree = 2625.502 kJ mol^{-1}

energy surface. Energies other than the MP4SDQ//HF will be referred to specifically in the text. All energies are uncorrected for zero-point vibrational energy unless otherwise stated.

The HF/6–31G*//HF/6–31G*, MP4SDQ/6–31G*//HF/6–31G* and zero-point vibrational energies of these species are given in table 5 together with MP4SDQ/6–31G*//MP2/6–31G* and QCISD(T)/6–31G*//MP2/6–31G* energies for species for which they were calculated. The important points to notice from this table are that the MP4SDQ//HF energy of CN is *lower* that the MP4SDQ//MP2 energy and that the transition-state species TS_3 has a relative energy above the energy of the reactants at the HF//HF level but below the energy of the reactants at the MP4SDQ//HF level. The relative energetics of TS_3 will be further discussed later. The apparent discrepancy in the CN energies indicates that the partial inclusion of correlation energy in the optimization (MP2 level) does not represent the correlation effects in this species very well. As a result of this, the energies quoted relative to reactants at the MP4SDQ//MP2 level probably overestimate the true energy differences slightly. The MP4SDQ//MP4SDQ energy of this species is only *ca.* 1 kJ mol^{-1} below the MP4SDQ//HF energy indicating this overestimation at the MP4SDQ//MP2 level will be small.

The thermochemistry of the possible products channels from this reaction are summarized below where it can be seen that there are four exoergic sets of products. The quoted energies include a scaled (see below) correction for zero-point vibrational energy. The relative energies of species on pathways to exoergic products, with the exception of $N_2 + CH_3$, are plotted in figure 8. The energies plotted in this figure are uncorrected for zero-point vibrational energy.

$$
\begin{aligned}
NH_3 + CN &\longrightarrow N_2H + CH_2\,(^1A_1) && \Delta E = 239.9 \text{ kJ mol}^{-1} \\
&\longrightarrow N_2H + CH_2\,(^3B_1) && \Delta E = 167.7 \text{ kJ mol}^{-1} \\
&\longrightarrow NH + \textit{cis}\ HCNH && \Delta E = 177.2 \text{ kJ mol}^{-1} \\
&\longrightarrow NH + \textit{trans}\ HCNH && \Delta E = 154.3 \text{ kJ mol}^{-1} \\
&\longrightarrow NH + H_2CN && \Delta E = 106.6 \text{ kJ mol}^{-1}
\end{aligned}
$$

$$\longrightarrow \quad NH_2 + HNC \quad \Delta E = -75.4 \text{ kJ mol}^{-1}$$
$$\longrightarrow \quad H_2NCN + H \quad \Delta E = -125.3 \text{ kJ mol}^{-1}$$
$$\longrightarrow \quad NH_2 + HCN \quad \Delta E = -162.4 \text{ kJ mol}^{-1}$$
$$\longrightarrow \quad N_2 + CH_3 \quad \Delta E = -327.5 \text{ kJ mol}^{-1}$$

Additional calculations done on the reactants NH_3 and CN and the products NH_2, HNC and HCN following the G-1 procedure[4] show some important results. The first is that at this level of theory, which has been shown to give energies close to experimentally determined ones [94], the exoergicities of reaction to form NH_2 + HNC and NH_2 + HCN are reduced to 26.4 and 88.0 kJ mol^{-1} respectively. Secondly, a significant contribution to the G-1 energy (*ca.* 0.05 hartree) arises from the inclusion of higher polarization functions (*2df*) in the basis set. This suggest that a larger basis set, which includes higher polarization functions on the non-hydrogen atoms, would improve the accuracy of the results obtained for all species. Such a basis set would stabilize species with stretched bonds more than other species. Higher level optimizations for all species would also increase accuracy, however higher level calculations using bigger basis sets for such a *large* system as this, would place impractical demands on both computer CPU time and disk-storage space.

The harmonic vibrational frequencies calculated for all species are given in table 6. In an extensive study, DeFrees and McLean [95] have shown that calculated HF/6–31G* vibrational frequencies generally overestimate the corresponding experimentally determined anharmonic ones by *ca.* 12%. These workers conclude that the application of an empirical scaling factor of 0.89 results in a mean error of only 49 cm^{-1}. The vibrational frequencies and zero-point vibrational energies quoted are unscaled.

Reaction of CN with NH_3 can result in the initial formation of four possible complexes depending on their relative orientations. Of these, we were able to optimize structures for those resulting from orientation of the C or N end of CN toward the

[4]These calculations were done as part of a study of the HNC⇌HCN equilibrium in conjunction with the experimental determination of the products of reaction in chapter 7.

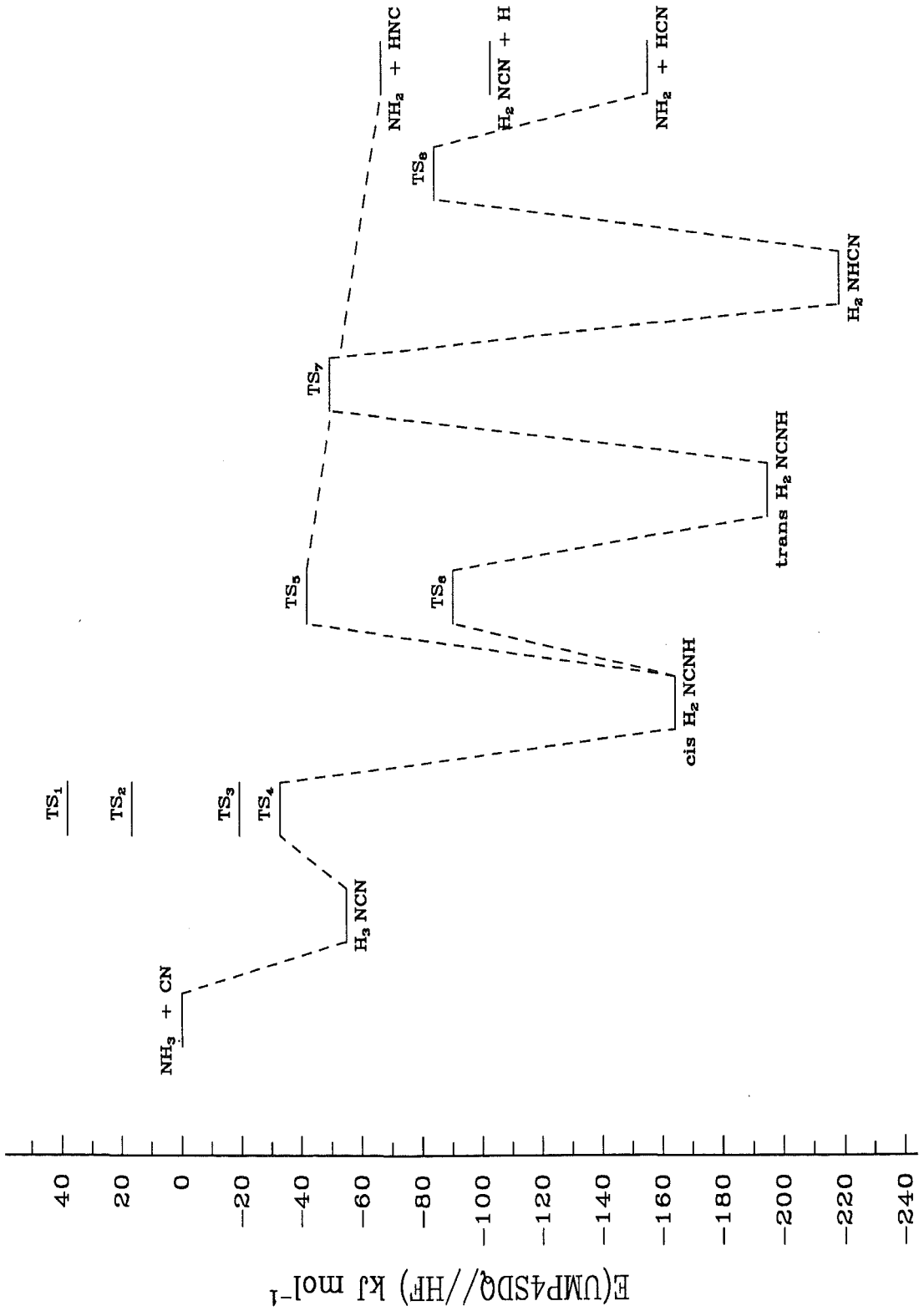

Figure 8: Relative energies of species conceivably involved in the reaction of CN with NH_3

Species	Harmonic Vibrational Frequencies (cm^{-1})					
CN	σ 1982					
NH	σ 3528					
N_2	σ_g 2758					
CH_2 ($^3B_1$)	A_1 1238	A_1 3327	B_2 3527			
CH_2 ($^1A_1$)	A_1 1567	A_1 3151	B_2 3177			
NH_2	A_1 1710	A_1 3606	B_2 3707			
N_2H	A′ 1264	A′ 1661	A′ 3276			
HCN	π 889	σ 2438	σ 3679			
HNC	π 541	σ 2309	σ 4094			
CH_3	A_2'' 307	E′ 1540	A_1' 3285	E′ 3461		
NH_3	A_1 1208	E 1849	A_1 3690	E 3823		
H_2CN	B_1 1033	B_2 1073	A_1 1436	A_1 1639	A_1 3234	B_2 3319
cis HCNH	A′ 1013	A″ 1063	A′ 1267	A′ 1664	A′ 3250	A′ 3582
trans HCNH	A′ 1033	A″ 1100	A′ 1332	A′ 1701	A′ 3295	A′ 3678
H_3NCN	E 66	182	E 369	1170	E 1827	2056
	3709	E 3857				
trans H_2NCNH	375	495	540	755	1092	1185
	1397	1788	1933	3771	3776	3922
HHNHNC	120	131	197	275	390	867
	871	1706	2314	3643	3744	3818
HHNHCN	107	120	155	252	365	1021
	1022	1708	2422	3560	3634	3734
H_2NCN	461	532	691	1159	1324	1805
	2603	3788	3891			
cis H_2NCNH	334	480	534	780	1044	1153
	1344	1801	1965	3598	3764	3904
H_2NHCN	376	555	694	977	1154	1298
	1416	1766	1825	3293	3789	3898
HCN_2H_2	667	841	948	1016	1106	1141
	1255	1589	1826	3200	3764	3888
H_2NHNC	154	560	701	1010	1232	1440
	1509	1624	1849	3734	3768	3830
CH_3N_2	180	505	912	1147	1243	1543
	1622	1628	1690	3235	3328	3330
HNCHNH	611	656	848	1077	1197	1234
	1299	1510	1592	3329	3685	3715

Species	Harmonic Vibrational Frequencies (cm^{-1})					
HN_2CH_2	866	982	1055	1101	1242	1298
	1365	1430	1669	3299	3394	3736
TS_1	3051i	300	327	679	1010	1011
	1441	1466	1754	2010	3716	3810
TS_2	651i	155	208	401	448	851
	1657	1707	2242	2630	3736	3866
TS_3	1904i	163	179	329	594	983
	1630	1632	1822	2147	3702	3809
TS_4	1336i	307	331	509	633	718
	1144	1288	1801	2168	3774	3899
TS_5	645i	172	339	619	663	886
	941	1726	2102	3649	3750	3884
TS_6	856i	194	525	670	1111	1130
	1210	1816	2077	3407	3727	3822
TS_7	1048i	279	528	535	617	667
	1130	1297	1808	2206	3793	3906
TS_8	697i	132	333	727	867	902
	975	1723	1798	3540	3651	3754
TS_9	576i	371	406	1073	1116	1247
	1339	1662	1899	3206	3282	3681
TS_{10}	446i	462	809	965	1189	1241
	1408	1573	1796	3355	3685	3787

Table 6: Calculated Hartree-Fock harmonic vibrational frequencies

H (H_3) end of NH_3 (H_2NHCN and H_2NHNC respectively) and from orientation of the C end of CN toward the N end of NH_3 (H_3NCN). The formation of H_3NCN and H_2NHNC would be favoured by dipole-dipole forces. We were unable to optimize a structure resulting from collision with the N end of CN oriented towards the N end of NH_3. Our closest approximation to this structure has a energy only 4 kJ mol^{-1} below the energy of the reactants and 4.5 kJ mol^{-1} higher in energy than the reactants with the inclusion of zero-point vibrational energies. A normal co-ordinate analysis of this structure shows that it possesses two imaginary vibrations meaning it is neither an intermediate or transition-state species. All other collision complexes optimized are stable relative to the energy of the reactants.

The formation of the H_2NHNC intermediate proceeds over a barrier lying 16 kJ mol^{-1} higher in energy than the reactants. As a result of this barrier, the rate constant for reaction *via* this pathway would be expected to exhibit a positive temperature dependence. The H_2NHNC intermediate has a geometry essentially consisting of an NH_2 and a HNC molecule connected by a long bond which suggests that this pathway is a direct H-abstraction mechanism. At the Hartree-Fock level of theory, formation of the H_2NHCN complex proceeds over a barrier lying 43.4 kJ mol^{-1} higher in energy than the reactants and like H_2NHNC, this species has a geometry essentially consisting of an NH_2 and a HCN molecule connected by a long bond suggesting a H-abstraction mechanism. Inclusion of correlation energy lowers the energy of this species to below that of the reactants however all attempts to optimize this structure at the MP2 level failed. The reasons for this are unclear, but preliminary indications from the MP2 optimizations suggest that the MP2 geometry would be significantly different from the HF geometry. Therefore the accuracy of the MP4SDQ//HF energies is questionable and we believe the Hartree-Fock energy better represents the relative energetics of this species than does the MP4SDQ energy. Both of these species have barrierless pathways to products HNC + NH_2 and HCN + NH_2 respectively.

The H_3NCN intermediate has no barriers to formation and has possible pathways involving dissociation of a H atom or 1,3 migration of a H atom available to it. Our results show that the barrier to H dissociation, to form H_2NCN and H, lies 37.7 kJ mol^{-1} above the energy of the reactants. The rate constant for reaction *via* this mechanism would therefore be expected to display a positive dependence on temperature, that is increase as the temperature is increased. The barrier to migration of H from N to N′ proceeds over a barrier 21.9 kJ mol^{-1} above the energy of the H_3NCN intermediate and 33.0 kJ mol^{-1} *below* the energy of the reactants. At the MP4SDQ//MP2 and QCISD(T)//MP2 levels of theory this barrier lies 23.7 and 33.5 kJ mol^{-1} above the energy of the H_3NCN intermediate and 37.7 and 9.3 kJ mol^{-1} below the energy of the reactants respectively. The true energetics of this barrier is likely to be better represented by the QCISD(T) energy than the MP4SDQ energies.

A *secondary* barrier of this form on the potential-energy surface is the origin of a reaction rate constant displaying a *negative* dependance on temperature. As the temperature is raised the number of states with sufficient energy to redissociate to reactants increases relative to the number of states with sufficient energy for H-migration. The effect of this is that the apparent rate of disappearance of reactants decreases as the temperature is raised.

Following H-migration, the *cis*-form of the H_2NCNH intermediate has pathways involving isomerism to the *trans*-form or dissociation to products NH_2 and HNC available to it. This intermediate is very assymetric indicating that considerable contortion of the molecular skeleton occurred during the H-transfer process. Our results show the barrier to dissociation to products is 48.4 kJ mol^{-1} higher in energy than the barrier to isomerism. From the *trans* H_2NCNH intermediate, further rearrangement involving migration of the same H atom from N′ to C leads to the products NH_2 and HCN. The results of the G-1 calculations mentioned earlier, which showed that the exoergicities of reaction to form NH_2 and HCN or NH_2 and HNC to be considerably less than those calculated at the MP4SDQ//HF level, suggest that more extensive calculations, at higher levels of theory and with bigger basis sets, may show the pathway to formation of NH_2 + HNC to be less favoured than the pathway to formation of NH_2 + HCN.

Reaction *via* this mechanisms would be expected to proceed at a rate controlled by the relative rates of passage across the secondary barrier and on to products and of dissociation back to reactants. The form of this potential energy surface is similar to that thought to be characteristic of a radical-radical association reaction where the collision complex rearranges *via* a four-centre transition state to yield products [96]. This is a somewhat surprising similarity since this is a reaction between a radical and a neutral molecule.

5.5 Conclusions

The methods of *ab initio* molecular orbital theory have been used to calculate the structures and relative energies of species conceivably involved in the reaction of CN with NH_3. Geometries of these species were optimised at the Hartree-Fock and levels of theory with energies calculated at the MP4SDQ//HF, MP4SDQ//MP2 and QCISD(T)//MP2 levels.

The results show that there are four energy allowed sets of reaction products possible; namely NH_2 + HNC, H_2NCN + H, NH_2 + HCN and N_2 + CH_3 in order of increasing exoergicity. Complete mechanistic pathways to all sets of products, with the exception of N_2 + CH_3, have been found. Initial collision complexes on the pathways to the formation of all other sets of exoergic products are all stable relative to the energy of the reactants.

Barriers to reaction lying on the pathways to formation of HNC + NH_2 and HCN + NH_2 *via* direct H-abstraction mechanisms, and H_2NCN + H means that the rate constants for reaction *via* these pathways would be expected to display positive temperature dependences. A *secondary* barrier to reaction lying on a separate pathway to the formation of NH_2 + HCN and/or HNC indicates that the rate constant for reaction *via* this mechanism would display a negative temperature dependence.

The accuracy and limitations of the methods used in relation to the results obtained has been discussed.

A paper based on this work is in preparation [97].

Chapter 6

Kinetics of reactions of CN with NH_3 and ND_3

6.1 Introduction

The cyanogen radical (CN) is known to be an important species in a wide range of chemical systems. It is one of the most abundant and widely distributed of interstellar molecules, its electronic and rotational emissions having been observed with high spatial resolution over a large number of interstellar regions, originating from numerous astronomical sources [98,99,100] including stars, cometary coma and dust and molecular clouds. It is thought to be an important intermediate in processes controlling the nitrogen balance in planetary atmospheres [101] and interstellar clouds [102]. Electronic and vibrational CN emissions have also been of interest due to the possibility of laser action. Gain coefficients and quenching behaviours of emissions from excited CN molecules have been measured [103] to determine the viability of development of a CN chemical-laser.

CN-radicals are commonly observed transient species in flames [104,105] and are thought to play an important part in processes controlling the production of the pollutant NO from hydrocarbon flames [106] and from flames doped with nitrogen

compounds [107]. Studies have demonstrated that although the organically bound fuel-N is initially converted to HCN, the large increase in production of NO observed from hydrocarbon flames doped with nitrogenous fuels [108] has a rate determining step consistent with the reaction [107,109]

$$CN + OH \longrightarrow NCO + H$$

To understand the complex chemistry occurring in many practical chemical systems such as these, computer modelling is necessary. In order for these models to be accurate, knowledge of the rate coefficients of many component reactions over wide ranges of reaction conditions are required. Such information is vital if these models are to be used predictively, as done by Herbst and Klemperer [110] to predict the observed correlation [111] between the abundances of CN and CO in interstellar clouds. Towards this end, a number of studies of the rate of reactions of cyanogen radicals with species known to be present and thought to be important in such systems have been undertaken (table 7).

The data in these tables represents work done in the area of CN-radical kinetics during the past decade. The rate coefficient listed is either a generally agreed upon value or an intermediate value where a spread of rata constants have been reported. Where possible results showing the dependence of the rate constant on temperature and/or vibrational excitation of CN are quoted. The temperature range and data listed are taken from the first reference cited. Of all the studies undertaken, the reactions of CN with O_2 [87,113,117,123,124,125,128,135,136,138,139,140,141] and H_2 [86,113,114,117,118,123,124,139,141] have received the most attention. Both reactions have been studied over wide temperature ranges extending down to temperatures found in *warm* interstellar clouds in the case of CN + O_2. The now well established room-temperature rate constant for this reaction has been used as a benchmark value in many studies.

In this study we report room temperature rate coefficients for the reactions of CN-radicals with NH_3 and ND_3. To date, four previous measurements of the rate

Species	Temp (K)	Rate coefficient ($cm^3\ s^{-1}$)	Ref
O_2	99-716	$2.49 \pm 0.02 \left(\frac{T}{298}\right)^{-0.5\pm0.015} \times 10^{-11}$	[112]
	294-716	$1.86 \pm 0.08 \exp\left(\frac{1150\pm150}{RT}\right) \times 10^{-11}$	[87]
H_2	295-768	$2.4 \pm 0.7 \left(\frac{T}{298}\right)^{1.6\pm0.2} \exp\left(\frac{-1340\pm90}{T}\right) \times 10^{-12}$	[113]
		$0.42 \pm 0.38 \left(\frac{T}{298}\right)^{2.8\pm0.6} \exp\left(\frac{-790\pm290}{T}\right) \times 10^{-12}$	
D_2	295-768	$0.79 \pm 0.15 \left(\frac{T}{298}\right)^{2.2\pm0.1} \exp\left(\frac{-1330\pm60}{T}\right) \times 10^{-12}$	[113,114,86]
		$4.3 \pm 1.8 \left(\frac{T}{298}\right)^{1.1\pm0.3} \exp\left(\frac{-1930\pm140}{T}\right) \times 10^{-12}$	
CH_3C_2H	294	$2.1 \pm 0.5 \times 10^{-10}$	[115]
		$2.3 \pm 0.5 \times 10^{-10}$	
C_5H_{12}	294	$1.6 \pm 0.2 \times 10^{-10}$	[115]
$C(CH_3)_4$	294	$1.1 \pm 0.1 \times 10^{-10}$	[115]
		$1.1 \pm 0.1 \times 10^{-10}$	
C_7H_{16}	294	$2.3 \pm 0.2 \times 10^{-10}$	[115]
		$2.6 \pm 0.3 \times 10^{-10}$	
CH_3OH	294	$1.2 \pm 0.2 \times 10^{-10}$	[115]
		$1.3 \pm 0.2 \times 10^{-10}$	
C_2F_3H	294	$4.2 \pm 0.3 \times 10^{-11}$	[115]
		$4.6 \pm 0.3 \times 10^{-11}$	
C_2F_4	294	$2.5 \pm 0.3 \times 10^{-11}$	[115]
		$2.6 \pm 0.3 \times 10^{-11}$	
HCl	295-764	$0.78 \pm 0.17 \exp\left(\frac{-18000\pm800}{RT}\right) \times 10^{-11}$	[116,117,118]
		$0.58 \pm 0.06 \exp\left(\frac{-15800\pm400}{RT}\right) \times 10^{-11}$	
HBr	295-764	$2.0 \pm 0.4 \exp\left(\frac{-7700\pm700}{RT}\right) \times 10^{-11}$	[116,117,118]
		$2.4 \pm 0.3 \exp\left(\frac{-8300\pm400}{RT}\right) \times 10^{-11}$	
HI	295-764	$6.1 \pm 0.6 \exp\left(\frac{300\pm300}{RT}\right) \times 10^{-11}$	[116,117,118]
		$7.2 \pm 0.2 \exp\left(\frac{200\pm100}{RT}\right) \times 10^{-11}$	
NO	295	$1.42 \pm 0.01 \times 10^{-12}$	[87,119,120]
	294-716	$4.95 \pm 0.2 \exp\left(\frac{1090\pm220}{RT}\right)$	[87,119,120]

Species	Temp (K)	Rate Coefficient ($cm^3\ s^{-1}$)	Ref
CH_4	292-1488	$(1 \pm 2)T^{2.64\pm0.24} \exp\left(\frac{220\pm150}{T}\right) \times 10^{-19}$	[119–123, 112, 113]
C_2H_2	294-700	$3.49 \pm 0.26 \exp\left(\frac{571\pm23}{T}\right) \times 10^{-11}$	[126,123,115]
C_2H_4	294-700	$4.72 \pm 0.25 \exp\left(\frac{509\pm20}{T}\right) \times 10^{-11}$	[126,123,115]
C_2H_6	294-984	$(3.7 \pm 0.2)T^{2.7\pm0.2} \exp\left(\frac{810\pm80}{T}\right) \times 10^{-19}$	[122,121,123,127,115]
C_3H_6	rt	$2.3 \pm 0.3 \times 10^{-10}$	[123]
C_3H_8	292-1270	$(2 \pm 3)T^{1.22\pm0.2} \exp\left(\frac{400\pm150}{T}\right) \times 10^{-14}$	[121,122,127,115]
Cl_2	rt	$6.0 \pm 0.3 \times 10^{-12}$	[128]
F_2	rt	$6.4 \pm 0.8 \times 10^{-14}$	[128]
HCN	296-578	$10^{-11.41\pm0.15} \times \exp\left(\frac{-670\pm100}{T}\right)$	[129]
BrCN	296-578	$10^{-10.7\pm0.4} \times \exp\left(\frac{-1340\pm330}{T}\right)$	[129]
CH_3CN	296-578	$10^{-10.19\pm0.10} \times \exp\left(\frac{-1140\pm70}{T}\right)$	[129]
HC_2CN	rt	$1.70 \pm 0.08 \times 10^{-11}$	[130]
H_2O	518-1027	$1.33 \pm 0.13 \exp\left(\frac{-31200\pm600}{RT}\right) \times 10^{-11}$	[131,132]
NO_2	297-740	$10^{-10.40\pm0.12} \times \exp\left(\frac{-186\pm33}{T}\right)$	[119]
N_2O	300-740	$10^{-11.8\pm0.4} \times \exp\left(\frac{-3560\pm181}{T}\right)$	[133]
CO_2	2510-3510	$6.6 \exp\left(\frac{-19200}{T}\right) \times 10^{-10}$	[134,135]
N	300	$1.00 \pm 0.13 \times 10^{-10}$	[136,134]
O	2510-3510	$1.03 \exp\left(\frac{-1000}{T}\right) \times 10^{-11}$	[134,137,138]

Table 7: Results of previous studies of the reaction of CN-radicals. For species which have two entries in the table, the upper entry represents CN ($v'' = 0$) and the lower entry represents CN ($v'' = 1$). T is the temperature at which the measurements were made. 'rt' indicates room temperature. The gas constant R = 8.314 J K^{-1} mol^{-1}. All rate coefficients listed are expressed in 'per molecule' units, that is, $cm^3\ s^{-1}$ implies cm^3 $molecule^{-1}$ s^{-1}

Year	v''	Temp (K)	Rate Coefficient ($cm^3\ s^{-1}$)	Ref
1968	-	687	$8.8 \pm 5.0 \times 10^{-12}$	[142]
1972	0	300	2.1×10^{-11}	[143]
	2	300	2.5×10^{-11}	
	4	300	3.8×10^{-11}	
	0	375	1.8×10^{-11}	
	4	375	2.3×10^{-11}	
1987	-	295	$2.5 \pm 0.5 \times 10^{-11}$	[117]
1988	0	294-716	$1.52 \pm 0.23 \exp\left(\frac{-1500 \pm 600}{RT}\right) \times 10^{-11}$	[87]
	1		$1.55 \pm 0.15 \exp\left(\frac{-2600 \pm 400}{RT}\right) \times 10^{-11}$	

Table 8: Results of previous studies of the reaction of CN with NH_3

constant for the reaction CN with NH_3 have been reported but no measurements of the rate constant for the reaction of CN with ND_3. The reaction of CN with NH_3 was first studied by Boden and Thrush [142] in 1968. They generated CN-radicals by reaction of C_2N_2 with O atoms at 687K and monitored their time evolution by absorption spectroscopy. The analysing light for these measurements was generated by a microwave discharge in a mixture of Ar, N_2 and CH_4 which emitted CN $\tilde{B} \rightarrow \tilde{X}$ radiation. The rate coefficient they obtained, along with those reported by subsequent workers are shown in table 8.

Bullock *et al.* [143] extended this work four years later, including a study of the dependences of the rate constant on temperature and on vibrational excitation of CN. They produced CN-radicals by pulse-radiolysis of dilute mixtures of C_2N_2 and NH_3 in argon and monitored the decay of CN in the $v'' = 0, 2$ and 4 vibrational levels by absorption spectroscopy, using a high-pressure xenon-lamp, at 300 and 375K. They found that the rate coefficient exhibited a negative dependence on temperature and a positive dependence on vibrational excitation of CN. The rate constant they determined from extrapolation of their data to 687K essentially shows

agreement with that determined by Boden and Thrush at this temperature. More recently, de Juan *et al.* [117] and Sims and Smith [87] have studied this reaction using laser-photolysis and laser-induced fluorescence to generate and monitor CN respectively. The results obtained by Sims and Smith, which span a wide temperature range, provide support for the negative temperature dependence and positive dependence on vibrational excitation of CN of the rate coefficient found by Bullock *et al.*, although they report a room-temperature rate constant somewhat higher than that of previous workers.

All previous studies of the reaction of cyanogen with ammonia make use of the well known CN $\tilde{B}\rightarrow\tilde{X}$ electronic system, in either absorption or emission to monitor the CN decay. In this study we monitor the CN concentration *via* the (1,0) vibrational band of the ground electronic state.

6.2 Experimental

Cyanogen radicals were produced by 193.3 nm photolysis of C_2N_2 in mixtures of C_2N_2, He and either NH_3 or ND_3, by the unfocussed output of an ArF excimer-laser. The excimer-laser was operated at a frequency of *ca.* 10 Hz and produced pulses with energies of approximately 50 mJ, as measured by a Scientech model 364 power/energy meter. The low pulse energies combined with the small absorption cross-section of C_2N_2 at 193 nm (*ca.* 1.1×10^{-19} cm^2 [114]) ensured that pseudo first-order conditions were maintained throughout all experiments with $[NH_3]$ or $[ND_3] \gg [CN]$.

The photolysis cell used for these experiments (see section 2.2.6) consisted essentially of a length of 50 mm internal-diameter glass tubing approximately 1200 millimetres long, with ground-glass flanges at either end onto which calcium fluoride windows were attached. Calcium fluoride was chosen because of its high optical transparency from the vacuum-ultraviolet through to infra-red wavelengths, allowing both photolysis and probe laser beams to introduced to the cell co-linearly.

The excimer-laser and diode-laser beams enter from opposite ends of the cell and the diode-laser beam makes four passes diagonally through the entire length of the volume swept out by the excimer-laser beam. The reaction gas mixture flows into the cell from the end where the excimer-laser beam enters. Additional buffer gas flows into the cell through four ports around each window designed to reduce the deposition of CN-polymer on them.

The intensity of the diode-laser beam was monitored by focussing it into a Judson liquid-nitrogen cooled, mercury-cadmium-telluride detector with a KRS-5 lens. The detector output was amplified by a matched Judson PA-100 pre-amplifier and taken to the transient recorder or the oscilloscope. Cyanogen rovibrational line positions were calculated using the spectroscopic constants of Cerny *et al.* [144] and were in excellent agreement with those observed by Davies and Hamilton [145]. The diode-laser was tuned to the P(10) ($v = 0 \rightarrow 1$) line of the ground ($\tilde{X}^2\Sigma^+$) electronic state at *ca.* 2003.06254 cm^{-1}. The absolute frequency was determined by calibration with known CO line positions [146] interpolated by the fringes of the etalon.

The experimental setup is shown in figure 9. A 10-volt pulse produced by a variable frequency, square-wave generator simultaneously triggers the photolysis laser and the transient recorder. The transient recorder is configured to allow the collection of data from the pre-trigger region, so that the value of I_0 (intensity at $t = 0$) may be determined, as well as from the post-trigger region in which the transient CN absorption decays. The number of points digitized per pulse and the sampling rate of the recorder were selected so that the entire decay of the absorption of CN-radicals was recorded and the experimental repetition rate was kept as high as possible. Typically the decays of CN-radicals from 500 photolysis laser pulses were averaged. Decreasing the repetition rate increases the data collection time of an experiment and exacerbates problems associated with the diode-laser frequency *drifting* due to instability in the refrigerator temperature. This problem was minimized by checking to ensure the diode-laser was centered on the CN rovibrational line before each measurement was taken. The excimer laser, the diode laser and the transient digitizer are all triggered from separate opto-isolated circuits to reduce

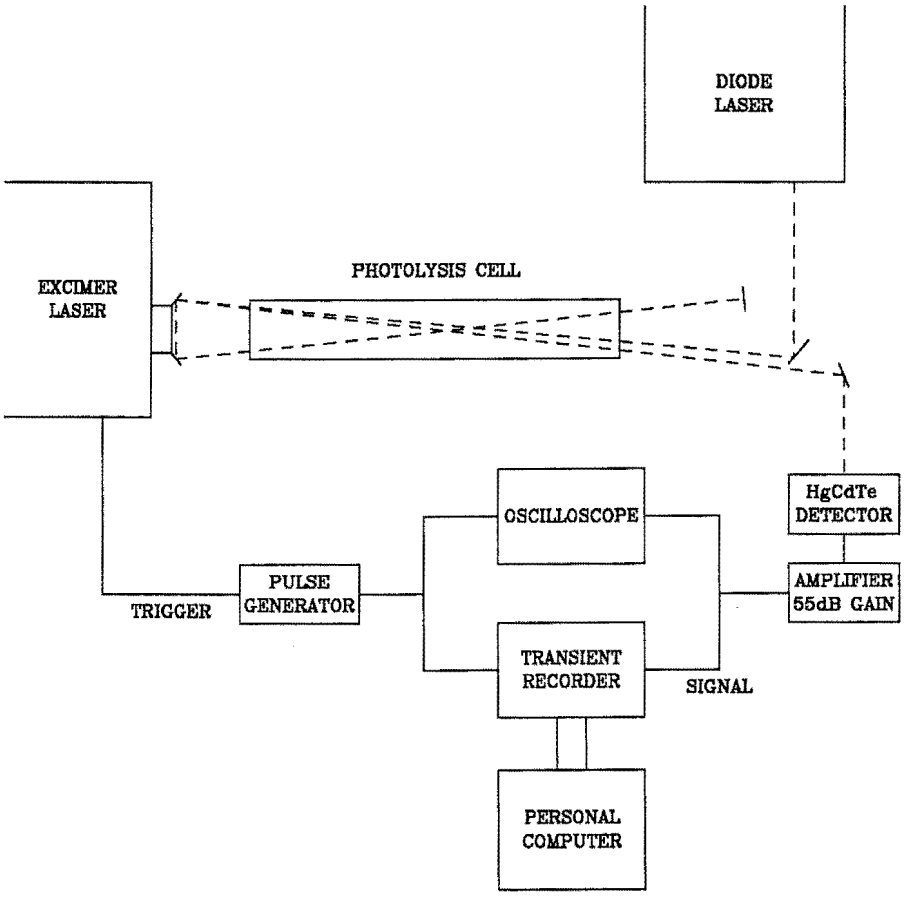

Figure 9: Experimental configuration for the collection of kinetic data using excimer-laser photolysis/diode-laser absorption spectroscopy

pick-up associated with the excimer laser discharge.

Flow rates of reagent molecules were measured with calibrated Tylan mass flowmeters and controlled with needle valves. Cell pressure, typically around 2 torr, was measured using a MKS model 122AA 0-10 torr Baratron. Reactant partial pressures were calculated from the measured flow rates and total pressure. All experiments were conducted at room temperature (296 ± 2) K. The purity, handling and preparation of gases used in this experiment has been discussed previously in section 2.3.

6.3 Results and Discussion

In our reaction system CN radicals can be removed by reaction with NH_3, the radical precursor C_2N_2, the reaction products HCN and NH_2 (see chapter 7), NH_3 photolysis products NH_2 and H and other CN-radicals, or *via* diffusion out of the active volume[1].

Since $[NH_3] \gg [NH_2]$, [NH], [H], [HCN] and [CN] the rate of removal of CN-radicals with time may be expressed as

$$\frac{-d[\mathrm{CN}]}{dt} = k_{\mathrm{diff}}[\mathrm{CN}] + k_{\mathrm{C_2N_2}}[\mathrm{CN}][\mathrm{C_2N_2}] + k_{\mathrm{NH_3}}[\mathrm{CN}][\mathrm{NH_3}] \tag{4}$$

Solution of this equation and imposing the boundary condition that at $t = 0$, [CN] $= [\mathrm{CN}]_0$ yields

$$[\mathrm{CN}] = [\mathrm{CN}]_0 \exp -k't \tag{5}$$

where $k' = k_{\mathrm{diff}} + k_{\mathrm{C_2N_2}}[\mathrm{C_2N_2}] + k_{\mathrm{NH_3}}[\mathrm{NH_3}]$. Combining this with the Beer-Lambert law yields an expression relating the experimentally observed absorption intensity as a function of time, to the concentration of CN-radicals.

$$\ln\left(\ln\left(\frac{\mathrm{I_0}}{\mathrm{I_t}}\right)\right) = \ln\left(\epsilon[\mathrm{CN}]_0 l\right) - k't \tag{6}$$

Figure 10 shows time-resolved plots of the transient absorption of CN in the presence of two differing concentrations of ND_3. Both curves are the results obtained from averaging over 500 photolysis laser pulses. The pseudo-first-order decay constant is obtained from the slope of a plot of the natural logarithm of absorption versus time (equation 6) as shown in figure 11. The first 50 microseconds of each decay were not included in the fitting procedure, to ensure any residual effects of pickup from the excimer-laser discharge are eliminated. The linearity of plots obtained confirms that CN was being removed by first-order processes. The bimolecular rate coefficient k, is obtained from the slope of a plot of the pseudo first-order rate constants as a function of the reactant concentration (figure 12).

[1]The active volume in this context is the volume of the cell swept out by the excimer-laser beam.

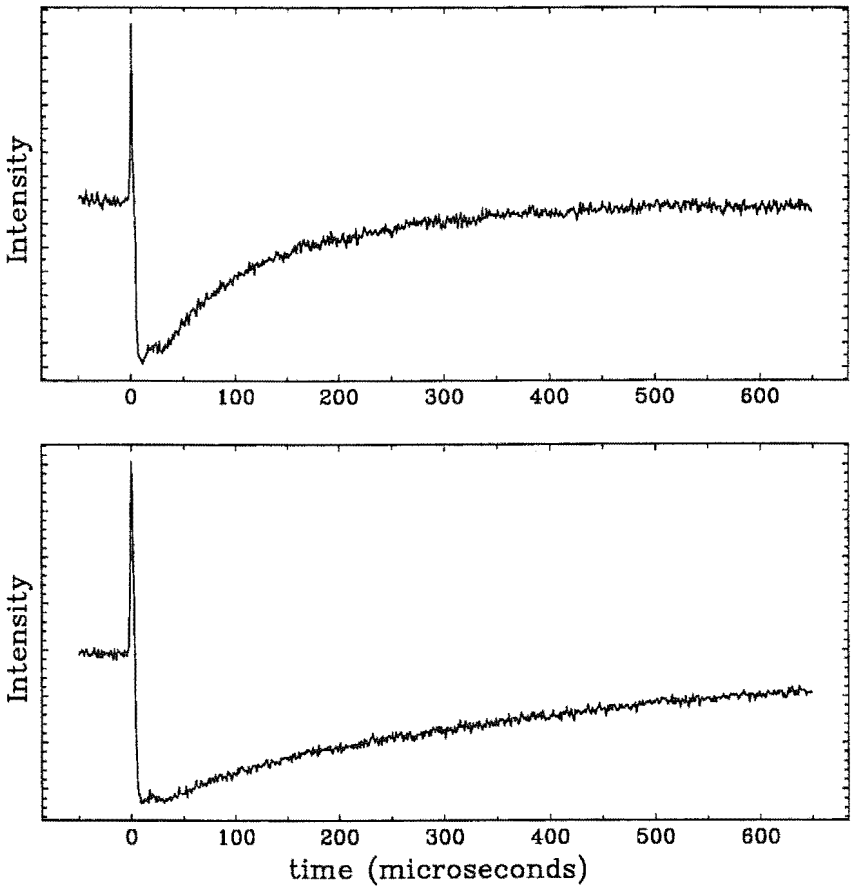

Figure 10: Transient absorption profiles of CN-radicals in the presence of ND_3. Upper trace $[ND_3] = 2.13 \times 10^{14}$ cm^{-3}; Lower trace $[ND_3] = 0.74 \times 10^{14}$ cm^{-3}.

The intercept of figure 12 represents the sum of the rates of removal of CN by all processes other than reaction with NH_3 (or ND_3) including reaction with C_2N_2. At the partial pressures of C_2N_2 used, the contribution to the intercept from reaction with C_2N_2 [147] is small. The negative[2] intercept we obtain is almost certainly due to overestimation of the actual NH_3 concentration in the active volume. NH_3 is depleted in the active volume by photolysis at 193 nm [148] and as a result of this the concentrations we calculate (see section 2.3) will slightly overestimate the actual concentration of NH_3 in the region where CN-radicals are produced. The

[2]The intercept is in fact statistically zero.

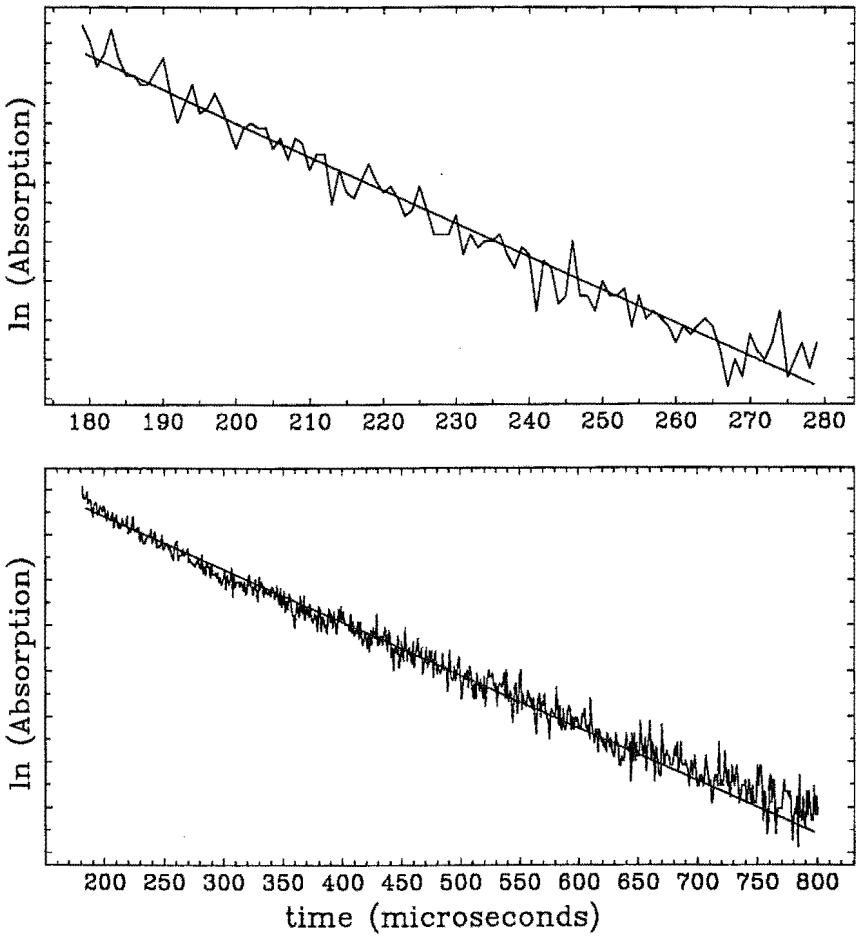

Figure 11: Pseudo first-order decay plots for CN in the presence of ND_3. The data from figure 10 was used to create these plots

effect of this will be that the data points in our Stern-Volmer plot (figure 12) will be shifted in the [reactant] co-ordinate toward more positive values, hence our negative intercept. The single-photon absorption cross-section of NH_3 is 4.5×10^{-18} cm^2 [149] so that together with the slow reactant flow-rates we employ, *significant* NH_3 depletion may occur. Since $[NH_3]$ is at least in a 500-fold excess of [CN], NH_3 photolysis would not affect our pseudo first-order reaction conditions or the decay constants we obtain. Similar arguments apply to the reaction of CN with ND_3 although depletion by photolysis will occur to lesser extent since ND_3 has a smaller

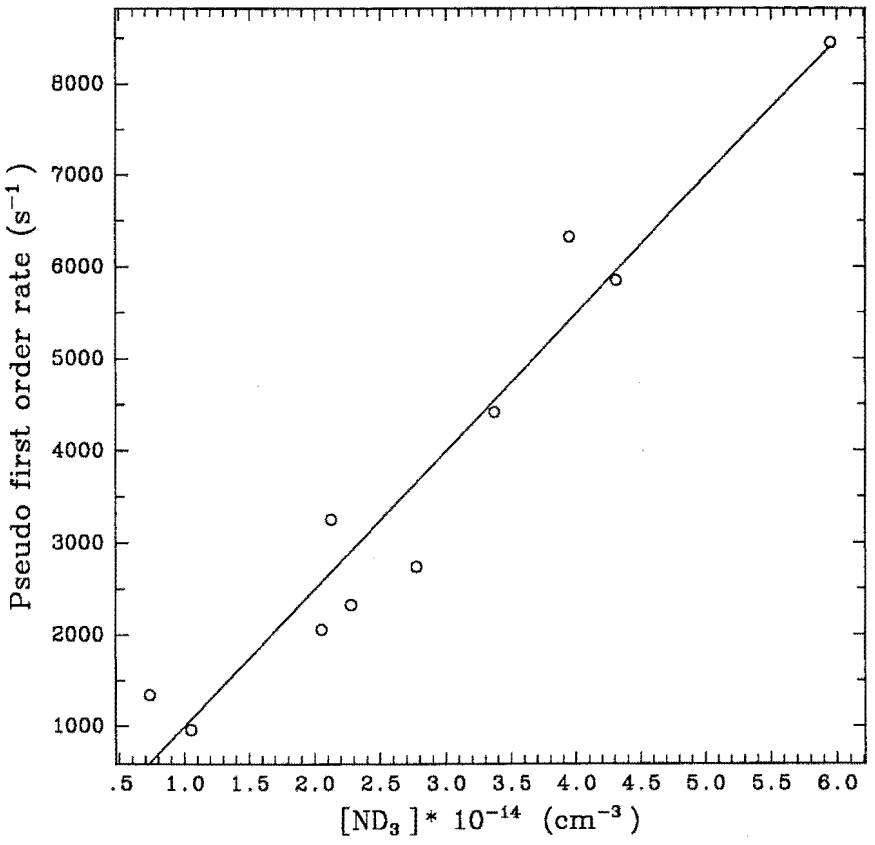

Figure 12: Stern-Volmer plot for the reaction of CN with ND_3

single-photon absorption coefficient[3] at 193 nm.

Photolysis of C_2N_2 at 193 nm has been shown to produce CN-radicals in both the $v'' = 0$ and $v'' = 1$ vibrational levels of the ground electronic state [151,152] with rotational temperatures of around 900K. Measurements of the relative population of each state indicate that between 13 [151] and 26% [152] of CN-radicals are produced in the $v'' = 1$ level. Population of higher vibrational levels was not observed. Although rotational equilibration to 300K has been shown to be rapid [124], and

[3]Although to date the single-photon absorption coefficient of ND_3 at 193 nm has not been measured, studies such as the jet-cooled spectra obtained by Vaida *et al.* [150] indicate that a smaller value is likely.

Species	v''	Temp (K)	Rate Coefficient ($cm^3\ s^{-1}$)	Ref
NH_3	0	300	2.1×10^{-11}	[143]
	-	295	$2.5 \pm 0.5 \times 10^{-11}$	[117]
	0	295	$2.9 \pm 0.1 \times 10^{-11}$	[87]
	1	294	$4.5 \pm 0.3 \times 10^{-11}$	
	0	296	$3.0 \pm 0.4 \times 10^{-11}$	this work
ND_3	0	296	$1.5 \pm 0.3 \times 10^{-11}$	this work

Table 9: Room temperature rate constants for the reaction of CN with NH_3

would occur in the time we wait before fitting decays, vibrational relaxation occurs on a longer timescale. The major pathways for deactivation of CN ($v'' = 1$) are *via* energy transfer to C_2N_2 and by reaction with NH_3. Vibrational energy transfer to NH_3 is unlikely to be important due to a large difference in the vibrational frequencies of CN and NH_3. Energy transfer to C_2N_2 [124], repopulating the $v'' = 0$ level should only be competitive with reaction with NH_3 [87] at low NH_3 concentrations. Systematic removal of data points corresponding to low NH_3 concentrations does not affect the rate coefficient we obtain beyond the errors we quote. Therefore it would seem that the small fraction of CN-radicals formed in the $v'' = 1$ vibrational state are not effecting our analysis of CN ($v'' = 0$) radicals to a discernable degree and that the rate constant we report is a good measure of the rate at which CN ($\tilde{X}\ ^2\Sigma^+, v'' = 0$) radicals react with NH_3.

The results obtained, together with the room-temperature rate coefficients obtained by other workers are shown in table 9. The quoted uncertainty for our results represents the 95% confidence level obtained from a Students-t test of the linear-least-squares fit.

Our results are in excellent agreement with recent study of Sims and Smith [87] and are also in good agreement with the earlier study of de Juan *et al.* [117] from the same laboratory.

The results of the experimental studies of this reaction show that it displays characteristics normally associated with radical-radical reactions [153]; those being the rate of reaction is close to the collisional rate and displays a negative dependence on temperature. Despite the kinetic data available, the mechanism by which CN reacts with NH_3 is unclear. As Sims and Smith [87] point out, this reaction has a rate constant several orders of magnitude faster than the reaction of CN with other H-atom containing small molecules such as H_2 and CH_4 where the H–X bond strength is less than in NH_3. Experimental evidence to date indicates that the reactions of CN with H_2 and CH_4 proceed *via* a direct H-abstraction type mechanism [123], so it seems unlikely that reaction with NH_3 does also. In addition to this, *ab initio* theoretical studies of the reactions of CN with H_2 [83] and NH_3 (see chapter 5) show that there are barriers of 16–40 kJ mol^{-1} on the pathways to products *via* direct H-abstraction mechanisms. The rate coefficients for reaction *via* these mechanisms would be expected to display positive temperature dependences as observed for reaction with H_2 [113] but not for reaction with NH_3. Therefore it would seem that CN does not react with NH_3 *via* a direct H-abstraction type mechanism as the barrier on the pathway to products is inconsistent with both the observed fast rate and negative temperature dependence. Similar reasoning would suggest that reaction of CN with NH_3 to form H_2NCN + H *via* the mechanism presented in chapter 5 would also be inconsistent with the observed experimental data since this pathway also has a barrier to reaction.

Recent theoretical investigations into the origin of the negative temperature dependence [153,154] indicate that the fate of such reactions may be determined by long-range intermolecular forces such as dipole and quadrupole interactions. Dynamical calculations of the rate of capture over a dipole-dipole potential by Phillips [97] show the capture rate to be *ca.* 7× greater than the measured rate of reaction. This implies that there is a secondary barrier on the reaction pathway.

The results of the *ab initio* molecular orbital theory study presented in chapter 5 show that there is another possible pathway for reaction in which dipole-dipole forces orient CN and NH_3 to form the H_3NCN intermediate. Reaction to products

from this intermediate proceeds over a secondary barrier lying 33.5 kJ mol^{-1} higher in energy than the intermediate but 9.3 kJ mol^{-1} lower than the energy of the reactants at the QCISD(T)//MP2 level of theory. A secondary barrier of this form would explain the negative temperature dependence and be consistent with fast rate of reaction observed and the results of Phillips. As the temperature is raised the number of states with sufficient energy to redissociate to reactants increases relative to the number of states with sufficient energy for H-migration. The effect of this is that the apparent rate of disappearance of CN decreases as the temperature is raised.

Additional calculations by Phillips, with the inclusion of a statistically based factor for the probability of crossing the secondary barrier gives calculated rates of reactions in good agreement with experimental values. The experimental (2.0) and calculated magnitudes of the kinetic isotope effect $\left(\left(\frac{k_H}{k_D}\right)\right)$ are also in agreement. Phillips notes that excellent agreement between the experimental and calculated rate of reaction and magnitude of the kinetic isotope effect can be obtained with a small adjustment to the height of this secondary barrier. His results suggest that the height of this barrier is bounded by the MP4SDQ//MP2 and QCISD(T)//MP2 energies. For reasons discussed in chapter 5 regarding the slow convergence of the unrestricted Møller-Plesset series and the limitations of the basis set used, this seems a reasonable conclusion.

This pathway is therefore the most likely mechanism of reaction of CN with NH_3 and ND_3. The observed products of reaction and the relationship to the conclusions drawn about the mechanism of reaction here will be discussed in chapter 7.

6.4 Conclusions

We have measured rate constants for the room temperature reactions of CN with NH_3 and ND_3. CN-radicals were produced by laser photolysis of C_2N_2 at 193 nm and their time evolution was monitored by infra-red absorption spectroscopy. The

results obtained were

$$\mathrm{CN} + \mathrm{NH_3} \quad k = 3.0 \pm 0.4 \times 10^{-11}\ \mathrm{cm^3\ s^{-1}}$$
$$\mathrm{CN} + \mathrm{ND_3} \quad k = 1.5 \pm 0.3 \times 10^{-11}\ \mathrm{cm^3\ s^{-1}}$$

All measurements are in good agreement with the results of previous workers.

Comparison of the results obtained with the results of other experimental and theoretical studies of the reaction of CN with NH_3, indicates that the reaction proceeds initially to a dipole-dipole favoured intermediate (H_3NCN) which subsequently rearranges over a secondary barrier and dissociates to give products.

A paper based on this work is in preparation [97].

Chapter 7

Products of reactions of CN with NH_3 and ND_3

7.1 Introduction

Complete characterization of a reaction requires that, in addition to kinetic studies, the products of reaction be determined. Since reactions involving free radicals may have more than one set of possible products, determination of the products that form and how the overall rate of reaction is partitioned between different product channels (branching ratio) is important. Although the likely products of reaction can often be determined on thermodynamic grounds, other forces, such as those controlling favourable orientation of reactants for collision or rearrangement and dissociation of any intermediate complexes formed, can often supercede thermodynamic considerations. Product determination can therefore provide fundamental information on the relative heights of barriers in the possible reaction channels, and the importance of other forces in determining which products form.

Of the many reactions of CN-radicals that have been studied, the products of reaction have been determined for only a few of these. Balla *et al.* observed the kinetic buildup of HCN from the reactions of CN with H_2 [114], CH_4 and C_2H_6 [121].

The rate constant they determined for the growth of HCN from the reaction of CN with H_2 was essentially the same as that they obtained for the disappearance of CN indicating that HCN and H are the sole products of reaction.

The NCO radical has been observed as a product of the reaction of CN with O_2 by many workers [140,155,156]. CO was also observed as a product of this reaction by Schmatjko and Wolfrum [157], who used a CO laser for time-resolved absorption measurements. From the observed vibrational distribution of CO they concluded that the reaction of CN with O_2 proceeds according to

$$\begin{aligned} CN + O_2 &\longrightarrow CO(v') + NO \quad (6 \pm 2)\% \\ &\longrightarrow NCO + O \quad (94 \pm 2)\% \end{aligned}$$

In a similar manner they determined that the reaction of CN with O proceeds according to

$$\begin{aligned} CN + O &\longrightarrow CO + N(^4S) \quad (20 \pm 10)\% \\ &\longrightarrow CO + N(^2D) \quad (80 \pm 10)\% \end{aligned}$$

Products of the reactions of CN with OCS and N atoms have also determined. Addison *et al.* [158] observed the spectrum of SCN from the reaction of CN with OCS and Kley *et al.* [159] observed C atoms from the reaction of CN with N atoms using vacuum-ultra-violet absorption spectroscopy.

Prior to this work, the products of the reaction of CN with NH_3 had only been partially characterized. Bullock *et al.* [143] observed the appearance of $NH_2(0,0,0)$ radicals from the pulse-radiolysis of C_2N_2 in the presence of NH_3. The rate constant the obtained for the growth of NH_2 was consistent with that they obtained for CN removal. The identity of the product(s) forming in addition to NH_2 remained to be determined.

7.2 Experimental

CN-radicals were produced by 248.5 nm photolysis of ICN in mixtures of ICN, NH_3 and Helium, using the unfocussed output of a KrF excimer laser. ICN rather

than C_2N_2 was used as the CN-radical source in these experiments to prevent NH_3 photolysis, which occurs at 193 nm. The reaction of photolysis products with CN radicals or C_2N_2 could have given rise to signals which may have been attributed to products of the reaction of CN with NH_3. Of particular concern would have been the reactions of H atoms. The photolysis cell and experimental setup for the observation of transient reaction profiles associated with the photolysis-laser pulse have been described in chapter 6. In this study we searched for the buildup of products after the photolysis-laser pulse rather than the decay of CN-radicals.

Mass analysis of samples of the reaction mixture was done using a Spectromass Dataquad quadrupole mass-spectrometer. Samples were taken from the pumpout port of the cell through a needle-valve. The quadrupole was pumped to pressures of *ca.* 10^{-8} torr by a Varian VHS-4 diffusion pump backed by a Welch Duo-Seal model 1376 mechanical pump. Analysis was done at pressures typically ranging from 5×10^{-6} to 5×10^{-5} torr as measured by an ion-gauge adjacent to the quadrupole. The diffusion pump and quadrupole are separated by a large liquid-nitrogen cold trap to prevent contamination of samples with diffusion pump oil fragments.

Infra-red diode laser spectra of static mixtures were obtained in a Scintrex model WC-2 1.5 metre White cell. The infra-red beam traversed a path length *ca.* 75 metres through the cell and was focussed upon its exit by a KRS-5 lens into a Judson liquid-nitrogen cooled, mercury-cadmium-telluride detector. The detector output was amplified by a matched Judson PA-100 pre-amplifier and displayed on the oscilloscope. The absolute frequency was determined using the known line positions [146] of either N_2O (ND_2, H_2NCN) or CO(HCN, HNC) reference gases interpolated by the fringes of the etalon.

Cell pressures were measured using either a MKS model 122AA 0–10 torr Baratron or a Texas Instruments model 144 quartz-spiral gauge. Pressures in the photolysis cell were typically 2–3 torr for flowing mixtures and 90–100 torr for static mixtures. Flow rates of reagent molecules were measured with calibrated Tylan mass flow-meters. All experiments were conducted at room temperature (296 ± 2)K. The purity, handling and preparation of reagent materials used in this experiment have

been discussed in section 2.3.

Ab initio molecular orbital theory energy calculations on the HCN/HNC equilibrium were performed using Gaussian90 [89].

7.3 Results and Discussion

The results of the *ab initio* molecular orbital theory calculations presented in chapter 5 indicate that there are four exoergic product channels in this reaction. These channels are summarized below. Energies quoted were calculated at the MP4SDQ//HF level of theory.

$$\begin{aligned} NH_3 + CN &\longrightarrow NH_2 + HNC \quad \Delta E = -75.4 \text{ kJ mol}^{-1} \\ &\longrightarrow H_2NCN + H \quad \Delta E = -125.3 \text{ kJ mol}^{-1} \\ &\longrightarrow NH_2 + HCN \quad \Delta E = -162.4 \text{ kJ mol}^{-1} \\ &\longrightarrow N_2 + CH_3 \quad \Delta E = -327.5 \text{ kJ mol}^{-1} \end{aligned}$$

It was shown that the production of H_2NCN + H proceeds over a barrier lying 37.7 kJ mol^{-1} above the energy of the reactants and therefore the formation of these products would be inconsistent with the experimentally observed fast reaction rate and negative dependence of the rate coefficient on temperature. The absence of a complete pathway to the formation of N_2 and CH_3 lead us to believe that these products were also unlikely to form although their possible production was not discounted entirely. The major problem with this reaction pathway was the inability to optimize a structure responsible for the formation of an N-N bond. Two complete mechanisms to the formation of both NH_2 and HNC and NH_2 and HCN were found, therefore these sets of products were thought to be the most likely reaction products at room temperature.

We mass-analysed samples taken from a flowing mixture of ICN, NH_3 and He while it was being irradiated at 248 nm and compared the resulting mass-spectra with those obtained with the laser off. The results showed a 15–25% increase in

signal at $\frac{m}{e} = 27$ when the excimer laser was incident upon the sample. Since only stable species are likely to survive the passage from where they are sampled to the quadrupole, the signal increase was assigned to the production of either HCN or HNC. Distinction between isomeric forms with the same mass-to-charge ratio is not possible using a quadrupole mass-spectrometer. No evidence for signal increases beyond that which occurred in background samples was found at $\frac{m}{e} = 28$ (N_2), or $\frac{m}{e} = 42$ and $\frac{m}{e} = 43$ (H_2NCN and H_2NCN/H^+), or at any other mass below $\frac{m}{e} = 43$ ($CN_2H_3^+$).

In order to determine whether HCN, HNC or both species were being produced by the reaction, the diode-laser was tuned to the P(9)(0,0,0 → 0,0,1) line of HCN at 2069.52008 cm^{-1} [160], then the R(8)(0,0,0 → 0,0,1) line of HNC at 2050.06122 cm^{-1} [161] and attempts were made to observe the kinetic buildup of these species after the photolysis-light pulse. However the infra-red line strengths of these molecules at these wavelengths were found to be too weak to enable their detection at the levels produced from a single pulse. To overcome this problem, static mixtures of reactants were irradiated at 248 nm for 30–45 minutes to increase the concentrations of products to measurable levels. To increase sensitivity further, the irradiated sample was transferred to the longer path-length White cell. Analysis of the resulting spectra showed the presence of the P(9) and P(15) lines of HCN at 2069.52008 cm^{-1} and 2050.42112 cm^{-1} respectively with percentage absorptions in excess of 20 × greater than background levels. No evidence for HNC was found in the region of the R(8) and R(15) lines at 2050.06122 cm^{-1} and 2069.15057 cm^{-1} respectively.

We performed additional *ab initio* molecular orbital theory calculations, following the G-1 procedure outlined by Pople *et al.* [94], to determine whether there was sufficient energy available from the reaction for HNC, should it form, to isomerize to HCN in the time before analysis. The results, plotted in figure 13 show that HNC lies 61.6 kJ mol^{-1} above HCN and the HNC/HCN isomerism transition-state (CHN (TS)) lies 186.1 kJ mol^{-1} above HCN. This means that the energy available from the reaction of CN with NH_3 to either set of products is less than half that required for isomerism of either HCN or HNC.

There have been few experimental determinations of the relative energies of HCN and HNC and only one "experimental" study of the magnitude of the activation barrier. The most recent study of the HCN/HNC energies by Pau and Hehre [162],

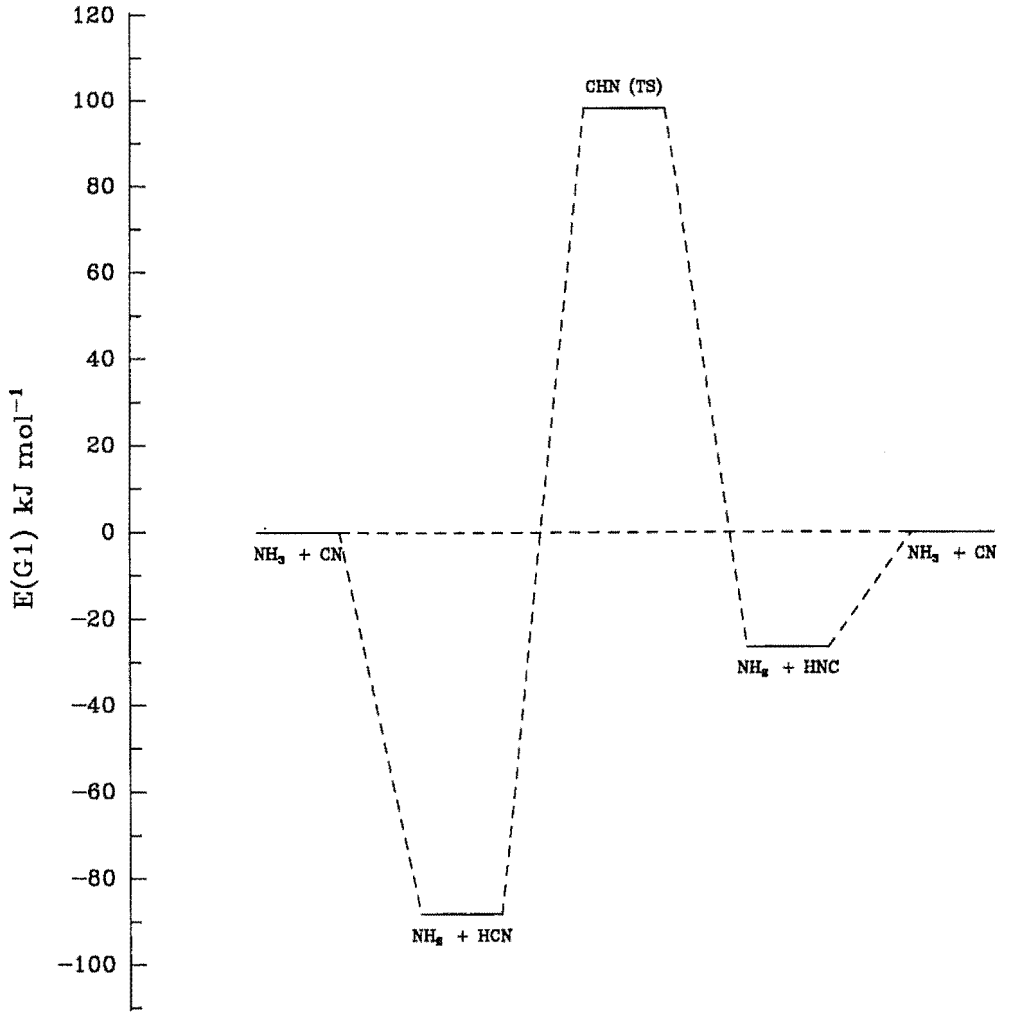

Figure 13: Calculated G-1 energies for the HCN⇌HNC equilibrium. Energies plotted represent that required for isomerization of either HCN or HNC relative to the energy available from the reaction of CN with NH_3 to the corresponding set of reaction products.

determined the HNC isomer to lie 61.9 ± 8.0 kJ mol^{-1} above the HCN isomer using Ion-Cyclotron Double-Resonance spectroscopy. This is in excellent agreement with our *ab initio* value. Our calculated geometries are also in good agreement with those determined experimentally [163,164] (table 10), and this is indicative of the degree of accuracy we might expect from our calculations in the transition region.

Species	Geometry	Reference
HCN	$r_{CN} = 1.153$ Å $r_{CH} = 1.065$ Å	[163]
	$r_{CN} = 1.176$ Å $r_{CH} = 1.069$ Å	this work
HNC	$r_{CN} = 1.169$ Å $r_{NH} = 0.994$ Å	[164]
	$r_{CN} = 1.186$ Å $r_{NH} = 1.002$ Å	this work
CHN (TS)	$r_{CN} = 1.194$ Å $r_{CH} = 1.188$ Å $r_{NH} = 1.389$ Å	[165]
	$r_{CN} = 1.195$ Å $r_{CH} = 1.176$ Å $r_{NH} = 1.407$ Å	this work

Table 10: Comparison of experimental and calculated geometries for HCN, HNC and the CHN (TS).

Recently Lee and Rendell [165] have reported an extensive *ab initio* study of the structure and energetics of the HCN⇌HNC transition-state. Their calculations, done using a coupled-cluster (CCSD(T)) method with very large basis sets show the CHN (TS) to lie 186.6 ± 4 kJ mol^{-1} above the HCN isomer. Their results are in good agreement with our findings. For reasons Lee and Rendell discuss [165], it would seem that the only "experimental" determination of the transition-state energy [166] is too low and that the *ab initio* values better represent the relative energy of this species.

From these results it would appear that should HNC form as a product of the reaction of CN with NH_3, there is insufficient energy available for it to isomerize to HCN. Since we do not observe HNC in our spectroscopic study we conclude that it is not a reaction product at room temperature.

In addition to the detection of HCN as a product of reaction, ND_2 radicals were detected in the regime of line positions calculated from energy levels determined by Meunchausen *et al.* [167], at approximately 1179.7 cm^{-1}. The assignment of the observed transient absorption to a line of ND_2 was done by photolysing a sample of pure ND_3 at 193 nm and observing a transient absorption at the same frequency.

NH was eliminated as the possible absorber as the frequency of the NH stretch is some 900 cm^{-1} higher in energy. The percentage absorption due to ND_2 produced by photolysing C_2N_2 or ICN in the presence of ND_3 was at least twice that due to ND_3 photolysis alone with identical ND_3 concentrations. The absorption buildup also occurred over a much longer timescale than that from the ND_3 photolysis which exhibited instantaneous production at a maximum concentration level. This indicates that ND_2 was being produced *both* from the photolysis of ND_3 *and* from the reaction of CN with ND_3. The intensity of the signal due to the kinetic buildup of ND_2 was, however, too weak for a rate coefficient to be determined from it.

The observation of ND_2 as a reaction product is in agreement with the work of Bullock *et al.* [143] who observed the formation of $NH_2(0,0,0)$ radicals in their pulse-radiolysis study of the reaction. The rate constant they obtained was in good agreement with that they obtained for the disappearance of CN(0,0) radicals although reduced response of their detection equipment resulted in higher experimental errors. In our study ND_2 rather than NH_2 was investigated simply because of the availability of a laser-diode covering the required spectral region.

The observation of these products is consistent with the conclusions drawn about the mechanism of reaction in the previous chapter. Phillips [97] has calculated the relative rates of passage across the barriers to formation of HCN + NH_2 and HNC + NH_2 (see chapter 5). His results show that the observed rate constant and kinetic isotope effect are both consistent with the proposed mechanism leading to the products NH_2 and HCN. The form of the potential-energy surface governing reaction *via* this mechanism would indicate that both HCN + NH_2 and HNC + NH_2 should be products of reaction, especially at elevated temperatures. The experimental observation of only one set of products suggests that other forces, rather that just the relative energetics of the potential-energy surface, may be controlling product formation. However, as mentioned in chapter 5, more extensive *ab initio* calculations may show the pathway to the formation of NH_2 + HNC to be energetically less favoured than the pathway to the formation of NH_2 + HCN, at room temperature. Further work is warranted to determine whether the production of NH_2 and HNC

occurs at higher reaction temperatures.

As mentioned previously, we found no evidence for the presence of N_2 in our mass spectra above background levels. However the background signal at $\frac{m}{e} = 28$ was higher than that at other mass-to-charge ratios of interest hence a small change in signal would have been harder to detect. We would have liked to have been able to probe for the presence of CH_3 radicals by infra-red kinetic spectroscopy, as this has been shown to be a sensitive method for CH_3 detection. However we were unable to do so as we did not have a laser-diode which covered the desired spectral region. Therefore we cannot rule out the presence of N_2 and CH_3 resulting from a minor reaction channel, but the results of the theoretical study presented in chapter 5 leads us to conclude that formation of these products would not be expected.

Similarly, no evidence was found for the presence of H_2NCN in our mass spectra beyond background levels. We did a spectroscopic search, similar to that outlined for HCN and HNC, for the presence of this species in the regime of the intense CN-stretch at *ca.* 2250 cm^{-1} [168]. We found no evidence for the presence of this species in our reaction mixtures. As mentioned in chapter 6, this formation of this species would involve reaction *via* a mechanism which has a barrier to reaction so would be inconsistent with the observed negative temperature dependence and fast rate of reaction.

7.4 Conclusions

The products of the reactions of CN with NH_3 and ND_3 have been determined using mass spectrometry and infra-red absorption spectroscopy. CN-radicals were produced by excimer-laser photolysis of ICN at 248 nm in both flowing and static mixtures also containing NH_3 or ND_3 and He.

The results obtained indicate than $NH(D)_2$ and H(D)CN are the sole products of these reactions at room temperature. No evidence was found for the production

of any other species from these reactions. The observation of $NH(D)_2$ as a reaction product is consistent with the results of previous workers.

Ab initio quantum chemical calculations on the HCN⇌HNC isomerization show that there is insufficient energy available from the reaction for either species to isomerize to the other supporting the accuracy of long timescale observations of HCN.

The results obtained have been discussed in terms of the conclusions drawn about the mechanism of reaction in the previous chapter and shown to be consistent with them. Further work is warranted to determine whether the production of NH_2 + HNC occurs in competition with production of NH_2 + HCN at elevated temperatures.

A paper based on this work is in preparation [97].

Chapter 8

Conclusions

The principal aim of this work was to study the reactions of cyanogen (CN) and boron hydride (BH) free radicals in the gas phase. The reactions of these species are particularly relevant to the chemistry of atmospheric and/or combustion systems. Observations made during the course of these kinetic studies and the existence of unresolved questions arising from studies of previous workers, led us to perform additional studies to characterize the emission observed during the photolyses of diborane and stannane, and to determine the products and mechanism of the reactions of CN with NH_3 and ND_3 using both experimental and theoretical methods. In this chapter, we will briefly summarize the results obtained and conclusions drawn from this work and suggest some areas in which this work may be extended.

A study of the kinetics of reactions of BH-radicals has provided the first measurements of bimolecular rate coefficients for the reactions of BH with NO and C_2H_4. The results obtained at room temperature were

$$\mathrm{BH} + \mathrm{NO} \longrightarrow \text{products} \quad k = 1.26 \pm 0.07 \times 10^{-10}\ \mathrm{cm^3\ s^{-1}}$$
$$\mathrm{BH} + \mathrm{C_2H_4} \longrightarrow \text{products} \quad k = 1.41 \pm 0.09 \times 10^{-10}\ \mathrm{cm^3\ s^{-1}}$$

BH ($^1\Sigma$) radicals were generated by excimer-laser photolysis of diborane at 193 nm and monitored by time-resolved laser-induced fluorescence. The effects of varying the temperature in the range 260–350K and the nature of the buffer gas on the

rate constants for these reactions has been investigated. In addition to these measurements, upper limits to the reactions of BH with O_2, C_2H_6, CH_4 and CO have been set. In each case, the results obtained have been interpreted in terms of the mechanism of reaction.

For the reaction of BH with NO, the observed rate of reaction and negative dependence of the rate coefficient on temperature have been shown to be consistent with the reaction being controlled by the rate of *capture* over a dipole-dipole potential. Comparison with the results of an *ab initio* study of this reaction indicates that the most likely products of reaction are HBO + $N(^2D)$ and/or BO + NH, although the presence of either of these sets of products has yet to be determined experimentally.

Boron containing combustion systems remain a poorly understood area of chemistry despite the evidence suggesting that they possess considerable potential as high energy fuels. There is considerable scope for further work on the reactions of boron hydrides and other small boron containing molecules, such as boron oxides and oxyhydrides, which are thought to be present in such systems. Detailed knowledge of many elementary reactions of these species is required if modelling of these combustions systems is to be successful. One of the main reasons for the lack of kinetic data on these species is that very little is known about the spectroscopy of these molecules. This makes detection and concentration monitoring using spectroscopic techniques, which are the most commonly used methods of detection in kinetic studies, impossible. Since both the HBO [48,49] and BH_2 [70] radicals have been observed spectroscopically, these species would seem good candidates for kinetic studies in the immediate future. Our results have also demonstrated that the 193 nm photolysis of diborane could be used as a source of BH_2 radicals.

Emission observed during the course of this work, from the 193 nm photolysis of diborane, led us to a study of the photodissociation of this species. These emissions were analysed and the identity of the probable emitter of each band observed was assigned on the basis of the dependence of band intensity on photolysis laser power, known thermochemistry and band structure. The emissions were assigned to two

news transitions of BH_2 as well as known transitions of BH ($\tilde{A}\rightarrow\tilde{X}$) and atomic boron(I). The production of BH and BH_2 was shown to arise from the absorption of two 193 nm photons while the production of excited B atoms results from the absorption of three 193 nm photons. Differences in selection rules governing transitions between states of differing geometry in absorption and emission, means that laser photolysis has considerable potential for generating new spectra. A higher resolution study of the emissions observed during the 193 nm photolysis of diborane is warranted. A similar study of the photodissociation of B_2D_6 would also prove useful to help confirm our assignments of new bands of BH_2 as well as to elucidate the spectroscopic nature of the emitting state.

Unexpected emissions observed during the course of this work, due the presence of stannane as an impurity in the diborane, led to a similar study of the photodissociation of this species. All emissions observed from the 193 nm photolysis of stannane were assigned to known atomic tin(I) transitions and were shown to arise from the absorption of a single 193 nm photon. The energy of the highest populated Sn(I) state observed relative to the energy available from a single 193 nm photon, implied that the photodissociation must proceed *via* the process

$$SnH_{4(g)} + h\nu_{193} \longrightarrow Sn_{(g)} + 2H_{2(g)} \qquad (7)$$

although the low intensities of the emissions observed suggested that this may only be a minor channel relative to

$$SnH_{4(g)} + h\nu_{193} \longrightarrow SnH_{2(g)} + H_{2(g)}$$

There is scope for further work on the photodissociation of stannane to determine the presence of H_2 and whether SnH_2 also forms.

A study of the kinetics of reactions of CN-radicals has provided the first measurement of the room temperature rate coefficient for the reaction of CN with ND_3, as well as a re-evaluation of the room temperature rate constant for the reaction of CN with NH_3. The results obtained were

$$CN + ND_3 \longrightarrow ND_2 + DCN \quad k = 1.5 \pm 0.3 \times 10^{-11}\ cm^3\ s^{-1}$$
$$CN + NH_3 \longrightarrow NH_2 + HCN \quad k = 3.0 \pm 0.4 \times 10^{-11}\ cm^3\ s^{-1}$$

CN ($^2\Sigma^+$) radicals were generated by excimer-laser photolysis of C_2N_2 at 193 nm and their time evolution was monitored by infra-red absorption spectroscopy. Prior to this work the reactions of CN with NH_3 and ND_3 were not well understood. Unresolved questions remaining from previous studies of the CN + NH_3 reaction motivated us to perform additional studies to determine the reaction products and mechanism.

By using the techniques of mass spectrometry and infra-red absorption spectroscopy, the products of reaction were found to be $NH(D)_2$ and H(D)CN at room temperature. *Ab initio* calculations, performed at the state-of-the-art G-1 level of theory, confirmed, that should HNC be forming as a product of reaction, there was insufficient energy available from the reaction for it to isomerize to HCN in the time before analysis.

To determine the mechanism of reaction, a further *ab initio* study was undertaken to calculate the structures and relative energies of species conceivably involved. The results obtained indicated that there were two possible mechanisms by which CN and NH_3 could react to form NH_2 and HCN. The results of all the kinetic studies done on this reaction show that the rate of reaction is fast and that the rate coefficient exhibits a negative dependence on temperature. Only one of the calculated mechanisms was shown to be consistent with these properties; a pathway in which reaction proceeds *via* a dipole-dipole favoured intermediate (H_3NCN) which subsequently rearranges over a secondary barrier and dissociates to give products.

This mechanism, however, would predict that both NH_2 + HCN and NH_2 + HNC should be products of reaction, especially at elevated temperatures. This suggested that either product formation was being controlled by forces other than the relative energetics of the potential energy surface or that that there were some limitations to the accuracy attainable from the *ab initio* calculations performed in this region of the potential energy surface. The results of the state-of-the-art level calculations done on the HCN⇌HNC equilibrium, which included calculations on the reactants and products of this reaction, indicated that the relative energetics of this region of the potential energy surface may change if higher level optimizations and energy

calculations with larger basis sets were performed, and favour the formation of NH_2 + HCN over NH_2 + HNC. There remains scope for such higher level calculations to be done on the regions of the potential energy surface which determine the relative favourability of these reaction channels as well as to more accurately determine the height of the secondary barrier. Together with the use of higher levels of theory in both the optimization of geometries and calculation of relative energies, use of improved basis sets which include d and f-type polarization functions and s and p-type diffuse functions would provide more quantitative results.

The limitations of the methods of *ab initio* molecular orbital theory with respect to accuracy of results attainable have been reported for many systems, and methods for overcoming and allowing for these limitations are being devised. From the results reported here, it is clear that calculations at the highest levels of theory using large basis sets are desirable if *quantitative* results are to be obtained. However, for *large* systems such as these, such calculations would place impractical demands on both computer CPU time and disk storage space. Developments in computer architecture will increase the viability of such calculations in the future. Currently calculations with carefully selected basis sets and with moderate inclusion of correlation effects, as was done in our study, are the most practical. Although there is no substitute for experimental data, this work has demonstrated that there is valuable information to be obtained from theoretical calculations.

The results of all studies of the reactions of CN with NH_3 and ND_3 were shown to be consistent with the reaction being controlled by the rates of capture over a dipole-dipole potential and of subsequent rearrangement and dissociation of the intermediate over a secondary barrier. This provides support for the theories suggesting that the fate of reactions exhibiting kinetic properties such as these, being determined by long range intermolecular forces. This is especially true for reactions such as BH with NO which lack any significant barriers on the reaction pathway.

The work done on these reactions could be extended in a number of areas. Studies to determine the effects of temperature on the rate constant for the reaction of CN with ND_3 and of rotational excitation of CN on the rate constants for both reactions

would provide valuable information. The results of such studies would also be useful for comparison to those calculated by statistically and dynamically based reaction rate theories. The fast rate of rotational equilibration of CN would mean that the latter of these two studies would need to be done at low pressures and possibly using the more sensitive laser-induced fluorescence method for detection of CN.

There also remains scope for more work to be done to determine whether HNC forms as a product of the reaction of CN with NH_3. Experimental techniques which associate the production of HNC with the photolysis laser pulse, such as infra-red kinetic spectroscopy, would be desirable since long timescale detection techniques are not completely conclusive due to the reactive nature of HNC. Our attempts to observe HNC and HCN using this technique suggest that detection of HNC in the region of the N–H stretch would be likely to be more sensitive than detection in the region of the N–C stretch. Resonance Enhanced Multi-Photon Ionization, which could distinguish between HCN and HNC on the basis of their differing ionization thresholds, would also be a suitable technique for this study. A study to determine if CH_3 radicals form as a reaction product could also be done. Infra-red absorption spectroscopy has been shown to be sensitive to the detection of this species and so infra-red kinetic spectroscopy would be an ideal technique for such an investigation.

In terms of the aims of this work, we have extended the understanding of the chemistry of the reactions of the gas phase free-radicals CN and BH, as well as the photochemistry of diborane and stannane. Despite the advances made in experimental physical chemistry, this work has demonstrated that the study of reactive species remains a major undertaking.

Bibliography

[1] L. R. Khundkar and A. H. Zewail, *Ann. Rev. Phys. Chem.*, p. 15. Annual Reviews Inc, (1990). and references therein.

[2] D. Imre, J. L. Kinsey, A. Sinha, and J. Krenos, *J. Phys. Chem.*, 88, (1984), p. 3956.

[3] P. R. Brooks, *Chem. Rev.*, 88, (1988), p. 407.

[4] M. D. Barnes, P. R. Brooks, R. F. Curl Jr, and P. W. Harland, *J. Chem. Phys.*, 94, (1991), p. 5245.

[5] M. D. Barnes, P. R. Brooks, R. F. Curl Jr, P. W. Harland, and B. R. Johnston, *J. Chem. Phys.*, (1991). in press.

[6] O. Svelto, *Principles of Lasers*. Plenum Press, 3rd ed., (1989).

[7] W. Demtröder, *Laser Spectroscopy*. Vol. 5 of *Springer Series in Chemical Physics*, Springer-Verlag, (1982).

[8] J. Pfab, *Ann. Rep. Prog. Chem. Sect. C*, p. 105. Vol. 84, Royal Society of Chemistry, (1987).

[9] G. Hancock, *J. Chem. Soc. Farad. Trans. 2*, 84, (1988), p. 429.

[10] W. F. Coleman, *J. Chem. Ed.*, 59, (1982), p. 441.

[11] S. R. Leone and C. B. Moore, *Chemical and Biochemical Applications of Lasers*, p. 1. Vol. 1, Academic Press, (1974).

[12] R. J. Donovan, *Ann. Rep. Prog. Chem. Sect. C*, p. 117. Vol. 84, Royal Society of Chemistry, (1987).

[13] W. M. Jackson, *J. Photochem.*, 17, (1981), p. 509.

[14] L. Pasternak, H. H. Nelson, and J. R. McDonald, *J. Chem. Ed.*, 59, (1982), p. 456.

[15] W. Tsang and A. Lifshitz, *Ann. Rev. Phys. Chem.*, p. 559. Annual Reviews Inc, (1990).

[16] W. C. Gardiner, ed., *Combustion Chemistry*. Springer-Verlag, (1984).

[17] J. A. Miller, R. J. Kee, and C. K. Westbrook, *Ann. Rev. Phys. Chem.*, p. 345. Annual Reviews Inc, (1990).

[18] G. A. Laguna and S. L. Baughcum, *Chem. Phys. Lett.*, 88, (1982), p. 568.

[19] A. Szabo and N. S. Ostlund, *Modern Quantum Chemistry*. Macmillan Publishing Co, (1982).

[20] I. N. Levine, *Quantum Chemistry*. Prentice Hall, 4th ed., (1991).

[21] W. J. Hehre, L. Radom, P. von R. Schleyer, and J. A. Pople, *Ab Initio Molecular Orbital Theory*. J. Wiley and Sons, (1986).

[22] J. Simons, *J. Phys. Chem.*, 95, (1991), p. 1017.

[23] P. J. Robinson and K. A. Holbrook, *Unimolecular Reactions*. Wiley-Interscience, (1972).

[24] I. W. M. Smith, *Kinetics and Dynamics of Elementary Gas Reactions*. Butterworths, (1980).

[25] M. J. Pilling and I. W. M. Smith, eds., *Modern Gas Kinetics*. Blackwell Scientific Publications, (1987).

[26] D. C. Clary, *Ann. Rev. Phys. Chem.*, p. 61. Annual Reviews Inc, (1990).

[27] M. Reich, R. Schieder, H. J. Clar, and G. Winnewisser, *Appl. Opt.*, 25, (1986), p. 130.

[28] H. J. Clar, R. Schieder, M. Reich, and G. Winnewisser, *Appl. Opt.*, 28, (1989), p. 1648.

[29] N. Rabjohn, ed., *Organic Syntheses.* Vol. 4, J. Wiley and Sons, (1967). p. 207.

[30] W. Jeffers, *Chem. & Ind.*, April 8 (1961), p. 431.

[31] G. W. Freeguard and L. H. Long, *Chem. & Ind.*, (1965), p. 471.

[32] G. W. Schaeffer and M. Emilius, *J. Amer. Chem. Soc.*, 76, (1954), p. 1203.

[33] M. W. Chase Jr, C. A. Davies, J. R. Downey Jr, D. F. Frurip, R. A. McDonald, and A. N. Syverud, "JANAF Thermochemical Tables, Third Edition," *J. Phys. Chem. Ref. Data*, 14, (1985). Suppl. 1.

[34] R. A. Yetter, H. Rabitz, F. L. Dryer, R. C. Brown, and C. E. Kolb, *Combust. Flame*, 83, (1991), p. 43.

[35] A. G. Gaydon and H. G. Wolfhard, *Flames, their structure, radiation and temperature.* Chapmann and Hall Ltd, 3rd ed., (1970). p. 349.

[36] G. K. Anderson and S. H. Bauer, *J. Phys. Chem.*, 81, (1977), p. 1146.

[37] P. M. Jeffers and S. H. Bauer, *J. Phys. Chem.*, 88, (1984), p. 5039.

[38] D. B. Bordchardt, J. G. Choi, K. Suziki, and S. H. Bauer, *J. Chem. Phys.*, 88, (1988), p. 6282.

[39] L. Pasternak, R. J. Balla, and H. H. Nelson, *J. Phys. Chem.*, 92, (1988), p. 1200.

[40] J. K. Rice, N. J. Caldwell, and H. H. Nelson, *J. Phys. Chem.*, 93, (1989), p. 3600.

[41] N. L. Garland, C. T. Stanton, J. W. Fleming, A. P. Baronavski, and H. H. Nelson, *J. Phys. Chem.*, 94, (1990), p. 4952.

[42] N. J. Caldwell, J. K. Rice, H. H. Nelson, G. F. Adams, and M. Page, *J. Chem. Phys.*, 93, (1990), p. 479.

[43] M. P. Irion and K. L. Kompa, *J. Chem. Phys.*, 76, (1982), p. 2338.

[44] J. A. Harrison. PhD thesis, University of Canterbury, (1988).

[45] J. W. C. Johns, F. A. Grimm, and R. F. Porter, *J. Mol. Spect.*, 22, (1967), p. 435.

[46] J. A. Harrison, R. F. Meads, and L. F. Phillips, *Chem. Phys. Lett.*, 150, (1988), p. 299.

[47] J. A. Harrison and R. G. A. R. Maclagan, *Chem. Phys. Lett.*, 146, (1988), p. 243.

[48] Y. Kawashima, K. Kawaguchi, and E. Hirota, *Chem. Phys. Lett.*, 131, (1986), p. 205.

[49] Y. Kawashima, Y. Endo, K. Kawaguchi, and E. Hirota, *Chem. Phys. Lett.*, 135, (1987), p. 441.

[50] M. Marshall, C. MacKay, and R. Wolfgang, *J. Amer. Chem. Soc.*, 86, (1964), p. 4741.

[51] J. DeHaven, M. T. O'Connor, and P. Davidovits, *J. Chem. Phys.*, 75, (1981), p. 1746.

[52] G. J. Green and J. L. Gole, *Chem. Phys. Lett.*, 69, (1980), p. 45.

[53] T. G. DiGiuseppe and P. Davidovits, *J. Chem. Phys.*, 74, (1981), p. 3287.

[54] W. M. Shaub and M. C. Lin, *NBS Special Publication*, 561, (1979), p. 1244.

[55] R. J. Donovan, C. Fotakis, A. Hopkirk, C. B. McKendrick, and A. Torre, *Can. J. Chem.*, 61, (1983), p. 1023.

[56] H. Shimohara and N. Nishi, *J. Chem. Phys*, 77, (1982), p. 234.

[57] N. Nishi and H. Shimohara, *J. Chem. Phys.*, 77, (1982), p. 246.

[58] R. D. Kenner, F. Rohrer, R. K. Browarzik, A. Kaes, and F. Stuhl, *Chem. Phys.*, 118, (1987), p. 141.

[59] V. M. Donnelly, A. P. Baronavski, and J. R. McDonald, *Chem. Phys.*, 43, (1979), p. 271.

[60] P. Lindberg, D. Raybone, J. A. Salthouse, T. M. Watkinson, and J. C. Whitehead, *Mol. Phys.*, 62, (1987), p. 1297.

[61] R. D. Kenner, R. K. Browarzik, and F. Stuhl, *Chem. Phys.*, 121, (1988), p. 457.

[62] E. Blum and G. Herzberg, *J. Phys. Chem.*, 41, (1937), p. 91.

[63] W. C. Price, *J. Chem. Phys*, 16, (1948), p. 894.

[64] T. Hirata and H. E. Gunning, *J. Chem. Phys.*, 27, (1957), p. 477.

[65] M. Bufalini and J. E. Todd, *J. Phys. Chem.*, 72, (1968), p. 3367.

[66] W. C. Kreye and R. A. Marcus, *J. Chem. Phys.*, 37, (1962), p. 419.

[67] J. H. Clark and R. G. Anderson, *Appl. Phys. Lett.*, 32, (1978), p. 46.

[68] M. P. Irion and K. L. Kompa, *J. Photochem.*, 32, (1986), p. 139.

[69] K. Kawaguchi, J. E. Butler, C. Yamada, S. H. Bauer, T. Minowa, H. Kanamori, and E. Hirota, *J. Chem. Phys.*, 87, (1987), p. 2438.

[70] G. Herzberg and J. W. C. Johns, *Proc. Roy. Soc. A*, 298, (1967), p. 142.

[71] S. H. Bauer, G. Herzberg, and J. W. C. Johns, *J. Mol. Spect.*, 13, (1964), p. 256.

[72] J. Fernandez, G. Lespes, and A. Dargelos, *Chem. Phys.*, 103, (1986), p. 85.

[73] D. R. Stull and H. Prophet, eds., *JANAF Thermochemical Tables, Second Edition*. National Bureau of Standards. NSRDS-NBS 37, (1971).

[74] J. A. Pople, B. T. Luke, M. J. Frisch, and J. S. Binkley, *J. Phys. Chem.*, 89, (1985), p. 2198.

[75] M. Page, G. F. Adams, J. S. Binkley, and C. F. Melius, *J. Phys. Chem.*, 91, (1987), p. 2675.

[76] J. A. Harrison, R. F. Meads, and L. F. Phillips, *Chem. Phys. Lett.*, 148, (1988), p. 125.

[77] J. Dufayard and O. Nedelec, *J. Chem. Phys.*, 69, (1978), p. 4708.

[78] G. H. F. Diercksen, N. E. Gruner, J. R. Sabin, and J. Oddershede, *Chem. Phys.*, 115, (1987), p. 15.

[79] D. D. Wagman, W. H. Evans, V. B. Porter, I. Halow, S. M. Bailey, and R. H. Schumm, Tech. Rep. 270.3, National Bureau of Standards, Washington DC, (1968).

[80] B. H. Mahan and R. Mandal, *J. Chem. Phys.*, 37, (1962), p. 207.

[81] M. A. King, G. D. Beverly, F. H. Koester, and R. P. Hollandsworth, *Inorg. Chem.*, 8, (1969), p. 2033.

[82] R. F. Meads, D. C. J. Marsden, J. A. Harrison, and L. F. Phillips, *Chem. Phys. Lett.*, 160, (1989), p. 342.

[83] R. A. Bair and T. H. Dunning, *J. Chem. Phys.*, 82, (1985), p. 2280.

[84] J. de Juan, S. Callister, H. Reisler, G. A. Segal, and C. Wittig, *J. Chem. Phys.*, 89, (1988), p. 1977.

[85] A. F. Wagner and R. A. Bair, *Int. J. Chem. Kinet.*, 18, (1986), p. 473.

[86] Q. Sun, D. L. Yang, N. S. Wang, J. M. Bowman, and M. C. Lin, *J. Chem. Phys.*, 93, (1990), p. 4730.

[87] I. R. Sims and I. W. M. Smith, *J. Chem. Soc. Farad. Trans. 2*, 84, (1988), p. 527.

[88] J. S. Binckley, M. J. Frisch, D. J. DeFrees, K. Raghavachari, R. A. Whiteside, H. B. Schlegel, E. M. Fluder, and J. A. Pople, *Gaussian 82*. Carnegie-Mellon University, Pittsburgh, (1982).

[89] M. J. Frisch, M. Head-Gordon, G. W. Trucks, J. B. Foresman, H. B. Schlegel, K. Raghavachari, M. Robb, J. S. Binkley, C. Gonzalez, D. J. DeFrees, D. J. Fox, R. A. Whiteside, R. Seeger, C. F. Melius, J. Baker, R. L. Martin, L. R. Kahn, J. J. P. Stewart, S. Topiol, and J. A. Pople, *Gaussian 90; Revision F*. Gaussian Inc, Pittsburgh, (1990).

[90] N. C. Handy, P. J. Knowles, and K. Somasundaram, *Theor. Chim. Acta.*, 68, (1985), p. 87.

[91] K. Raghavachari, *J. Chem. Phys.*, 82, (1985), p. 4607.

[92] R. H. Nobes, J. A. Pople, L. Radom, N. C. Handy, and P. J. Knowles, *Chem. Phys. Lett.*, 138, (1987), p. 481.

[93] J. A. Pople, M. Head-Gordon, and K. Raghavachari, *J. Chem. Phys.*, 87, (1987), p. 5968.

[94] J. A. Pople, M. Head-Gordon, D. J. Fox, K. Raghavachari, and L. A. Curtiss, *J. Chem. Phys.*, 90, (1989), p. 5622.

[95] D. J. DeFrees and A. D. McClean, *J. Chem. Phys.*, 82, (1985), p. 333.

[96] I. W. M. Smith, *J. Chem. Soc. Farad. trans. 2*, 87, (1991), p. 2271.

[97] R. F. Meads, R. G. A. R. Maclagan, and L. F. Phillips, in preparation.

[98] B. E. Turner and P. Thaddeus, *Astrophys. J.*, 211, (1977), p. 755. and references therein.

[99] A. P. C. Mann and D. A. Williams, *Nature*, 283, (1980), p. 721.

[100] W. F. Huebner, ed., *Physics and Chemistry of Comets.* Springer-Verlag, (1990).

[101] D. F. Strobel, *Planet. Space Sci.*, 30, (1982), p. 839.

[102] J. B. Pickles and D. A. Williams, *Astrophys. Space Sci.*, 52, (1977), p. 453.

[103] G. A. West and M. J. Berry, *J. Chem. Phys.*, 61, (1974), p. 4700.

[104] R. Bacis, D. Cerny, J. D'Incan, G. Guelachvili, and F. Roux, *Astrophys. J.*, 214, (1977), p. 946.

[105] Q. N. Le and M. Vanpee, *Combust. Flame*, 62, (1985), p. 193.

[106] A. N. Hayhurst and H. G. McLean, *Nature*, 251, (1974), p. 303.

[107] C. Morley, *Combust. Flame*, 27, (1976), p. 189.

[108] I. Glassman, *Combustion*. Academic Press, (1977). p. 219.

[109] B. S. Haynes, *Combust. Flame*, 28, (1977), p. 113.

[110] E. Herbst and W. Klemperer, *Astrophys. J.*, 185, (1973), p. 505.

[111] R. L. Dickman, W. B. Somerville, D. C. B. Whittet, D. McNally, and J. C. Blades, *Astrophys. J.*, 53, (1983), p. 55.

[112] I. R. Sims and I. W. M. Smith, *Chem. Phys. Lett.*, 151, (1988), p. 481.

[113] I. R. Sims and I. W. M. Smith, *Chem. Phys. Lett.*, 149, (1988), p. 565.

[114] R. J. Balla and L. Pasternak, *J. Phys. Chem.*, 91, (1987), p. 73.

[115] N. Sayah, X. Li, J. F. Caballero, and W. M. Jackson, *J. Photochem. Photobiol. A*, 45, (1988), p. 177.

[116] I. R. Sims and I. W. M. Smith, *J. Chem. Soc. Farad. Trans. 2*, 85, (1989), p. 915.

[117] J. de Juan, I. W. M. Smith, and B. Veyret, *J. Phys. Chem.*, 91, (1987), p. 69.

[118] J. de Juan, I. W. M. Smith, and B. Veyret, *Chem. Phys. Lett.*, 132, (1986), p. 108.

[119] N. S. Wang, D. L. Yang, and M. C. Lin, *Chem. Phys. Lett.*, 163, (1989), p. 480.

[120] M. B. Colket III, *Int. J. Chem. Kinet.*, 16, (1984), p. 353.

[121] R. J. Balla, K. H. Casleton, J. S. Adams, and L. Pasternak, *J. Phys. Chem.*, 95, (1991), p. 8695.

[122] B. Atakan and J. Wolfrum, *Chem. Phys. Lett.*, 186, (1991), p. 547.

[123] D. A. Lichtin and M. C. Lin, *Chem. Phys.*, 96, (1985), p. 473.

[124] X. Li, N. Sayah, and W. M. Jackson, *J. Chem. Phys.*, 81, (1984), p. 833.

[125] C. Anastasi and D. U. Hancock, *J. Chem. Soc. Farad. Trans. 2*, 84, (1988), p. 9.

[126] D. A. Lichtin and M. C. Lin, *Chem. Phys.*, 104, (1986), p. 325.

[127] W. P. Hess, J. L. Durant Jr, and F. P. Tully, *J. Phys. Chem.*, 93, (1989), p. 6402.

[128] R. C. Jensen, D. B. Walton, and R. D. Coombe, *Chem. Phys. Lett.*, 169, (1990), p. 441.

[129] S. Zabarnick and M. C. Lin, *Chem. Phys.*, 134, (1989), p. 185.

[130] J. B. Halpern, G. E. Miller, and H. Okabe, *Chem. Phys. Lett.*, 155, (1989), p. 347.

[131] A. Jacobs, M. Wahl, R. Weller, and J. Wolfrum, *Chem. Phys. Lett.*, 144, (1988), p. 203.

[132] A. Szekely, R. K. Hanson, and C. T. Bowman, *Int. J. Chem. Kinet.*, 16, (1984), p. 1609.

[133] N. S. Wang, D. L. Yang, M. C. Lin, and C. F. Melius, *Int. J. Chem. Kinet.*, 23, (1991), p. 151.

[134] D. Lindackers, M. Burmeister, and P. Roth, *Combust. Flame*, 81, (1990), p. 251.

[135] R. J. Balla and K. H. Casleton, *J. Phys. Chem.*, 95, (1991), p. 2334.

[136] A. R. Whyte and L. F. Phillips, *Chem. Phys. Lett.*, 98, (1983), p. 590.

[137] M. Y. Louge and R. K. Hanson, *Int. J. Chem. Kinet.*, 16, (1984), p. 231.

[138] D. F. Davidson, A. J. Dean, H. D. DiRosa, and R. K. Hanson, *Int. J. Chem. Kinet.*, 23, (1991), p. 1035.

[139] B. Atakan, A. Jacobs, M. Wahl, R. Weller, and J. Wolfrum, *Chem. Phys. Lett.*, 154, (1989), p. 449.

[140] J. L. Durant Jr and F. P. Tully, *Chem. Phys. Lett.*, 154, (1989), p. 568.

[141] A. Szekely, R. K. Hanson, and C. T. Bowman, *Int. J. Chem. Kinet.*, 15, (1983), p. 915.

[142] J. C. Boden and B. A. Thrush, *Proc. Roy. Soc. A*, 305, (1968), p. 107.

[143] G. E. Bullock, R. Cooper, S. Gordon, and W. A. Mulac, *J. Phys. Chem.*, 76, (1972), p. 1931.

[144] D. Cerny, R. Bacis, G. Guelachvili, and F. Roux, *J. Mol. Spect.*, 73, (1978), p. 154.

[145] P. B. Davies and P. A. Hamilton, *J. Chem. Phys.*, 76, (1982), p. 2127.

[146] G. Guelachvili and K. N. Rao, *Handbook of Infrared Standards*. Academic Press, (1986).

[147] D. E. Paul and F. W. Dalby, *J. Chem. Phys.*, 37, (1962), p. 592.

[148] H. Okabe, *Photochemistry of Small Molecules*. J. Wiley and Sons, (1978).

[149] M. Suto and L. C. Lee, *J. Chem. Phys.*, 78, (1983), p. 4515.

[150] V. Vaida, W. Hess, and J. L. Roebber, *J. Phys. Chem.*, 88, (1984), p. 3397.

[151] D. Eres, M. Gurnick, and J. D. McDonald, *J. Chem. Phys.*, 81, (1984), p. 5552.

[152] J. B. Halpern and W. M. Jackson, *J. Phys. Chem.*, 86, (1982), p. 973.

[153] M. J. Howard and I. W. M. Smith, *Prog. React. Kinet.*, 12, (1983), p. 57.

[154] D. C. Clary, *Mol. Phys.*, 53, (1984), p. 3.

[155] D. Patel-Misra, D. G. Sauder, and P. J. Dagdigian, *J. Chem. Phys.*, 93, (1990), p. 5448.

[156] H. Reisler, M. Mangin, and C. Wittig, *Chem. Phys.*, 47, (1980), p. 49.

[157] K. J. Schmatjko and J. Wolfrum, *Ber. Bungenses. Phys. Chem.*, 82, (1978), p. 419.

[158] M. C. Addison, A. J. Leitch, C. Fotakis, and R. J. Denovan, *J. Photochem.*, 10, (1979), p. 273.

[159] D. Kley, N. Washida, K. H. Becker, and W. Groth, *Chem. Phys. Lett.*, 15, (1972), p. 45.

[160] J. I. Choe, D. K. Kwak, and S. G. Kukulich, *J. Mol. Spect.*, 121, (1987), p. 75.

[161] J. B. Burkholder, A. Sinha, P. D. Hammer, and C. J. Howard, *J. Mol. Spect.*, 126, (1987), p. 72.

[162] C. Pau and W. J. Hehre, *J. Phys. Chem.*, 86, (1982), p. 321.

[163] G. Winnewisser, A. G. Maki, and D. R. Johnston, *J. Mol. Spect.*, 39, (197), p. 149.

[164] R. A. Cresswell and A. G. Robiette, *Mol. Phys.*, 36, (1978), p. 869.

[165] T. J. Lee and A. P. Rendell, *Chem. Phys. Lett.*, 177, (1991), p. 491. and references therein.

[166] J. N. Murrell, S. Carter, and L. O. Halonen, *J. Mol. Spect.*, 93, (1982), p. 307.

[167] R. E. Meunchausen, G. W. Hills, M. F. Merienne-LaFore, D. A. Ramsay, M. Vervloet, and F. W. Birss, *J. Mol. Spect.*, 112, (1985), p. 203.

[168] M. Birk and M. Winnewisser, *Chem. Phys. Lett.*, 123, (1986), p. 382.